NATIONAL ADVISORY COMMITTEE FOR AERONAUTICS

TECHNICAL NOTE

No. 1379

WIND-TUNNEL INVESTIGATION OF THE EFFECT OF POWER AND FLAPS ON THE STATIC LATERAL STABILITY AND CONTROL CHARACTERISTICS OF A SINGLE-ENGINE HIGH-WING AIRPLANE MODEL

By John R. Hagerman

Langley Memorial Aeronautical Laboratory
Langley Field, Va.

Washington
July 1947

NATIONAL ADVISORY COMMITTEE FOR AERONAUTICS

TECHNICAL NOTE NO. 1379

WIND-TUNNEL INVESTIGATION OF THE EFFECT OF POWER AND FLAPS ON THE STATIC LATERAL STABILITY AND CONTROL CHARACTERISTICS OF A SINGLE-ENGINE HIGH-WING AIRPLANE MODEL

By John R. Hagerman

SUMMARY

An investigation was conducted to determine the effect of power and of full-span slotted flaps on the static lateral stability and control characteristics of a single-engine high-wing airplane with tail on and tail off. The model combinations investigated included three power conditions - namely, propeller off, propeller windmilling, and power on - tested with flap neutral, single slotted flap, and double slotted flap.

The application of power with the flap neutral was found to make no appreciable change in the effective dihedral, to increase the directional stability at low lift coefficients, and to reduce the rudder effectiveness (rate of change of angle of yaw with rudder deflection). Deflection of the single slotted flap decreased the effective dihedral, increased the directional stability, and increased the rudder effectiveness. Deflection of the double slotted flap with power on decreased the effective dihedral, increased the directional stability, and decreased the rudder effectiveness. The addition of the tail surfaces increased the effective dihedral and the directional stability.

In comparing the high-wing and low-wing models, the high-wing model was found to have greater effective dihedral and greater rudder effectiveness than the low-wing model; however, the fin effectiveness on the high-wing model was found to be the smaller.

INTRODUCTION

The development and use of higher-powered engines on airplanes have introduced pronounced and important effects upon the stability and control characteristics of the airplane. Large slipstream effects

and increased wing loadings have been observed as a result of increased engine power.

In view of the aforementioned developments and problems resulting therefrom, a comprehensive investigation was undertaken at the Langley 7- by 10-foot tunnel to determine the effects of power, full-span single slotted and double slotted flaps, and vertical position of the wing on the stability and control characteristics of a model of a typical single-engine airplane. The results of the longitudinal-stability and lateral-stability investigations of the model as a low-wing airplane model are presented in references 1 and 2, respectively. The results of the longitudinal-stability investigation of the model as a high-wing airplane are presented in reference 3. The present paper deals with the investigation of the lateral stability and control characteristics of the model as a high-wing airplane model. In addition, the effect of wing position on lateral stability characteristics is included in this report.

COEFFICIENTS AND SYMBOLS

The results of the tests are presented in the form of standard NACA coefficients of forces and moments. Rolling-moment, yawing-moment, and pitching-moment coefficients are given about the center-of-gravity location (26.7 percent M.A.C.) which is shown in figure 1. The data are referred to the stability axes, which are a system of axes having their origin at the center of gravity and in which the Z-axis is in the plane of symmetry and perpendicular to the relative wind, the X-axis is in the plane of symmetry and perpendicular to the Z-axis, and the Y-axis is perpendicular to the plane of symmetry. The positive directions of the stability axes, of angular displacements of the airplane and control surfaces, and of hinge moments are shown in figure 2.

The coefficients and symbols are defined as follows:

C_L lift coefficient (Z/qS)

C_X longitudinal-force coefficient (X/qS)

C_Y lateral-force coefficient (Y/qS)

C_l rolling-moment coefficient (L/qSb)

C_m pitching-moment coefficient (M/qSc')

C_n	yawing-moment coefficient (N/qSb)
C_{h_r}	rudder hinge-moment coefficient $\left(H_r/qb_r\bar{c}_r^2\right)$
T_c'	effective thrust coefficient based on wing area $\left(T_{eff}/qS\right)$
Q_c	torque coefficient $\left(Q/\rho V^2D^3\right)$
V/nD	propeller advance-diameter ratio
η	propulsive efficiency $\left(T_{eff}V/2\pi nQ\right)$
Z	lift
X	longitudinal force
Y	lateral force
L	rolling moment
M	pitching moment
N	yawing moment
H	hinge moment, pound-feet
T_{eff}	propeller effective thrust, pounds
Q	propeller torque, pound-feet
q	free-stream dynamic pressure, pounds per square foot $\left(\rho V^2/2\right)$
S	wing area (9.44 sq ft on model)
c'	wing mean aerodynamic chord (M.A.C.) (1.36 ft on model)
$\bar{c}_r$	rudder root-mean-square chord back of hinge line (0.353 ft on model)
b	wing span, unless otherwise defined (7.458 ft on model)
b_r	rudder span along hinge line (1.508 ft on model)
V	air velocity, feet per second

D	propeller diameter (2.00 ft on model)
n	propeller speed, revolutions per second
ρ	mass density of air, slugs per cubic foot
α	angle of attack of fuselage center line, degrees
ψ	angle of yaw, degrees
δ	control-surface deflection with respect to chord line, degrees
β	propeller blade angle at 0.75 radius (25° on model)
Γ_{eff}	effective dihedral, degrees

Subscripts:

a	aileron
e	elevator
r	rudder
ψ	denotes partial derivatives of a coefficient with respect to angle of yaw $\left(\text{for example, } C_{l_\psi} = \frac{\partial C_l}{\partial_\psi}\right)$

MODEL AND APPARATUS

The tests were made in the Langley 7- by 10-foot tunnel which is described in references 4 and 5. The model was a $\frac{1}{5}$-scale model of a fighter-type airplane and is shown in figure 1. The wing was fitted with a 40-percent-chord double slotted flap which covered 93 percent of the span and was designed from data in reference 6. For the flap-neutral tests the flaps were retracted and the gaps between the flaps were faired to the airfoil contour with modeling clay. The rear flap of the double-slotted-flap configuration, which represented the flap for a single-slotted-flap configuration, had a 25.66-percent chord and was maintained at a setting of 30°. The front flap was retracted and faired to the airfoil contour with modeling clay. For the double-slotted-flap tests, the rear flap

was set at 30° relative to the front flap which in turn was set at 30° relative to the wing. With flaps deflected, there was about $\frac{1}{32}$-inch clearance between the end of the flap and the fuselage. No landing gear was used for these tests.

A detailed drawing of the tail assembly is shown in figure 3. During the preliminary stages of the investigation a conventional horizontal tail surface was found to be inadequate in providing longitudinal trim when the double slotted flap was deflected. As a result, an inverted Clark Y airfoil section equipped with a fixed leading-edge slot was used. When the model was tested with flap neutral and with the single slotted flap deflected, the tail slot was sealed; with the double slotted flap deflected, the slot was open. The vertical tail (fig. 3) was offset $1\frac{1}{2}^\circ$ to the left to help counteract the asymmetry in yawing moment due to slipstream rotation.

Power for the 2-foot-diameter, three-blade, right-hand, metal propeller used was obtained from a 56-horsepower water-cooled induction motor mounted in the fuselage nose. Propeller speed was measured by means of an electric tachometer which was accurate to within 0.2 percent. The dimensional characteristics of the propeller are given in figure 4.

Rudder hinge moments were measured by means of an electric strain gage mounted in the fin.

TESTS AND RESULTS

Test Conditions

The tests were made at dynamic pressures of 12.53 pounds per square foot for power-on tests with the double slotted flap deflected and 16.37 pounds per square foot for all other tests. These dynamic pressures correspond to airspeeds of about 70 and 80 miles per hour, respectively. The test Reynolds numbers were about 875,000 and 1,000,000 based on the wing mean aerodynamic chord of 1.36 feet.

Corrections

All power-on data have been corrected for tare effects caused by the model support strut. The power-off data, however, have not been corrected for tare effects because they have been found to be

relatively small and erratic on similar models, especially when the flaps are deflected. Jet-boundary corrections have been applied to the angles of attack, longitudinal-force coefficients, and tail-on pitching-moment coefficients. The corrections were computed as follows:

$$\Delta\alpha = 57.3\delta_w \frac{S}{C} C_L$$

$$\Delta C_X = -\delta_w \frac{S}{C} C_L^2$$

$$\Delta C_m = -57.3\left(\frac{\delta_T}{\sqrt{q_t/q}} - \delta_w\right) \frac{S}{C} \frac{\partial C_m}{\partial i_t} C_L$$

where

δ_w jet-boundary correction factor at wing (0.1125)

δ_T total jet-boundary correction factor at tail (varies between 0.200 and 0.210)

S model wing area (9.44 sq ft)

C tunnel cross-sectional area (69.59 sq ft)

$\frac{\partial C_m}{\partial i_t}$ change in pitching-moment coefficient per degree change in stabilizer setting as determined in tests

q_t/q ratio of effective dynamic pressure over the horizontal tail to free-stream dynamic pressure

Test Procedure

Propeller calibrations were made by measuring the longitudinal force for a range of propeller speed with the model at zero yaw, zero angle of attack, flaps neutral, and tail removed. The effective thrust coefficient was then computed from the relation

$$T_c' = C_{X_{(\text{propeller operating})}} - C_{X_{(\text{propeller removed})}}$$

The motor torque was also measured and the propeller efficiency computed. The results of the propeller calibration are shown in figure 5. Figure 6 illustrates the relation between T_c' and C_L, which is representative of a typical constant-speed propeller. For simplicity, a straight line variation of T_c' with C_L was used. The propeller speed required to simulate this thrust condition was determined from figures 5 and 6. The approximate amount of engine horsepower represented is given in figure 7 for various model scales and wing loadings. Tests were also made with the propeller off, propeller windmilling, and constant T_c'. The value of T_c' for the tests with the propeller windmilling was about -0.005.

At each angle of attack for power-on yaw tests the propeller speed was held constant throughout the yaw range. Since the lift and thrust coefficients vary with yaw when the propeller speed and angle of attack are held constant, the thrust coefficient is strictly correct only at zero yaw.

Lateral-stability derivatives were obtained from pitch tests at angles of yaw of $\pm 5^\circ$ (hereinafter termed slope tests) by assuming a straight-line variation between these points. The tests were made with the propeller off, propeller windmilling, constant power, and constant T_c'.

Owing to an error in part of the investigation of the double-slotted-flap configuration, some of the data are omitted.

Presentation of Results

An outline of the figures presenting the results of the investigation is given as follows:

	Figure
Effect of power on C_{l_ψ}, C_{n_ψ}, and C_{Y_ψ}:	
Flap neutral	8
Single slotted flap deflected	9
Double slotted flap deflected	10
Increments in C_{l_ψ}, C_{n_ψ}, and C_{Y_ψ} resulting from:	
Power (constant power minus propeller windmilling)	11
Flap deflection	12
Tail surfaces	13

DISCUSSION

The following discussion is concerned with the tail on the model except where otherwise noted.

Effective-Dihedral Derivative $\left(C_{l_\psi}\right)$

The variation of C_{l_ψ} with C_L (figs. 8 to 10) is generally smooth for all power conditions and flap configurations. In general, the yaw tests agree with the slope tests as is indicated by the large symbols on figures 8 to 10. (The large symbols represent slope values taken at zero yaw from the yaw tests.)

Effect of power.- The increments in C_{l_ψ} due to power (constant power minus propeller windmilling) are shown in figure 11. Application of power resulted in no appreciable change of effective dihedral for the flap-neutral case but decreased the effective dihedral with the single slotted and double slotted flap deflected $\left(C_{l_\psi} = 0.0002\right.$ is approx. equivalent to 1° of effective dihedral). This decrease in C_{l_ψ} with flaps deflected is caused by the lateral shift of the slipstream over the trailing wing as the airplane is sideslipped. The lateral center of pressure of the added lift due to power moves outboard and creates a rolling moment about the center of gravity.

The reduction in effective dihedral caused by power (complete model) ranged from 0.5° to -0.5° throughout the lift range for the flap-neutral configuration, from -0.5° to -3° for the single-slotted-flap configuration, and from -5.5° to -13° for the double-slotted-flap configuration.

Effect of flap deflection.- The effect of deflecting the single slotted flap on the effective dihedral is shown in figure 12. Inasmuch as the double-slotted-flap configuration was not investigated at a low enough lift coefficient to make a direct comparison with the flap-neutral configuration, a comparison of the increments of C_{l_ψ} between single-slotted-flap and double-slotted-flap deflections are presented in figure 12 to show the effect of the double slotted flap.

Deflecting the single slotted flap resulted in a decrease in effective dihedral with both power off and power on; however, deflecting the double slotted flap (in comparison with the single slotted flap) resulted in an increase of effective dihedral with power off and in a decrease with power on. The increase in effective dihedral with power off is thought to be caused by unsteady flow conditions resulting from the deflection of the double slotted flap.

Effect of tail surfaces.- The effect of the tail surfaces on the effective dihedral is shown in figure 13. The effective dihedral was increased with the addition of the tail surfaces for all conditions tested - the increase being slightly larger with power on than with power off.

It has been previously established that the rolling moment contributed by the vertical tail is dependent upon the distance from the X-axis to the center of pressure of the vertical tail. For a given lift coefficient the flap-neutral configuration (high angle of attack), therefore, would produce the smallest positive increment in C_{l_ψ}; and the double-slotted-flap configuration (low angle of attack), would produce the greatest positive increment in C_{l_ψ}. This trend is shown to occur for the flap-neutral and single-slotted-flap configurations. Because no double-slotted-flap tail-off data are available, increments in C_{l_ψ} resulting from the addition of the tail surfaces for this flap configuration are not presented.

Effect of wing position.- The high-wing model has less geometric dihedral (1.9°) than the low-wing model (5.8°) (reference 2). A comparison of the results in reference 2 and those presented herein, however, indicates that the high-wing model has greater effective dihedral when power is applied and when flaps are deflected than the low-wing model. An explanation of the greater effective dihedral of the wing in the high position is given in reference 7.

Directional-Stability Derivative (C_{n_ψ})

Effect of power.- The effects of power on C_{n_ψ} are presented in figure 11. With the tail off, power produced a destabilizing effect for the flap-neutral and single-slotted-flap configurations, with the destabilizing effect increasing with increasing lift coefficient. With the tail on, the resultant effect due to power was favorable for all flap configurations with the exception of the flap-neutral configuration which had a slight destabilizing power effect at low lift coefficients. The contribution of power to C_{n_ψ} (complete model) varied throughout the lift range from about 0.0001 to -0.0002 for the flap-neutral configuration, -0.0001 to -0.0011 for the single-slotted-flap configuration, and -0.0017 to -0.0004 for the double-slotted-flap configuration.

The addition of the windmilling propeller decreased the directional stability for all flap configurations with tail off and tail on, except for the double-slotted-flap configuration with tail on where the directional stability was increased. (See figs. 8 to 10.)

Effect of flap deflection.- Deflection of the single slotted flap produced a destabilizing effect on the directional stability with tail off above a lift coefficient of 0.8. (See fig. 12(a).) With tail on, the directional stability was increased with both power off and power on. (See fig. 12(b).) The contribution of ΔC_{n_ψ} produced by the single-slotted-flap deflection (complete model) varies from -0.00027 to 0.00003 with the windmilling propeller and from -0.00036 to -0.00039 for the constant-power condition. The data presented are generally in agreement with the theory that flap deflection increases the directional stability. (See references 8 and 9.)

Deflecting the double slotted flap had a favorable effect on the directional stability for all tail-on conditions. (See fig. 12(b).)

Effect of tail surfaces.- The addition of the tail surfaces increased the directional stability in all cases investigated. (See figs. 13(a) and 13(b).) The increments contributed by the tail increased with increased flap deflection and also increased with increased power.

The effect of tail configuration on the aerodynamic characteristics in yaw (from 40° to -40°) is presented in figures 14 to 16. The directional stability is less in all cases when the rudder is free than when held fixed. No rudder lock occurred for any of the

configurations tested. Rudder lock is determined by the reversal of the yawing-moment curve only when the reversal passes through zero yawing moment. The decreased slope of the yawing-moment curves at about $\pm 18^{\circ}$ yaw in figures 14(b) and 15(b) and at 18° yaw in figure 16(b), as well as the reversal of the yawing-moment curve at about -18° in figure 16(b), is probably due to vertical tail stall.

Effect of wing position.- A study of table I in reference 2 and table I in the present paper shows that raising the wing from a low-wing position to a high-wing position greatly reduced the fin effectiveness $\left(\Delta C_{n_\psi} \text{ due to tail}\right)$. (See reference 9.) The effect of wing-fuselage interference on fin effectiveness has been shown (reference 8) to be unfavorable for high-wing designs. For a high-wing airplane the vertical tail is mainly in a region of destabilizing sidewash. A more detailed explanation of this unfavorable interference is found in reference 9.

Directional Control and Trim

Effect of power on rudder-control and hinge-moment characteristics.- A summary of some of the principal rudder-control and hinge-moment parameters obtained from the results of the yaw tests (figs. 17 to 19) is given in table I.

The application of power decreased the rudder effectiveness $\frac{\partial \psi}{\partial \delta_r}$ with the flap neutral and with the double slotted flap deflected; however, with the single slotted flap deflected the rudder effectiveness was increased. The deflection of the single slotted flap (power on) increased the rudder effectiveness, whereas deflection of the double slotted flap (compared with the flap-neutral configuration) decreased the rudder effectiveness.

For the flap-neutral configuration only small changes occurred in the hinge-moment parameters $C_{h_{r_\psi}}$ and $\partial C_{h_r}/\partial \delta_r$ with power. The thrust coefficient is low for this condition (low C_L); therefore, power effects would also be expected to be low. For the single-slotted-flap and double-slotted-flap configurations, the application of power greatly increased the values of the hinge-moment parameters. This effect is especially noticeable on values of $C_{h_{r_\psi}}$ for the double-slotted-flap configuration.

Effect of power on trim.- A factor of prime importance to the pilot is the trim change with power. The dashed curve for $C_Y = 0$

on the yawing-moment curves (figs. 17 to 19) indicates points on the C_n-curve at which the lateral force is zero. The point at which the curve for $C_Y = 0$ intersects the C_n-axis gives the rudder deflection and yaw angle necessary to maintain straight flight with zero bank. The changes in rudder deflection required to trim with the wings level when power is applied and the corresponding changes in yaw angle are as follows:

Flap	α (deg)	$C_{L_{av}}$	$\Delta\delta_{r_{trim}}$ (deg)	$\Delta\psi_{trim}$ (deg)
Neutral	1.7	0.3	0	-1.5
Single slotted	9.6	1.9	-6	.2
Double slotted	9.4	3.1	2	.25

The foregoing data show that the trim changes caused by power are small; thus, good control is indicated.

Effect of wing position.- Higher values of $\partial\psi/\partial\delta_r$ were obtained with the high-wing model than with the low-wing model (reference 2). This difference is explained by the fact that whereas $\partial C_n/\partial\delta_r$ is nearly the same for both high-wing and low-wing models, the low-wing model has greater stability $\left(C_{n_\psi}\right)$ due probably to favorable side-wash characteristics at the tail.

Rudder deflections required to trim the high-wing design are small; thus, good control is indicated. The results for the low-wing design, however, indicate relatively large deflections to maintain trim.

The hinge-moment parameters $C_{h_{r_\psi}}$ and $\partial C_{h_r}/\partial\delta_r$ for the low-wing and high-wing models are within reasonable agreement.

CONCLUSIONS

Tests were conducted on a high-wing powered model of a typical fighter airplane with tail on and tail off equipped with full-span single slotted flap and full-span double slotted flap to investigate the effects of power and flap deflection on the static lateral stability and control characteristics. Effect of wing position on

lateral stability and control characteristics was also investigated. The following conclusions can be drawn from the data presented.

1. Effect of power:

(a) Application of power had no effect on the effective dihedral with the flap neutral; however, with the single slotted and double slotted flap deflected, application of power decreased the effective dihedral.

(b) The application of power increased the directional stability of the complete model except with flap neutral at low lift coefficients.

(c) The application of power decreased the rudder effectiveness with the flap neutral and with the double slotted flap deflected and increased rudder effectiveness with the single slotted flap deflected.

(d) Trim changes caused by power were small; thus, good control was indicated.

2. Effect of flap deflection:

(a) Deflecting the single slotted flap decreased the effective dihedral; however, deflecting the double slotted flap increased the effective dihedral with power off and decreased the effective dihedral with power on.

(b) Deflecting the single slotted flap increased the directional stability of the complete model with both power off and power on. Deflecting the double slotted flap increased the directional stability for all tail-on conditions.

(c) Deflecting the single slotted flap increased the rudder effectiveness for the power-on condition, whereas deflecting the double slotted flap (compared with the flap-neutral configuration) decreased the rudder effectiveness.

3. Effect of tail surfaces:

(a) The effective dihedral was increased with the addition of the tail surfaces.

(b) The tail surfaces added increments of directional stability for all flap and power conditions investigated.

4. Effect of wing position:

(a) For the high-wing model greater effective dihedral was apparent than for the low-wing model when power was applied and flaps were deflected.

(b) The fin effectiveness was less on the high-wing model than on the low-wing model.

(c) The rudder effectiveness was found to be greater on the high-wing model than on the low-wing model because of less directional stability for the high-wing model.

(d) Application of power resulted in small rudder deflections required to trim on the high-wing design and large rudder deflections on the low-wing design.

Langley Memorial Aeronautical Laboratory
National Advisory Committee for Aeronautics
Langley Field, Va., May 6, 1947

REFERENCES

1. Wallace, Arthur R., Rossi, Peter F., and Wells, Evalyn G.: Wind-Tunnel Investigation of the Effect of Power and Flaps on the Static Longitudinal Stability Characteristics of a Single-Engine Low-Wing Airplane Model. NACA TN No. 1239, 1947.

2. Tamburello, Vito, and Weil, Joseph: Wind-Tunnel Investigation of the Effect of Power and Flaps on the Static Lateral Characteristics of a Single-Engine Low-Wing Airplane Model. NACA TN No. 1327, 1947.

3. Hagerman, John R.: Wind-Tunnel Investigation of the Effect of Power and Flaps on the Static Longitudinal Stability and Control Characteristics of a Single-Engine High-Wing Airplane Model. NACA TN No. 1339, 1947.

4. Harris, Thomas A.: The 7 by 10 Foot Wind Tunnel of the National Advisory Committee for Aeronautics. NACA Rep. No. 412, 1931.

5. Wenzinger, Carl J., and Harris, Thomas A.: Wind-Tunnel Investigation of an N.A.C.A. 23012 Airfoil with Various Arrangements of Slotted Flaps. NACA Rep. No. 664, 1939.

6. Harris, Thomas A., and Recant, Isidore G.: Wind-Tunnel Investigation of NACA 23012, 23021, and 23030 Airfoils Equipped with 40-Percent-Chord Double Slotted Flaps. NACA Rep. No. 723, 1941.

7. Tucker, Warren A.: Wind-Tunnel Investigation of Effect of Wing Location, Power, and Flap Deflection on Effective Dihedral of a Typical Single-Engine Fighter-Airplane Model with Tail Removed. NACA TN No. 1061, 1946.

8. House, Rufus O., and Wallace, Arthur R.: Wind-Tunnel Investigation of Effect of Interference on Lateral-Stability Characteristics of Four NACA 23012 Wings, an Elliptical and a Circular Fuselage, and Vertical Fins. NACA Rep. No. 705, 1941.

9. Pass, H. R.: Analysis of Wind-Tunnel Data on Directional Stability and Control. NACA TN No. 775, 1940.

TABLE I

SUMMARY OF RUDDER-CONTROL AND HINGE-MOMENT PARAMETERS

Flap	Power	α (deg)	C_L	$C_{n_{\delta_r}}$	C_{n_ψ}	C_{n_ψ} (Tail off)	$\frac{\partial \psi}{\partial \delta_r}$	$C_{h_{r_\psi}}$	$\frac{\partial C_{h_r}}{\partial \delta_r}$
Neutral	Windmilling	1.7	0.3	-0.0011	-0.0011	0.0007	-0.85	-0.0014	-0.0058
Single slotted	Windmilling	9.6	1.9	-.0011	-.0012	.0004	-.85	-.0014	-.0062
Double slotted	Windmilling	9.4	2.8	-.0010	-.0011	-.0003	-.67	-.0005	-.0055
Neutral	Constant power	1.7	.3	-.0012	-.0011	.0007	-.78	-.0009	-.0075
Single slotted	Constant power	9.6	1.9	-.0018	-.0020	.0008	-.90	-.0043	-.0110
Double slotted	Constant power	9.4	3.1	-.0015	-.0035	.0009	-.37	-.0170	-.0108

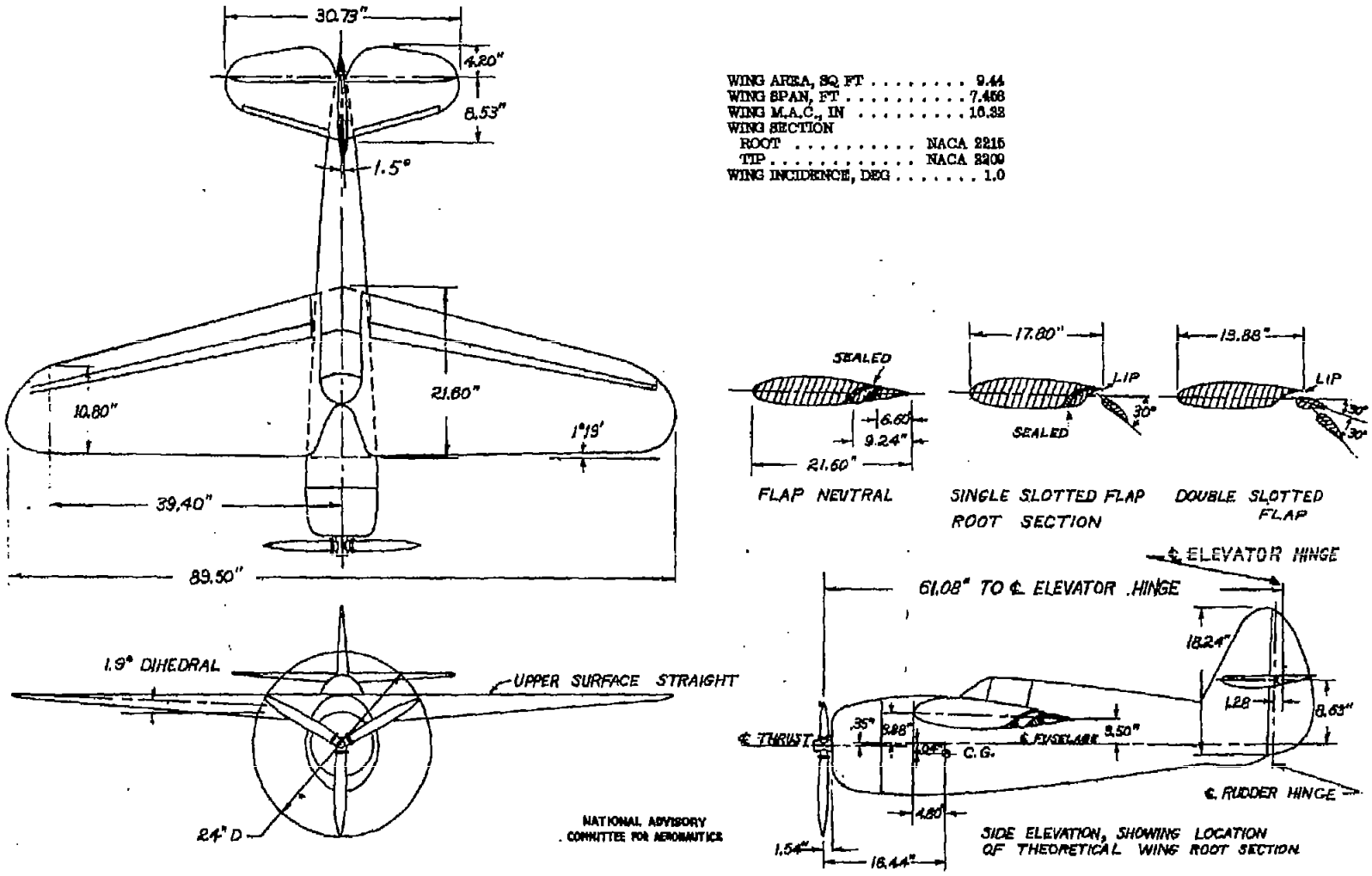

Figure 1.- Three-view drawing of the $\frac{1}{5}$-scale model as a single-engine high-wing airplane.

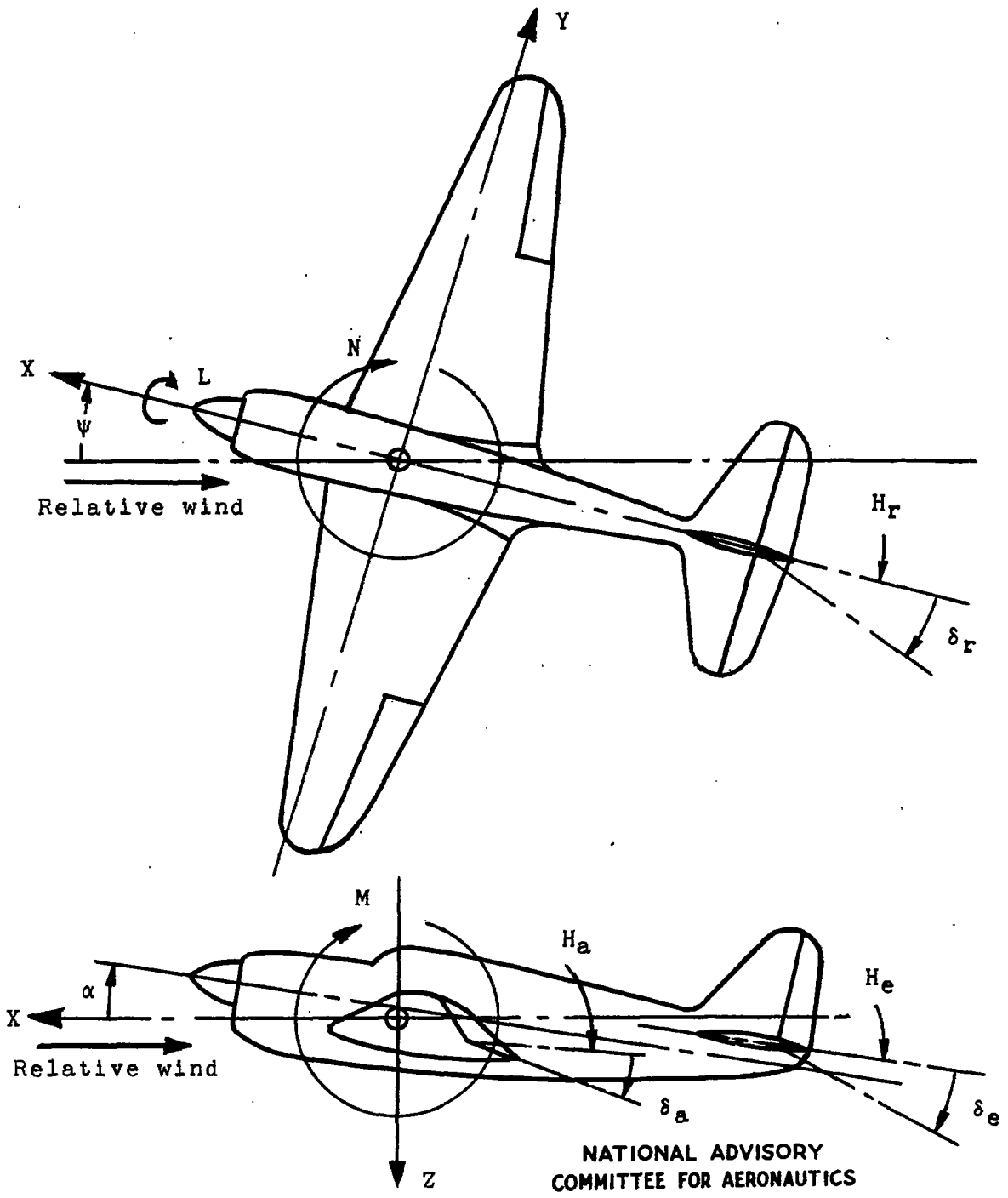

Figure 2.- System of axes and control-surface hinge moments and deflections. Positive values of forces, moments, and angles are indicated by arrows. Positive values of tab hinge moments and deflections are in the same directions as the positive values for the control surfaces to which the tabs are attached.

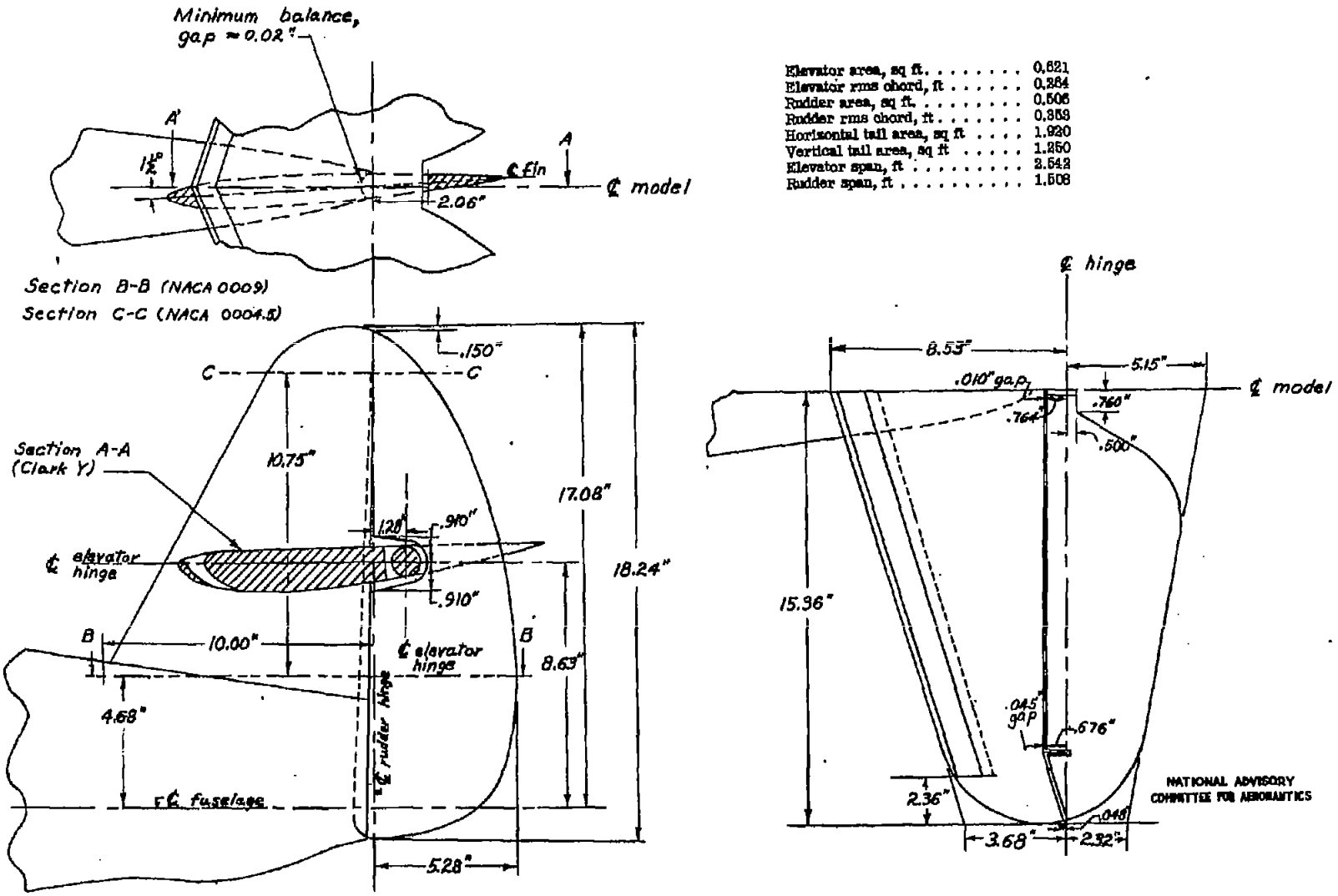

Figure 3.- Details and dimensions of the vertical and horizontal tails.

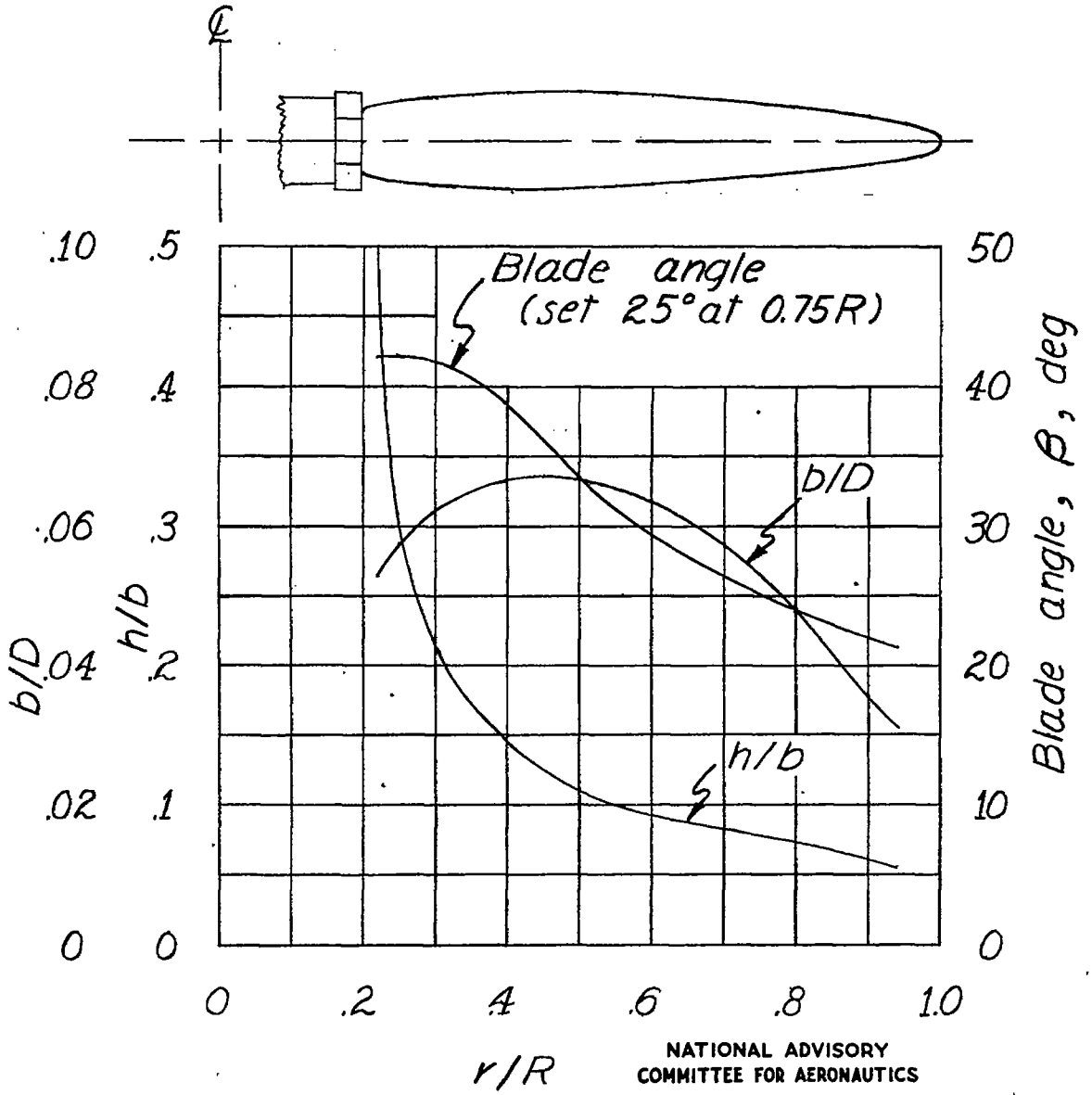

Figure 4.-Plan-form and blade-form curves for the model propeller. D, diameter; R, radius to tip; r, station radius; b, section chord; h, section thickness; RAF 6 airfoil section.

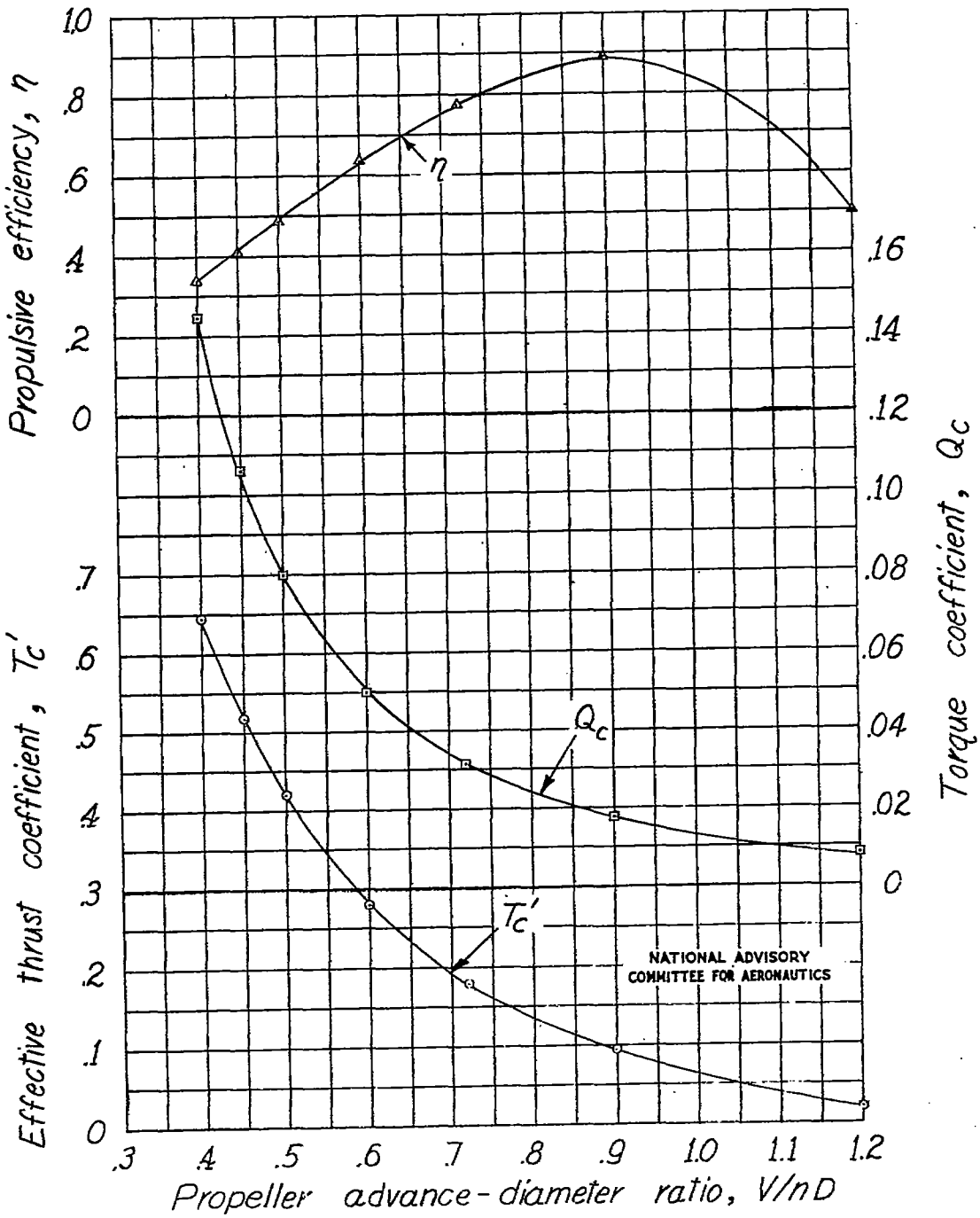

Figure 5.- Effective thrust coefficient, torque coefficient, and efficiency as functions of propeller advance-diameter ratio for the model as a high-wing airplane. $D = 2.0$ feet; $\beta = 25°$.

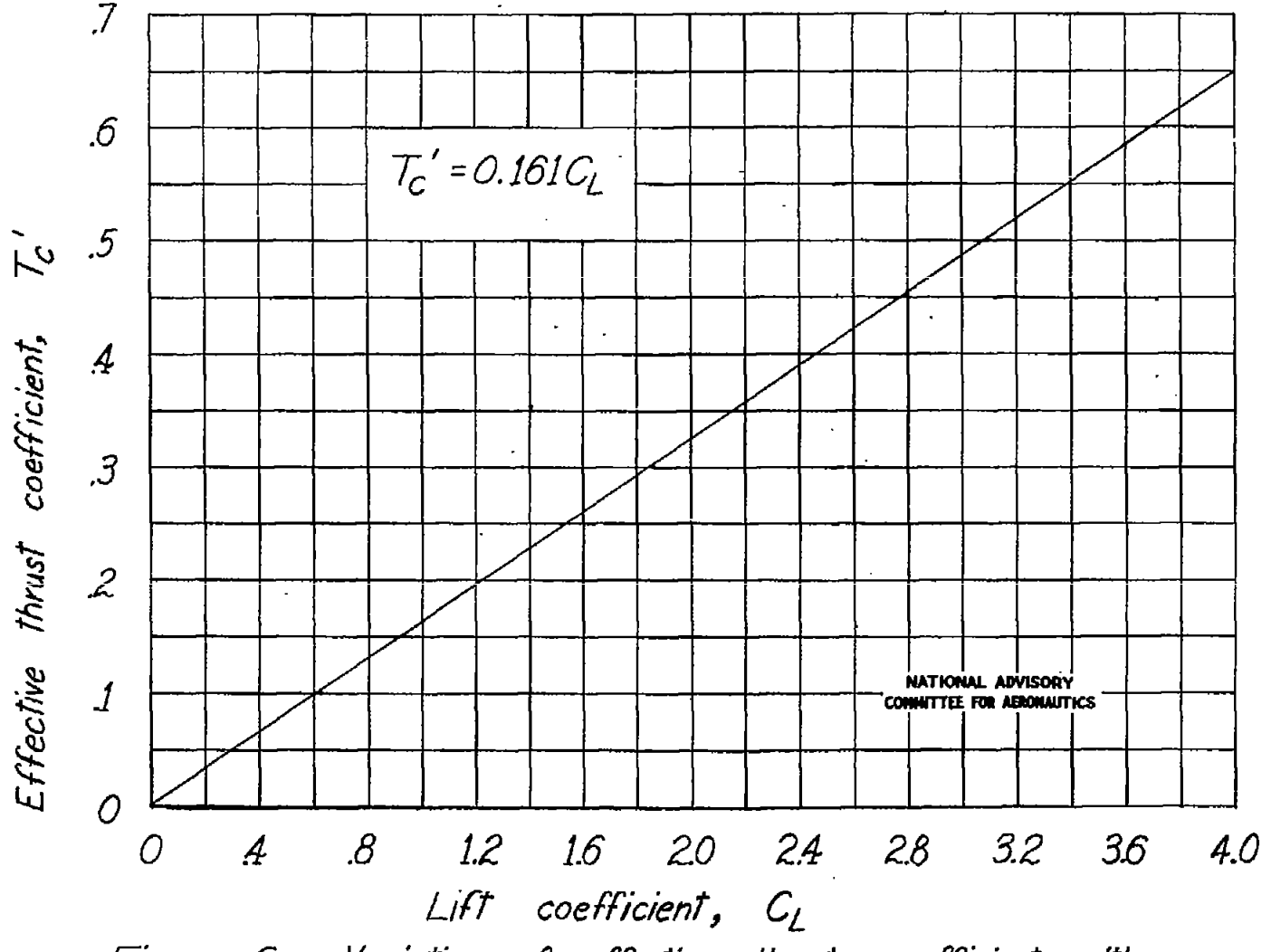

Figure 6.- Variation of effective thrust coefficient with lift coefficient for power-on tests.

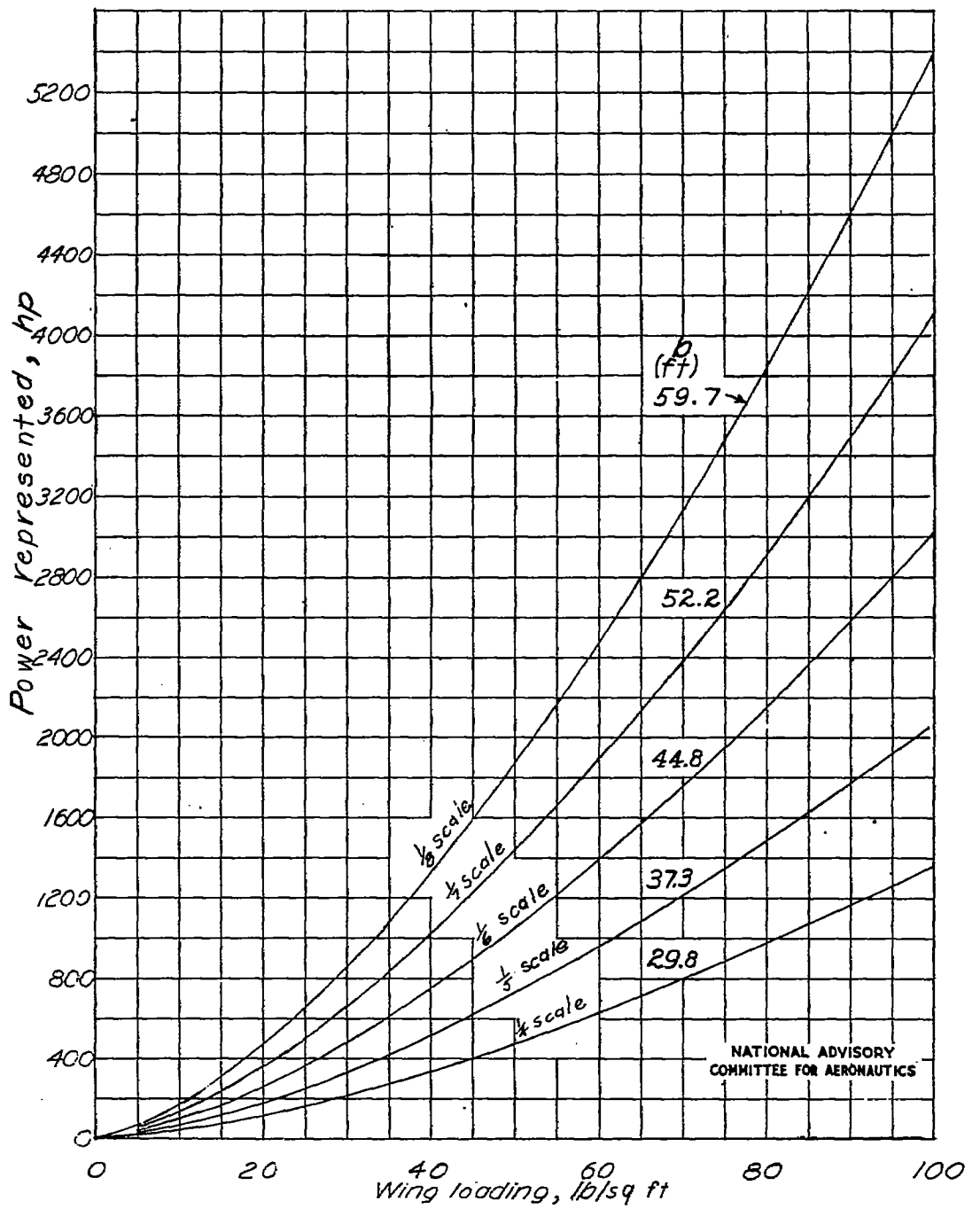

Figure 7.- Variation of approximate horsepower represented with airplane wing loading for various model scales.

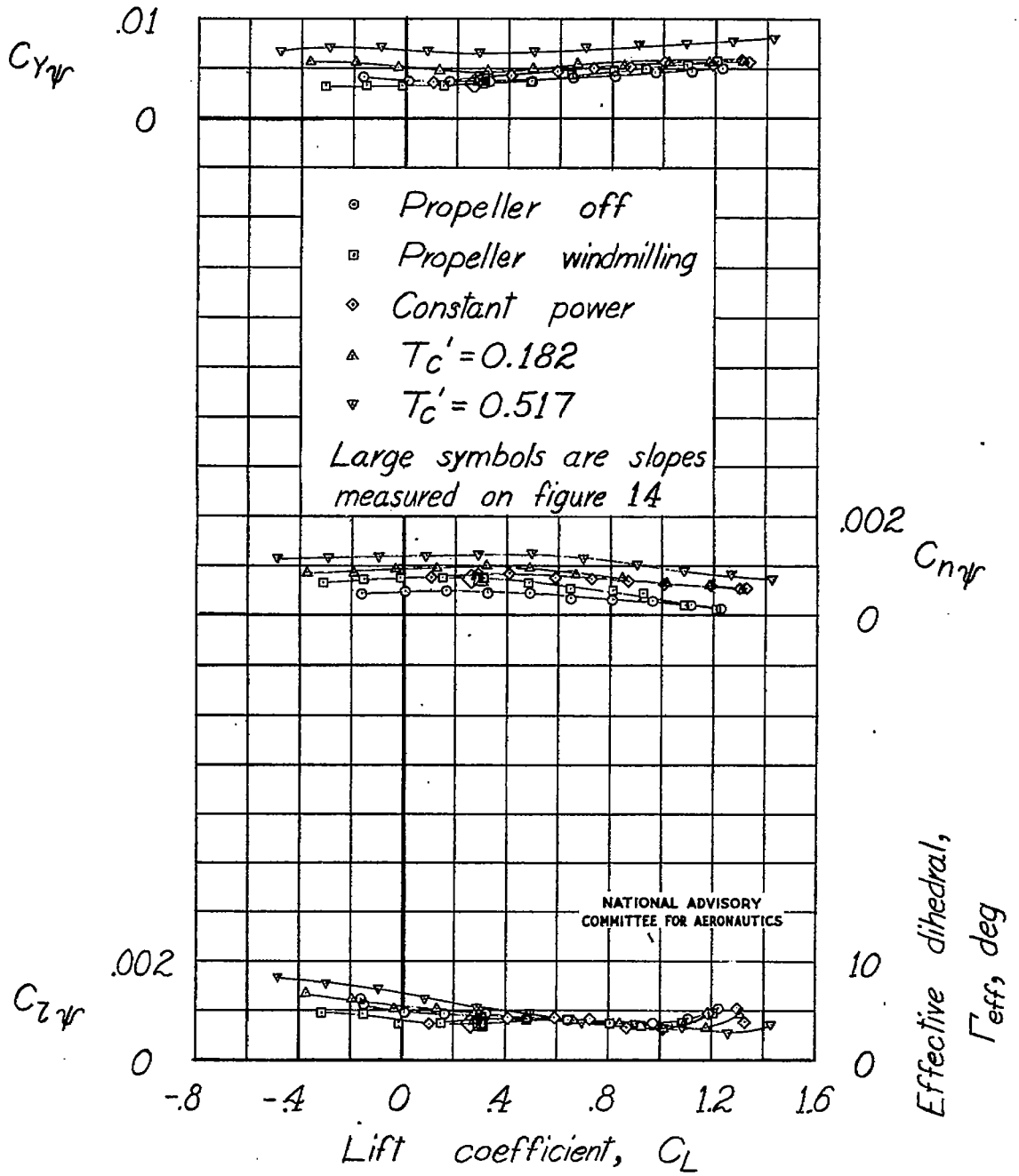

(a) Tail off.

Figure 8.- Effect of power on the variation of C_{l_ψ}, C_{n_ψ}, and C_{Y_ψ} with lift coefficient for the model as a single-engine high-wing airplane with flap neutral.

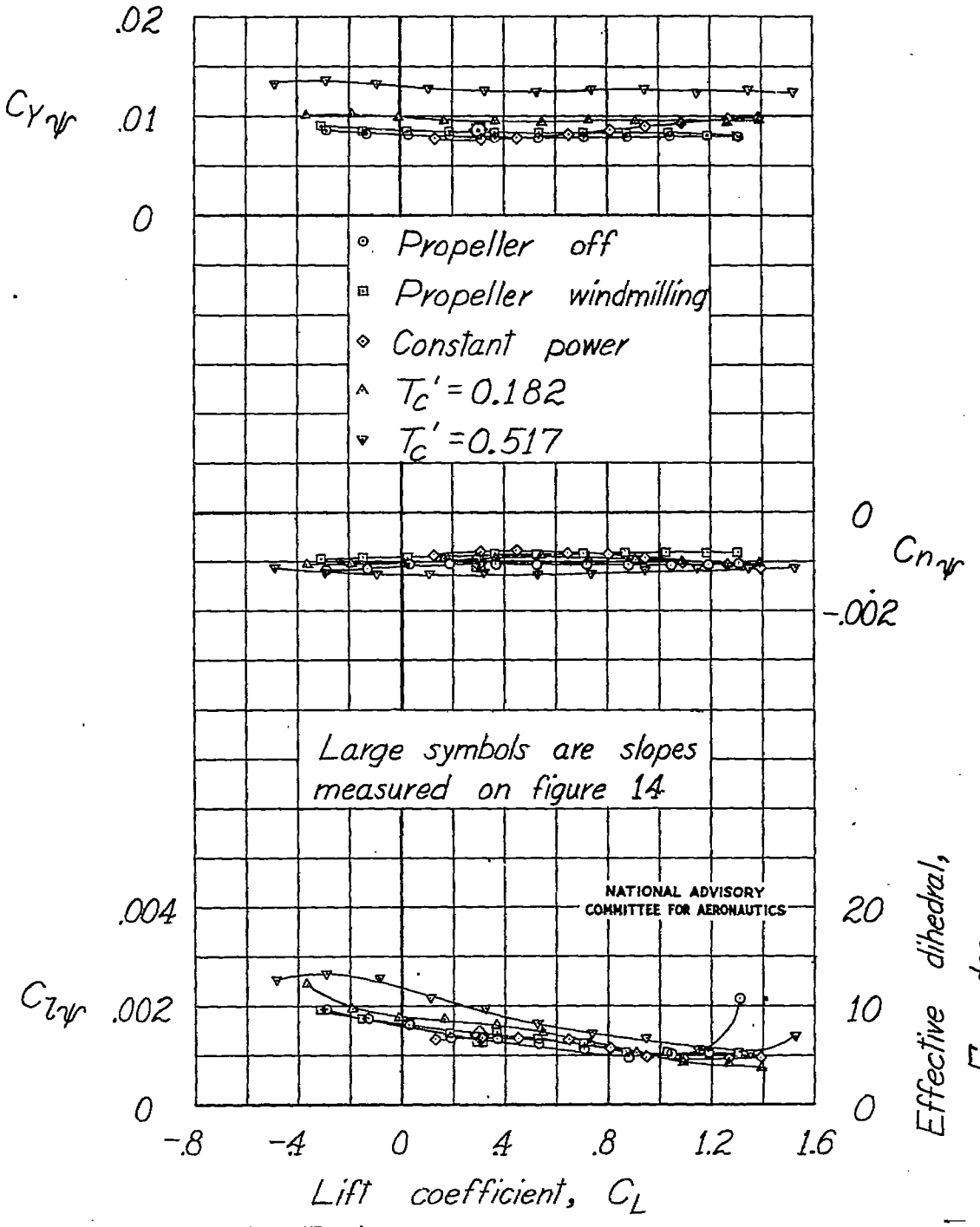

(b) Tail on.

Figure 8.- Concluded.

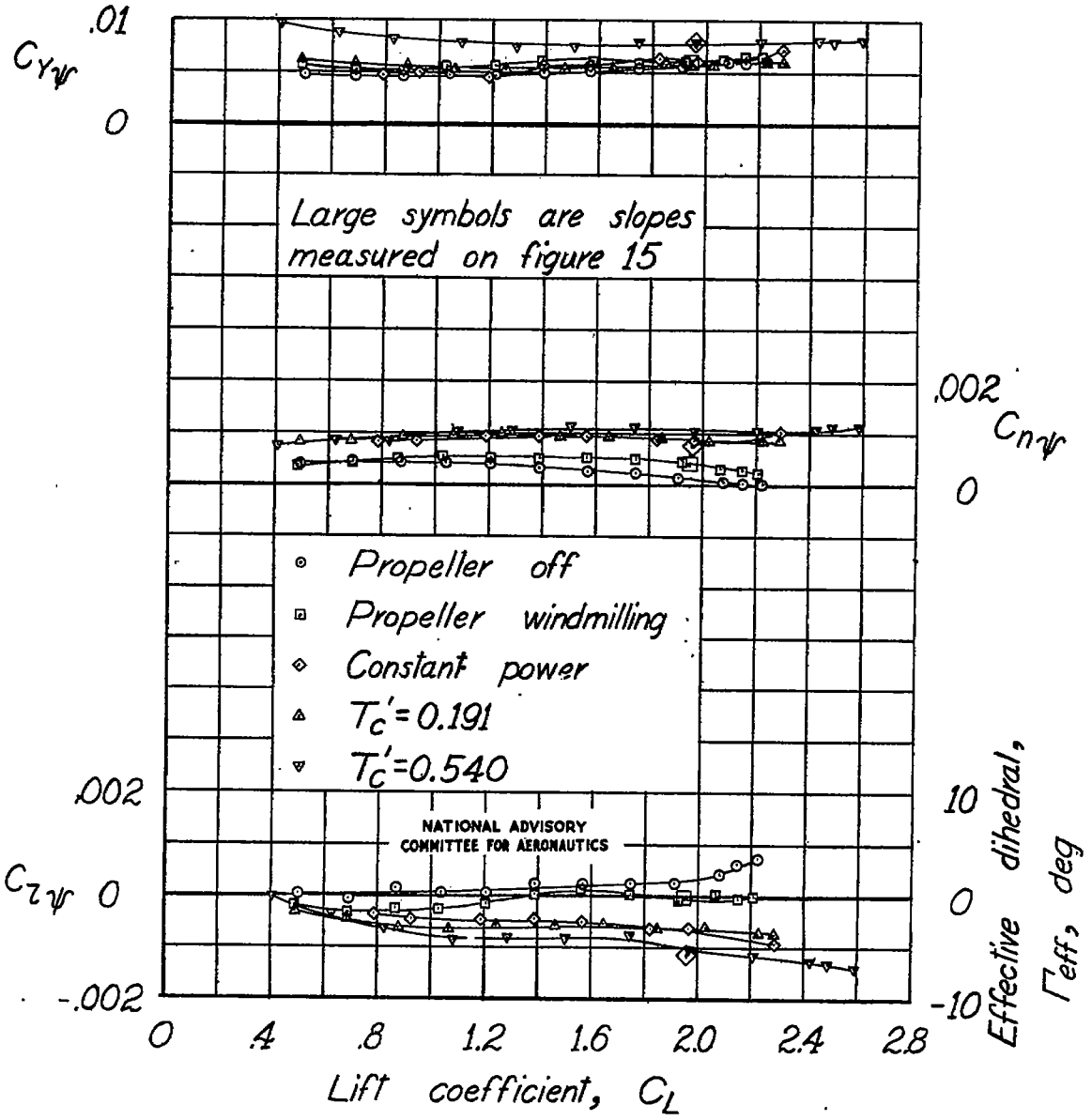

(a) Tail off.

Figure 9.-Effect of power on the variation of C_{l_ψ}, C_{n_ψ}, and C_{Y_ψ} with lift coefficient for the model as a single-engine high-wing airplane with a full-span single slotted flap.

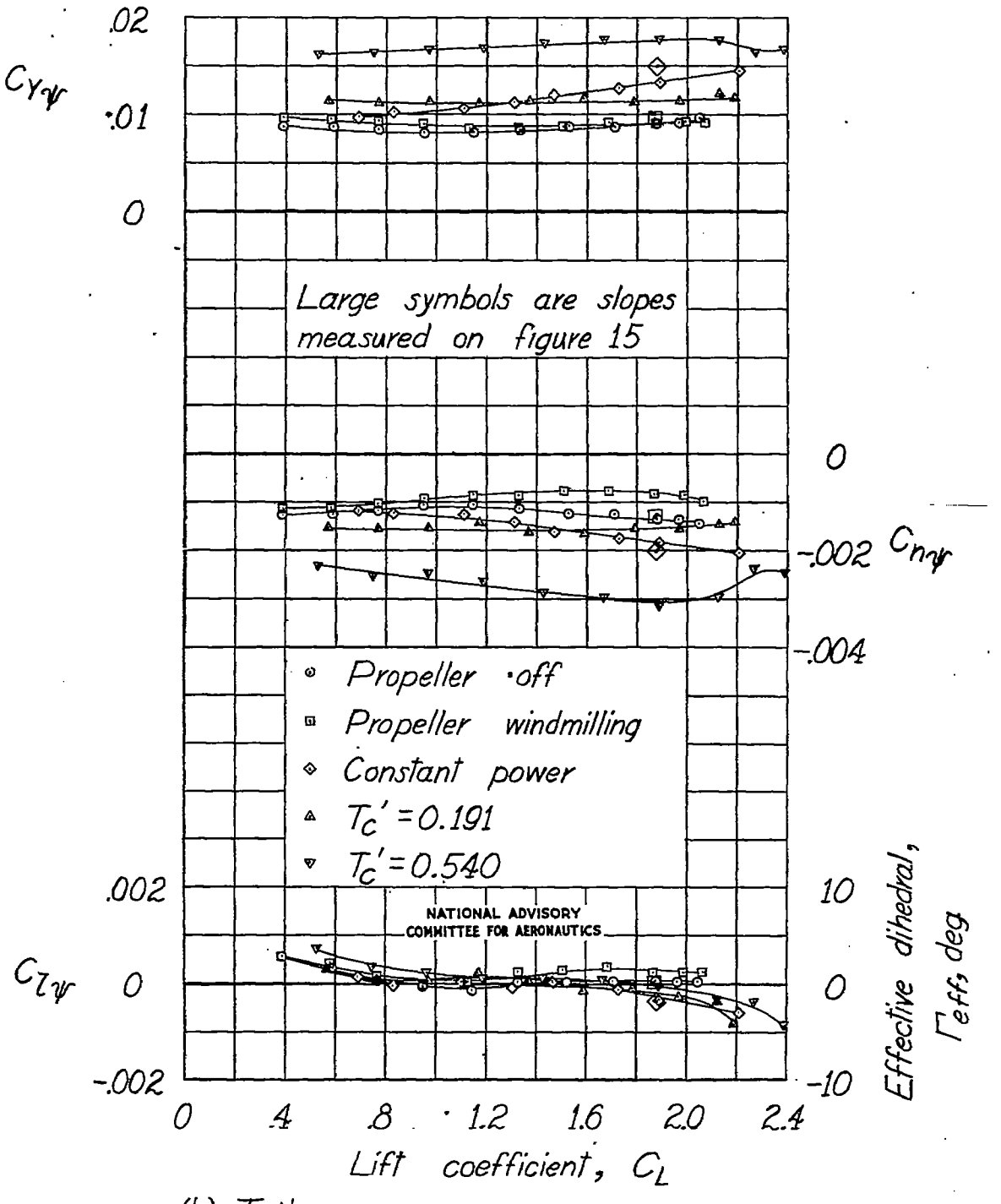

(b) Tail on.

Figure 9.– Concluded.

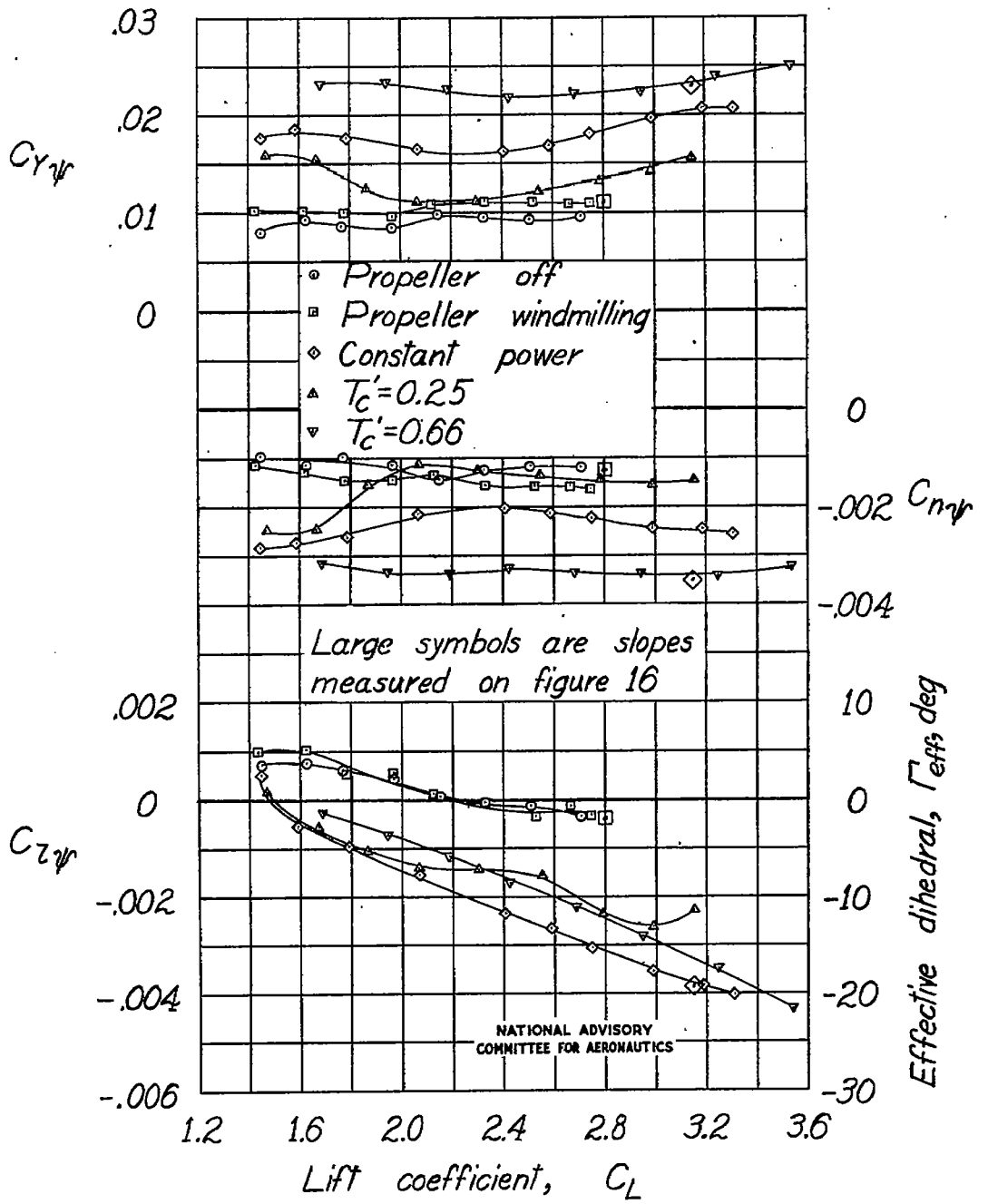

Figure 10.-Effect of power on the variation of C_{l_ψ}, C_{n_ψ}, and C_{Y_ψ} with lift coefficient for the model as a single-engine high-wing airplane with a full-span double slotted flap. Tail on.

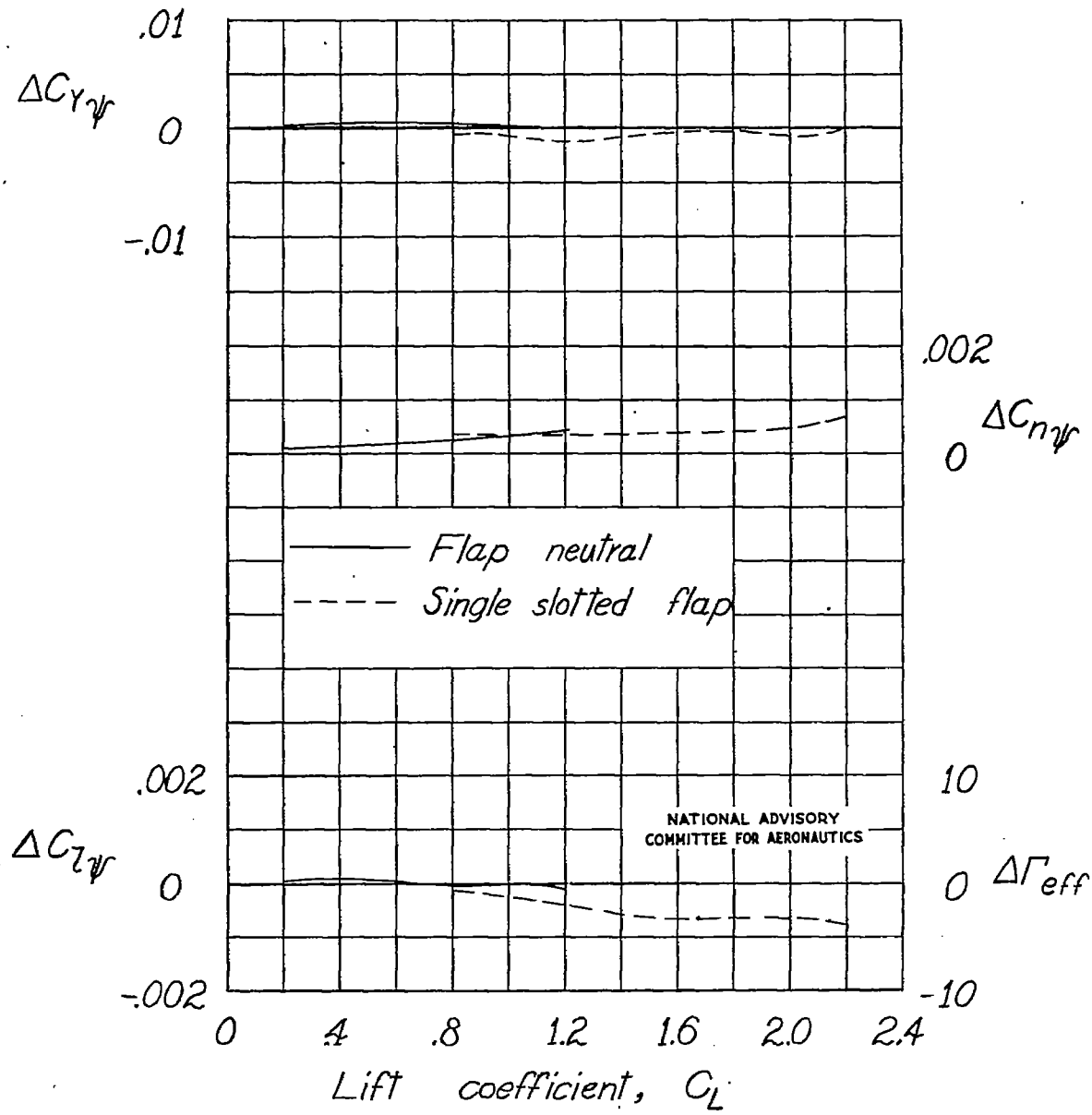

(a) Tail off.

Figure 11.- Increments in C_{l_ψ}, C_{n_ψ}, and C_{Y_ψ} resulting from power (constant power minus propeller windmilling) for the model as a single-engine high-wing airplane.

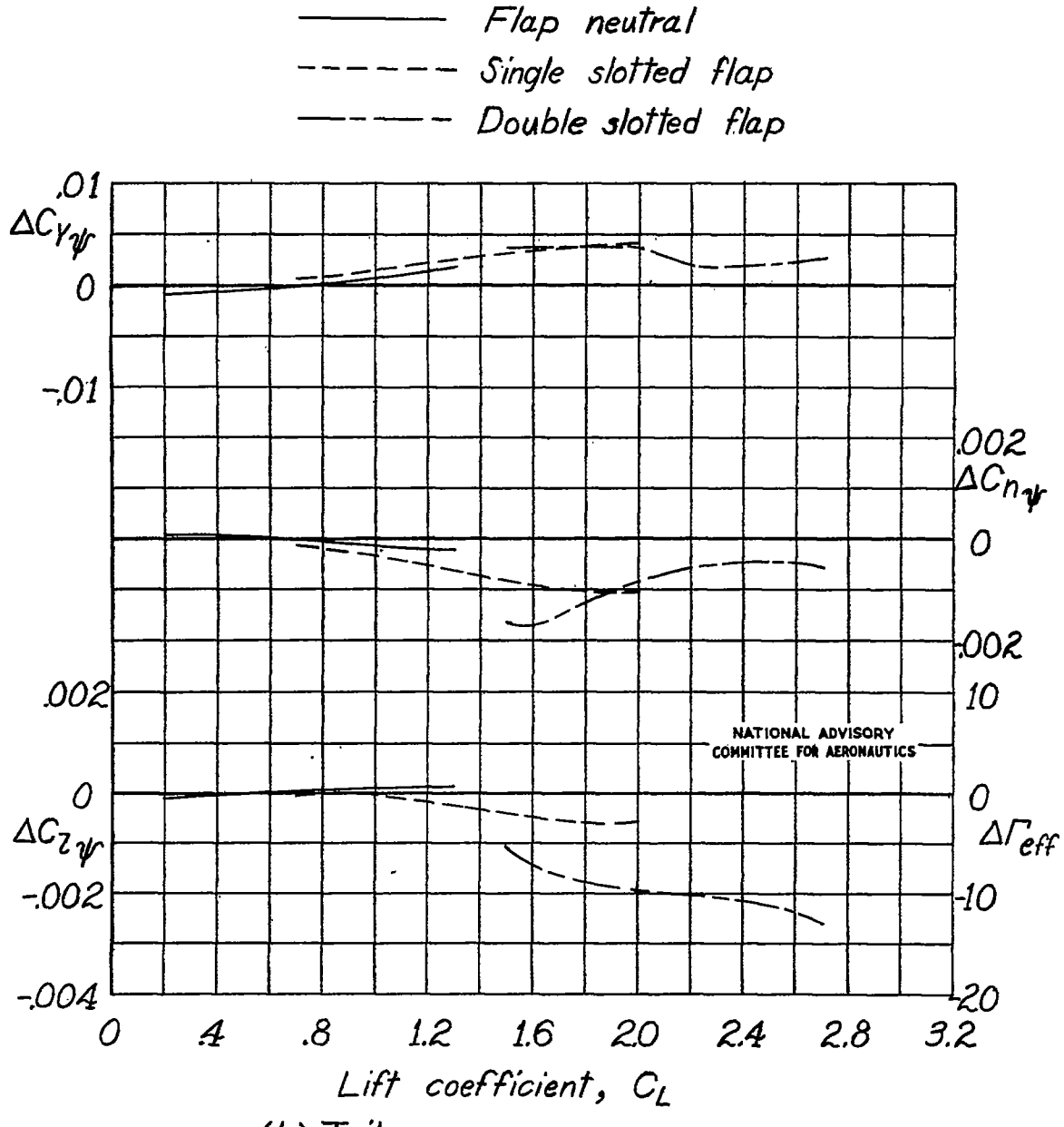

(b) Tail on.

Figure 11.- Concluded.

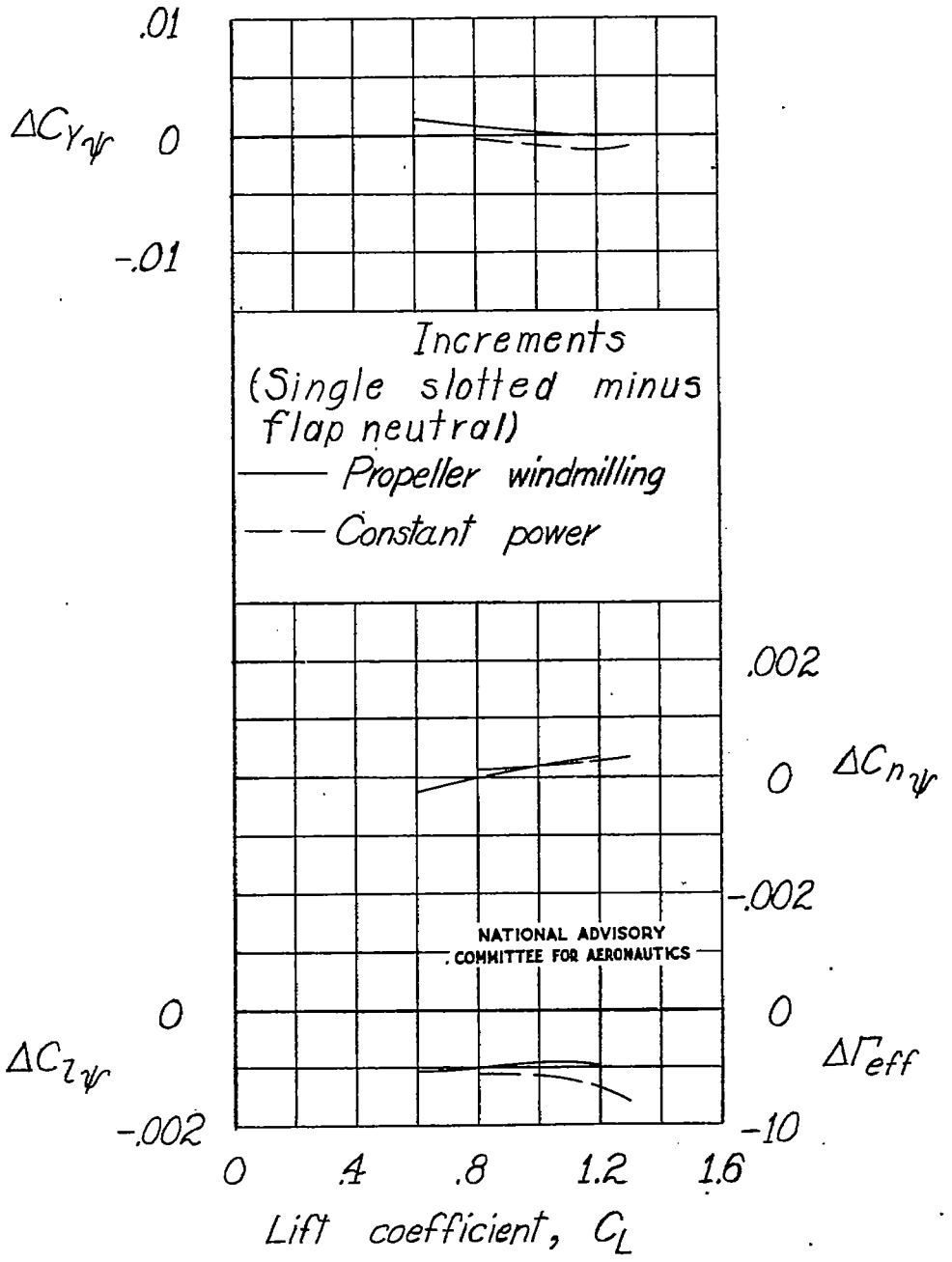

(a) Tail off.

Figure 12.–Increments in C_{l_ψ}, C_{n_ψ}, and C_{Y_ψ} resulting from flap deflection for the model as a single-engine high-wing airplane.

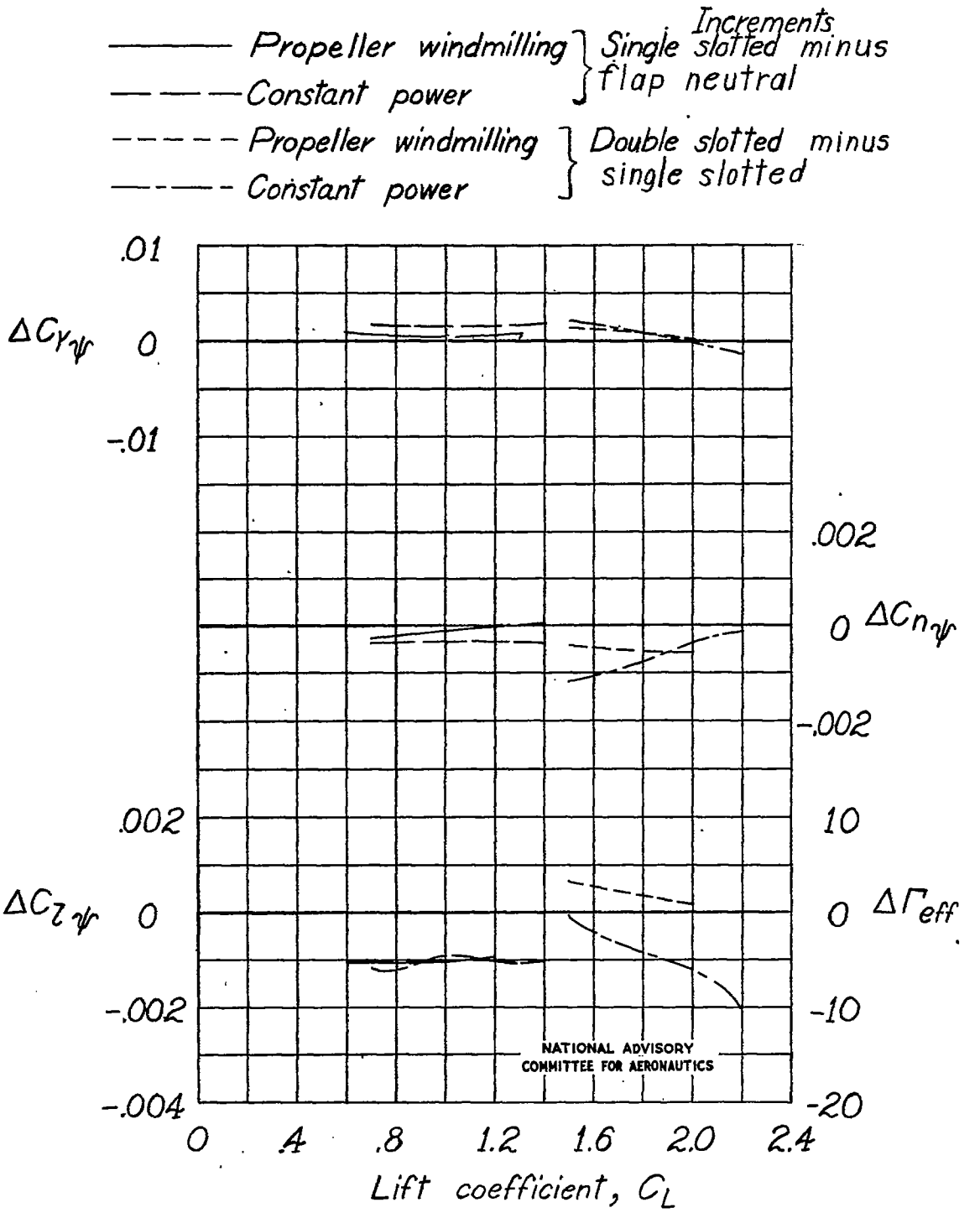

(b) Tail on.

Figure 12.- Concluded.

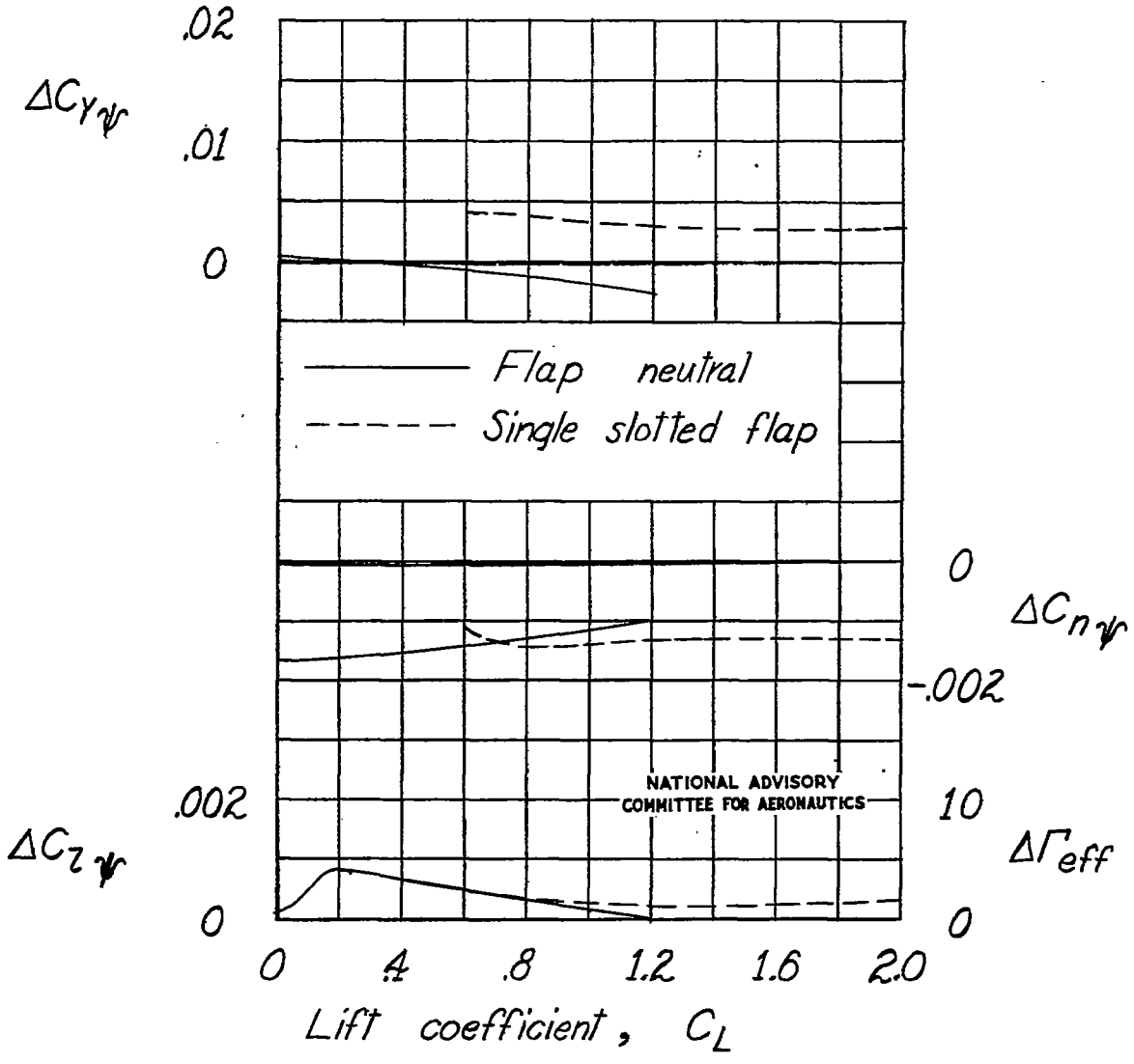

(a) Propeller windmilling.

Figure 13.- Increments in C_{l_ψ}, C_{n_ψ}, and C_{Y_ψ} contributed by the tail surfaces for the model as a single-engine high-wing airplane.

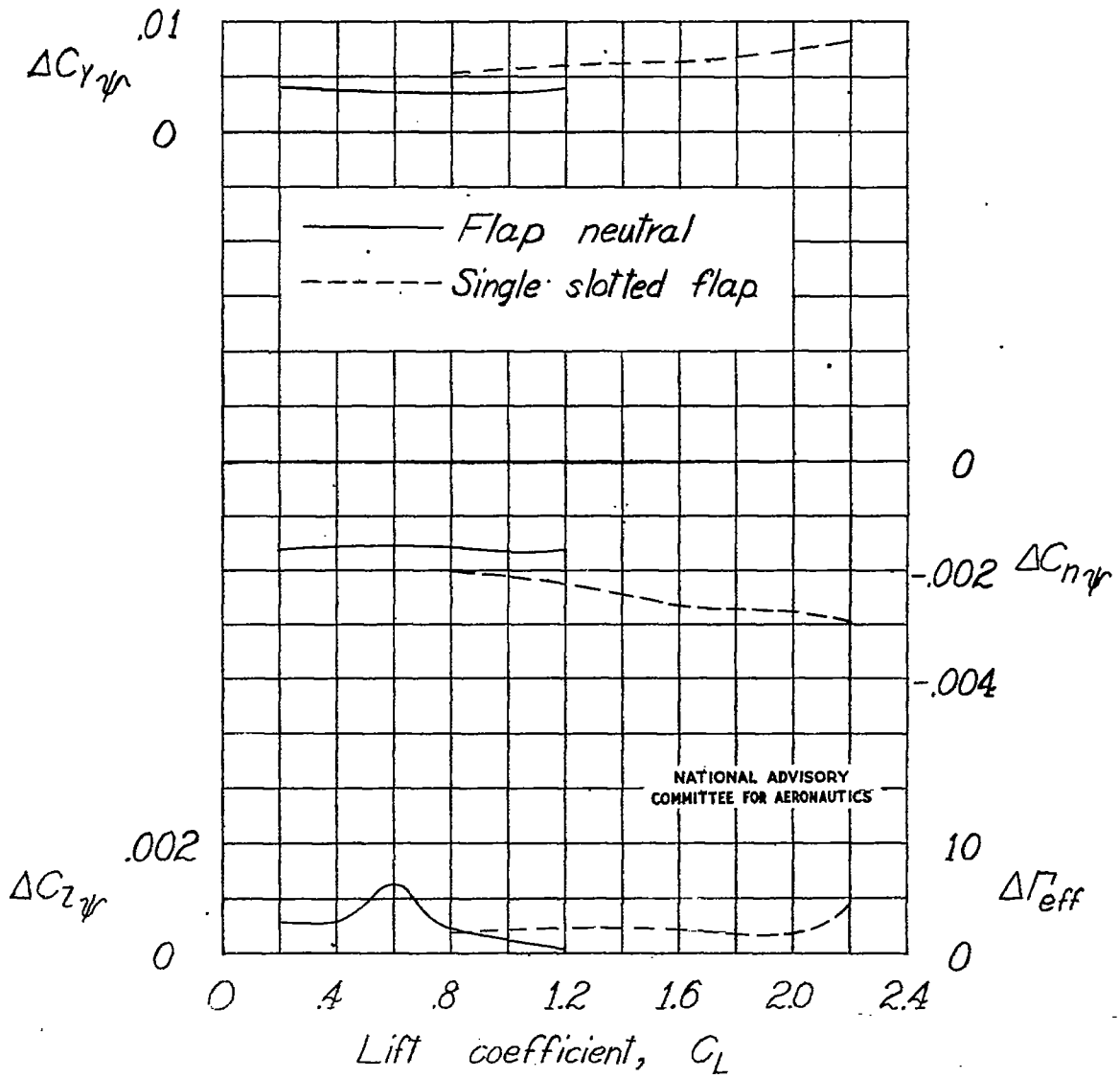

(b) Constant power.

Figure 13.- Concluded.

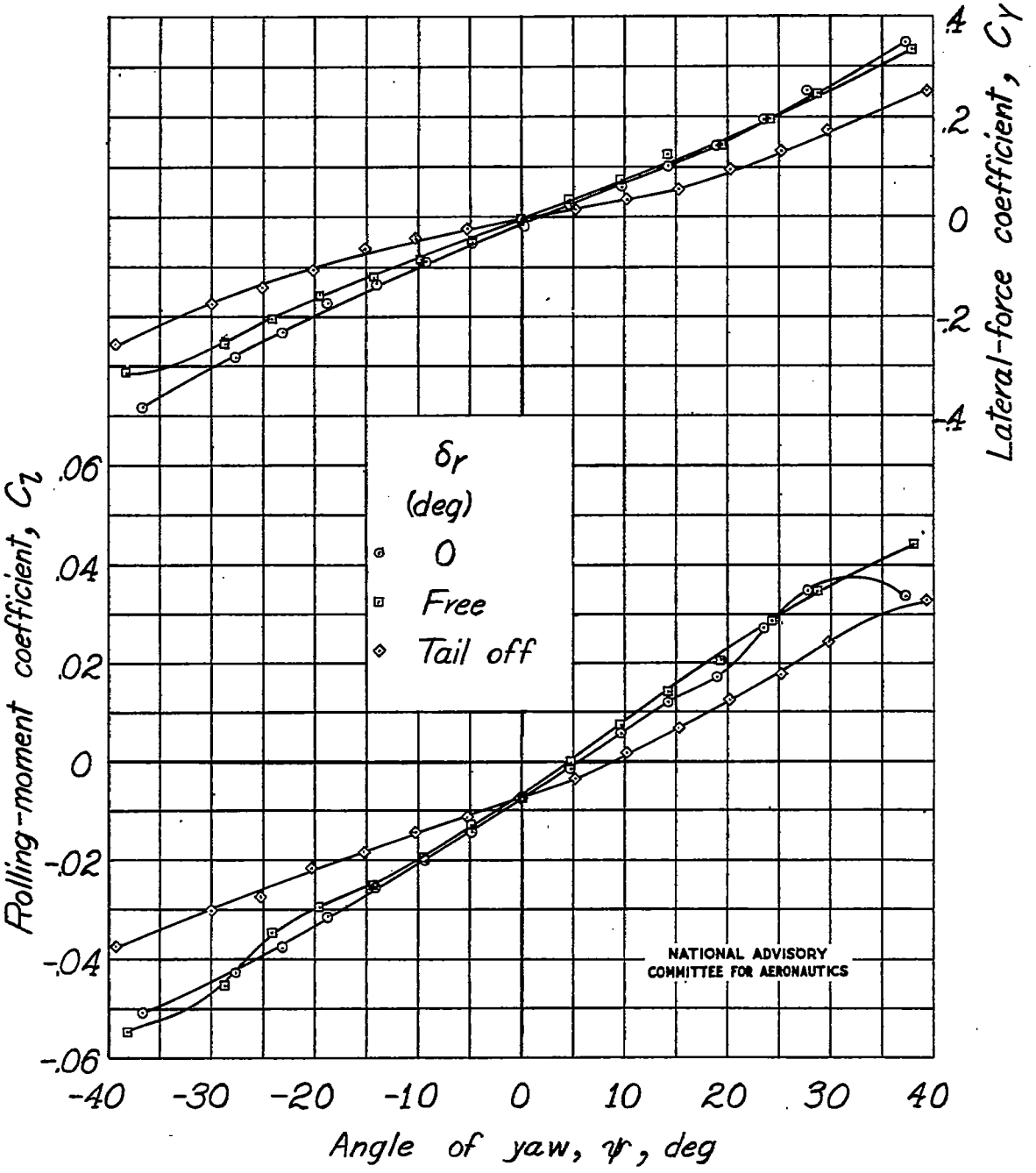

(a) Propeller windmilling.

Figure 14.- Aerodynamic characteristics in yaw of the model as a single-engine high-wing airplane with flap neutral. $\alpha \approx 1.7°$

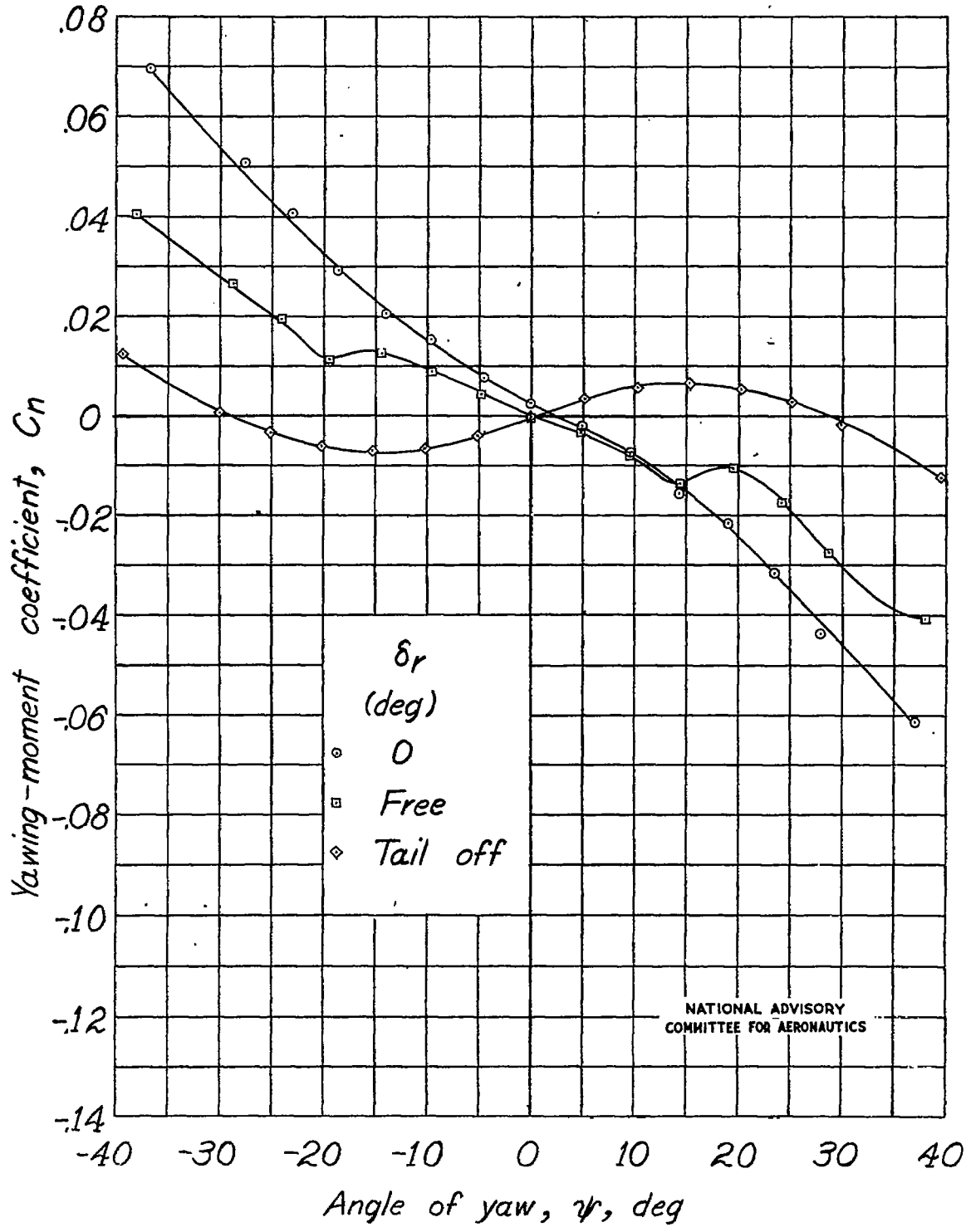

(a) Continued.

Figure 14.- Continued.

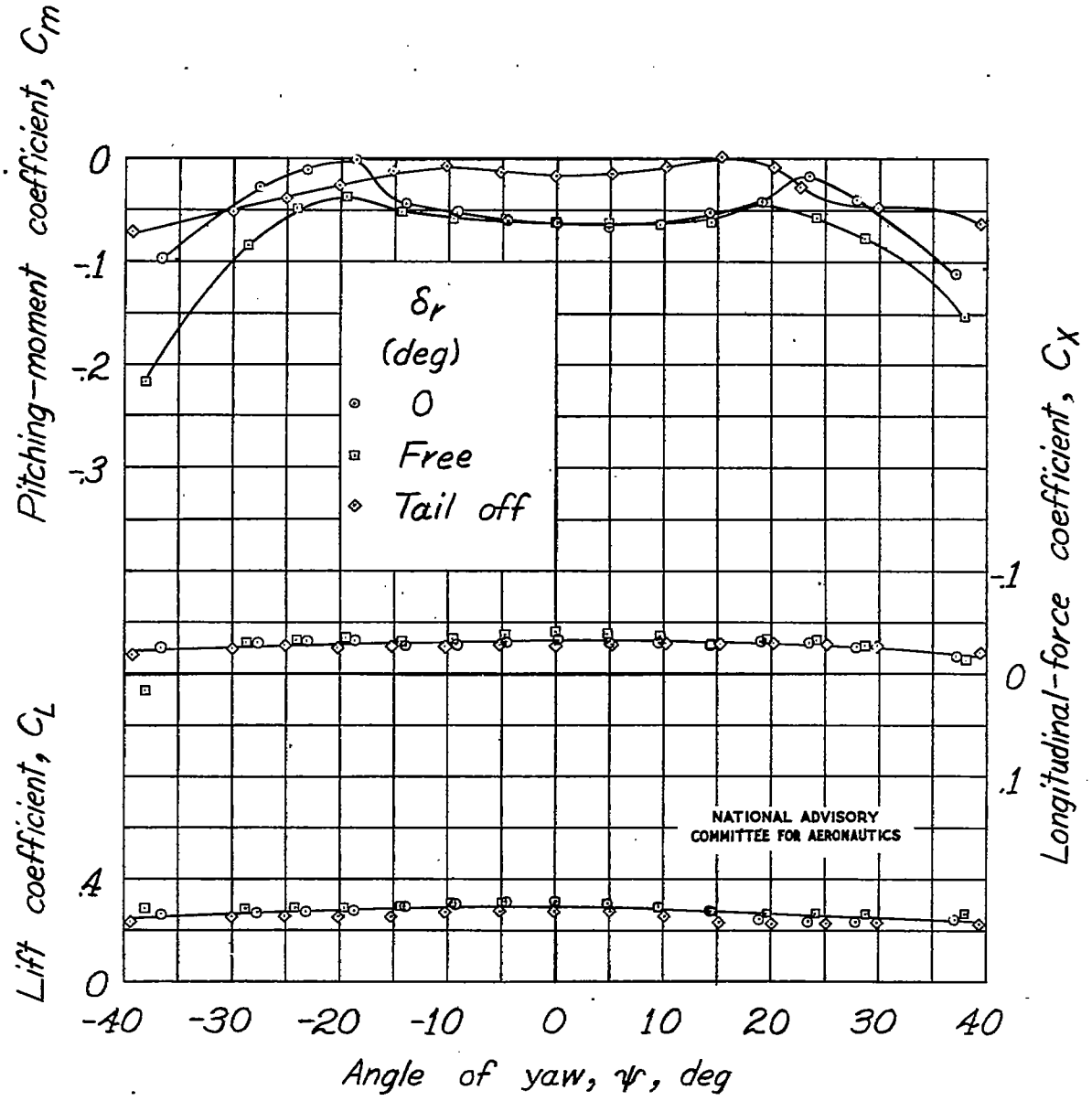

(a) Concluded.

Figure 14.- Continued.

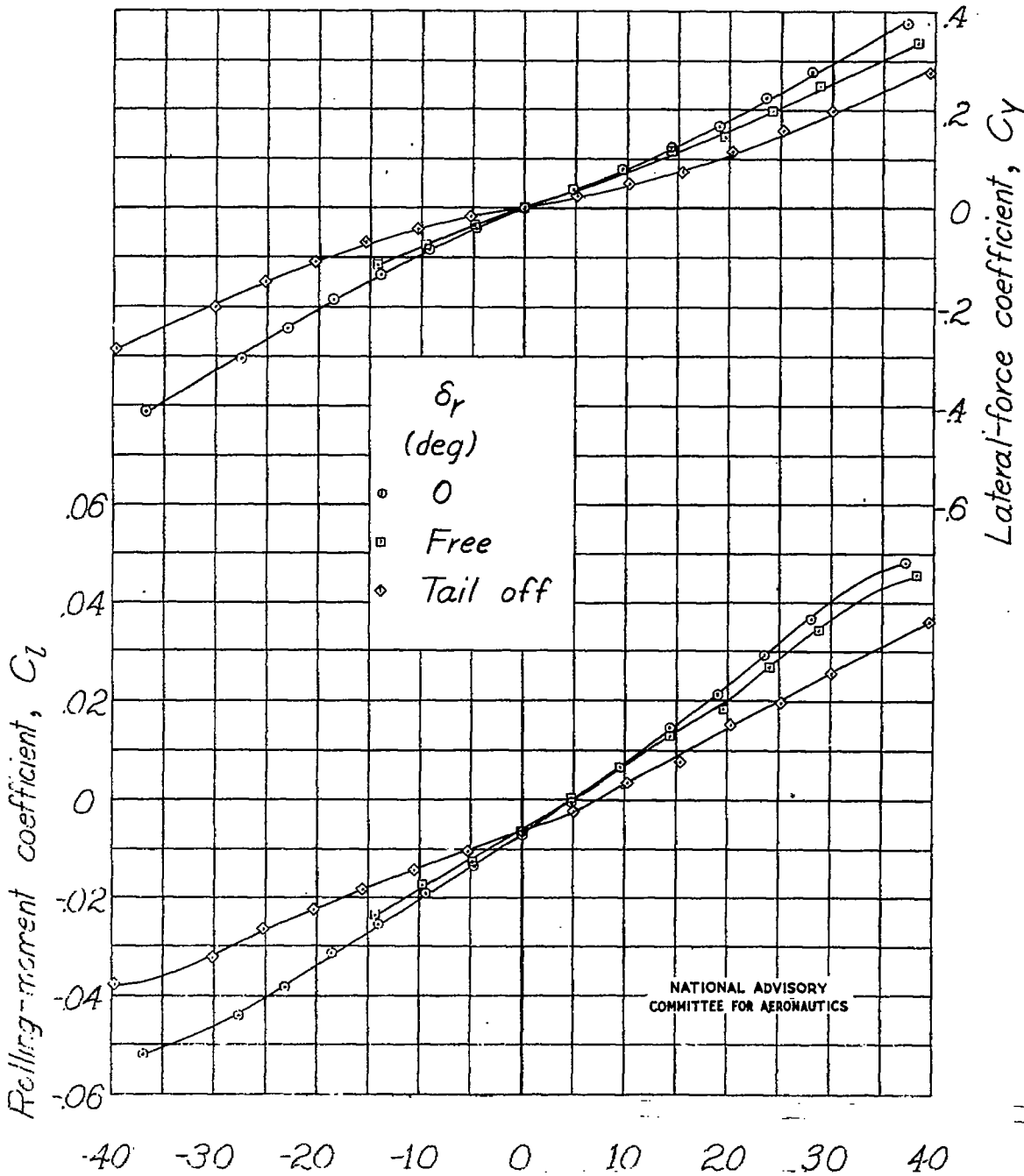

(b) Constant power.

Figure 14.-Continued.

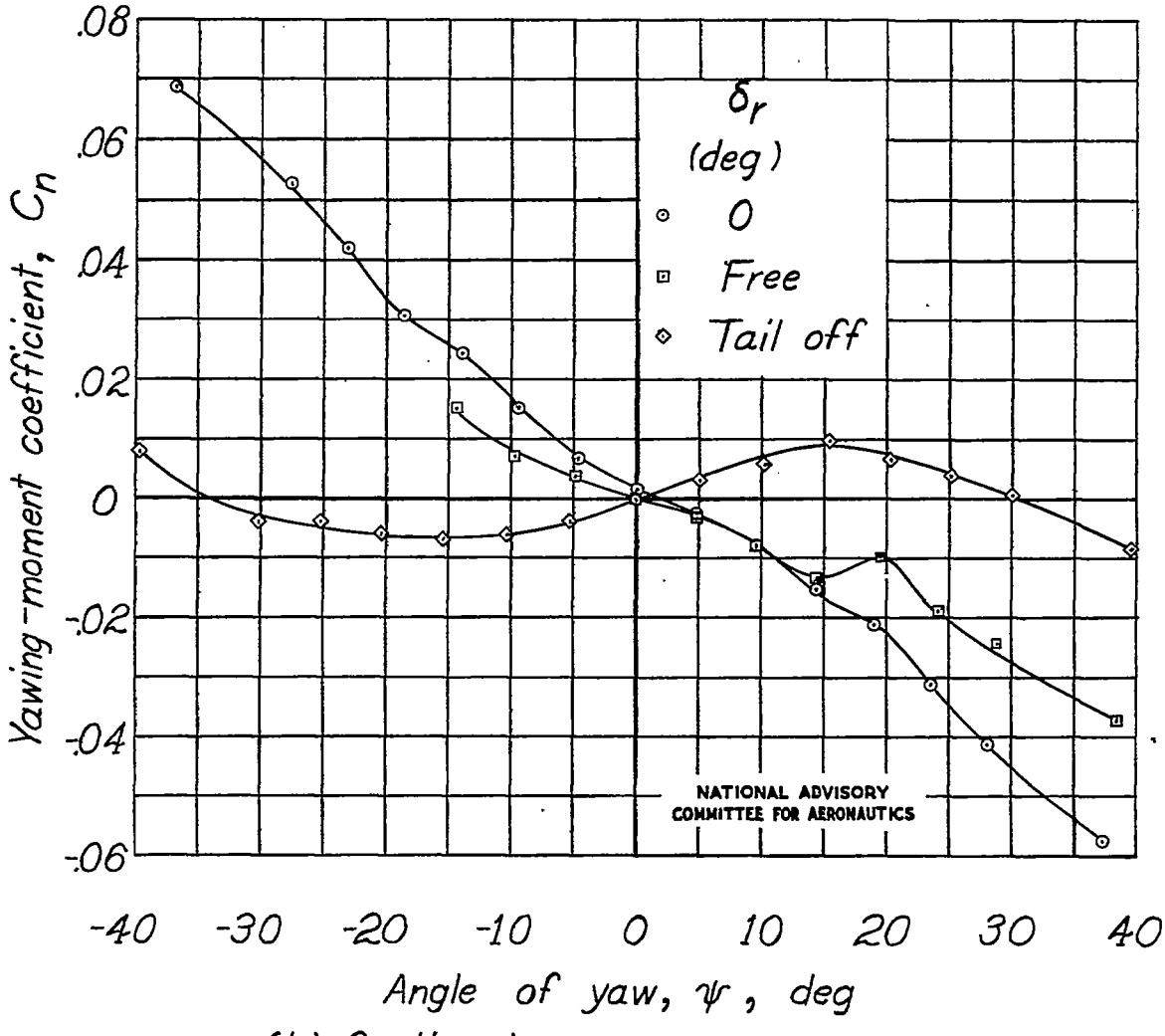

(b) Continued.

Figure 14.- Continued.

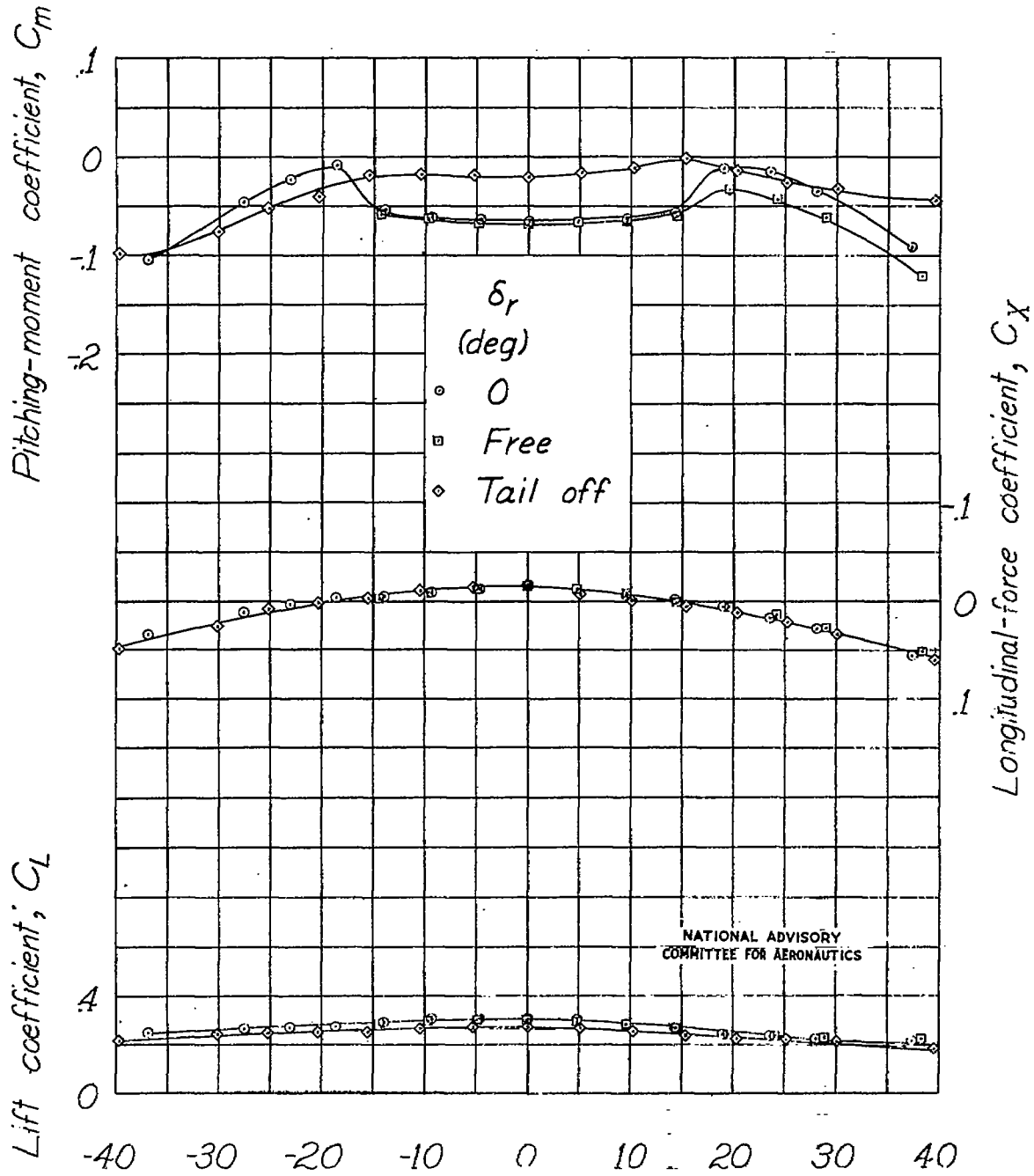

(b) Concluded.

Figure 14.—Concluded.

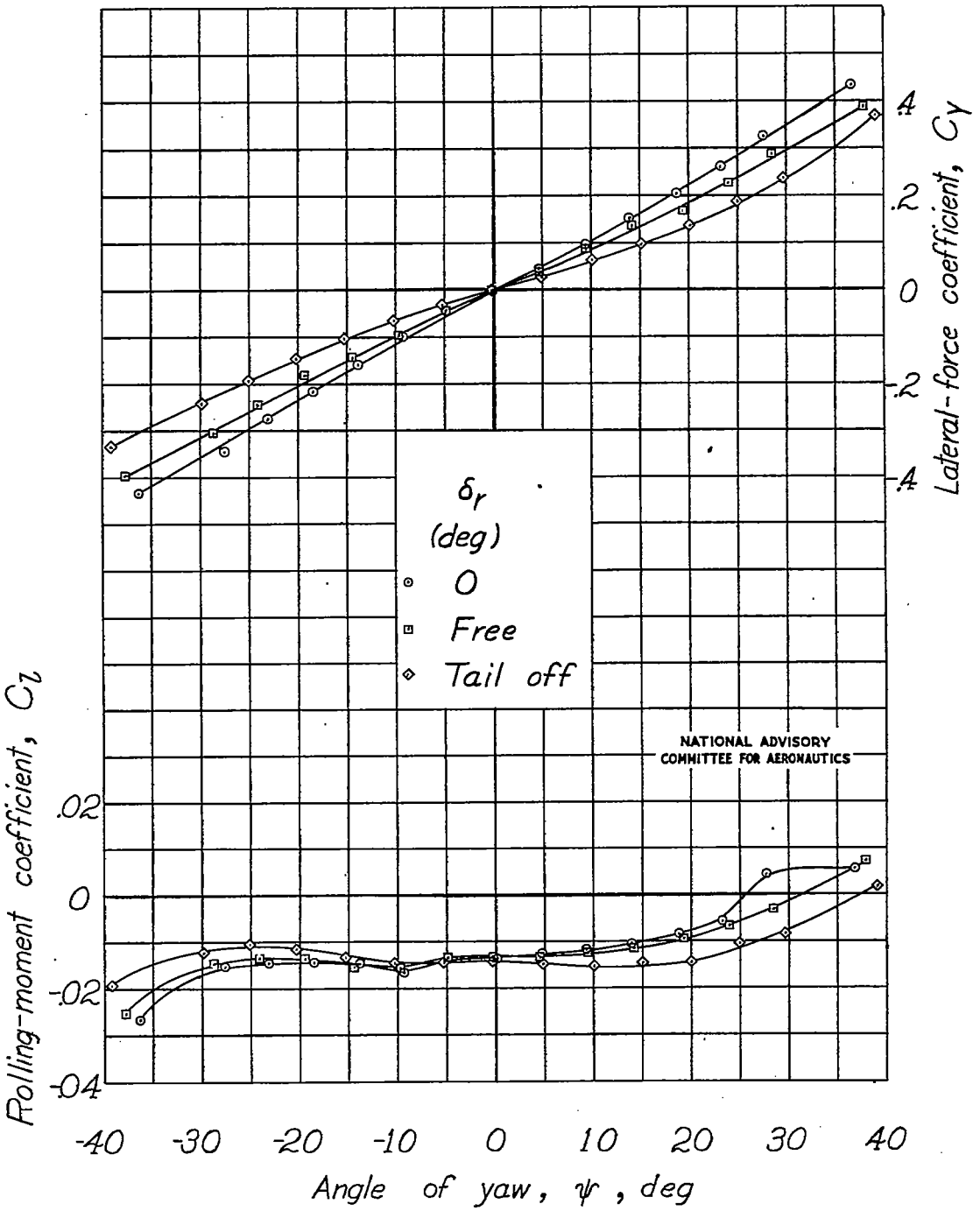

(a) Propeller windmilling.

Figure 15.- Aerodynamic characteristics in yaw of the model as a single-engine high-wing airplane with the full-span single slotted flap. $\alpha \approx 9.6°$.

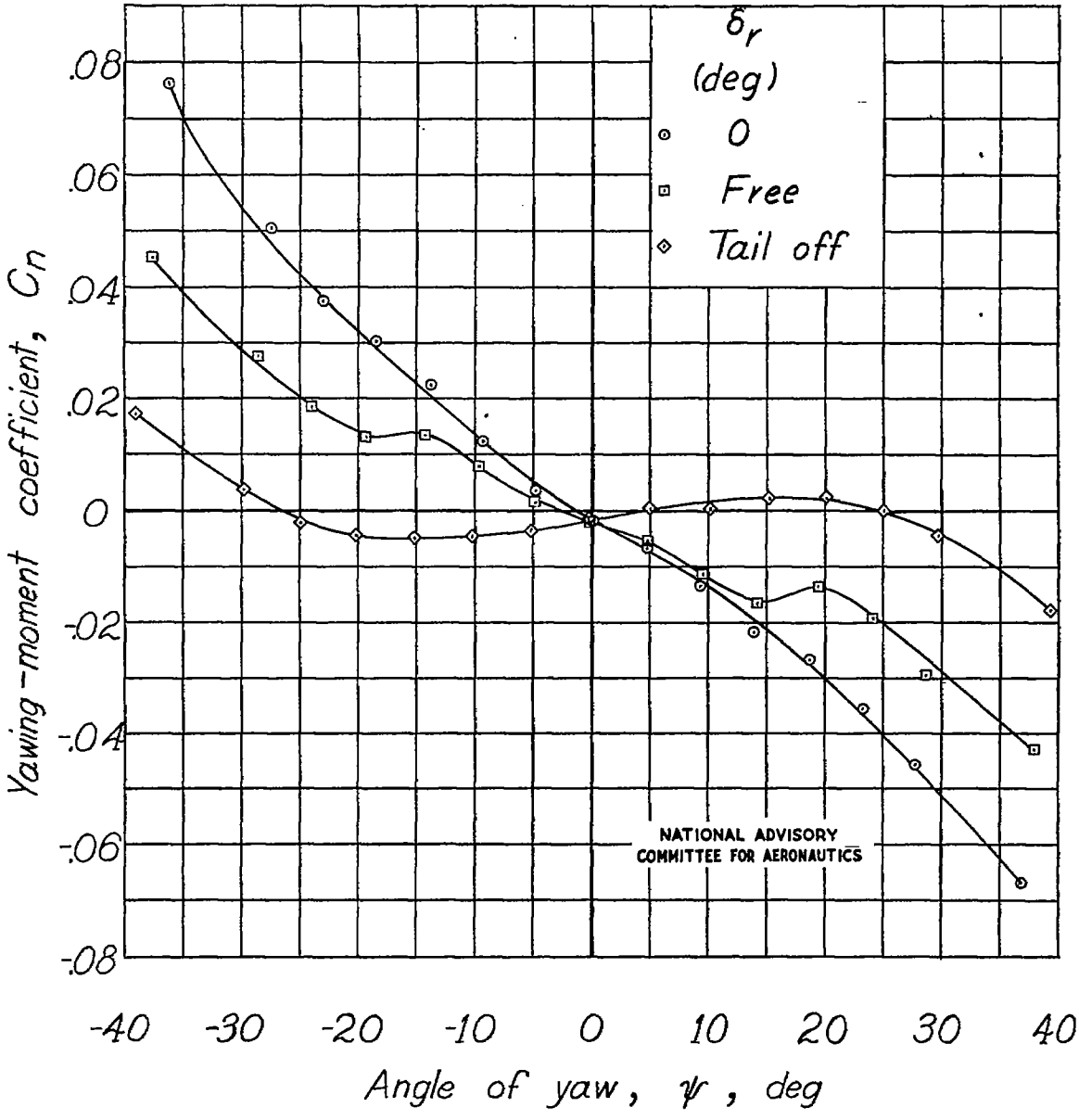

(a) Continued.

Figure 15.-Continued.

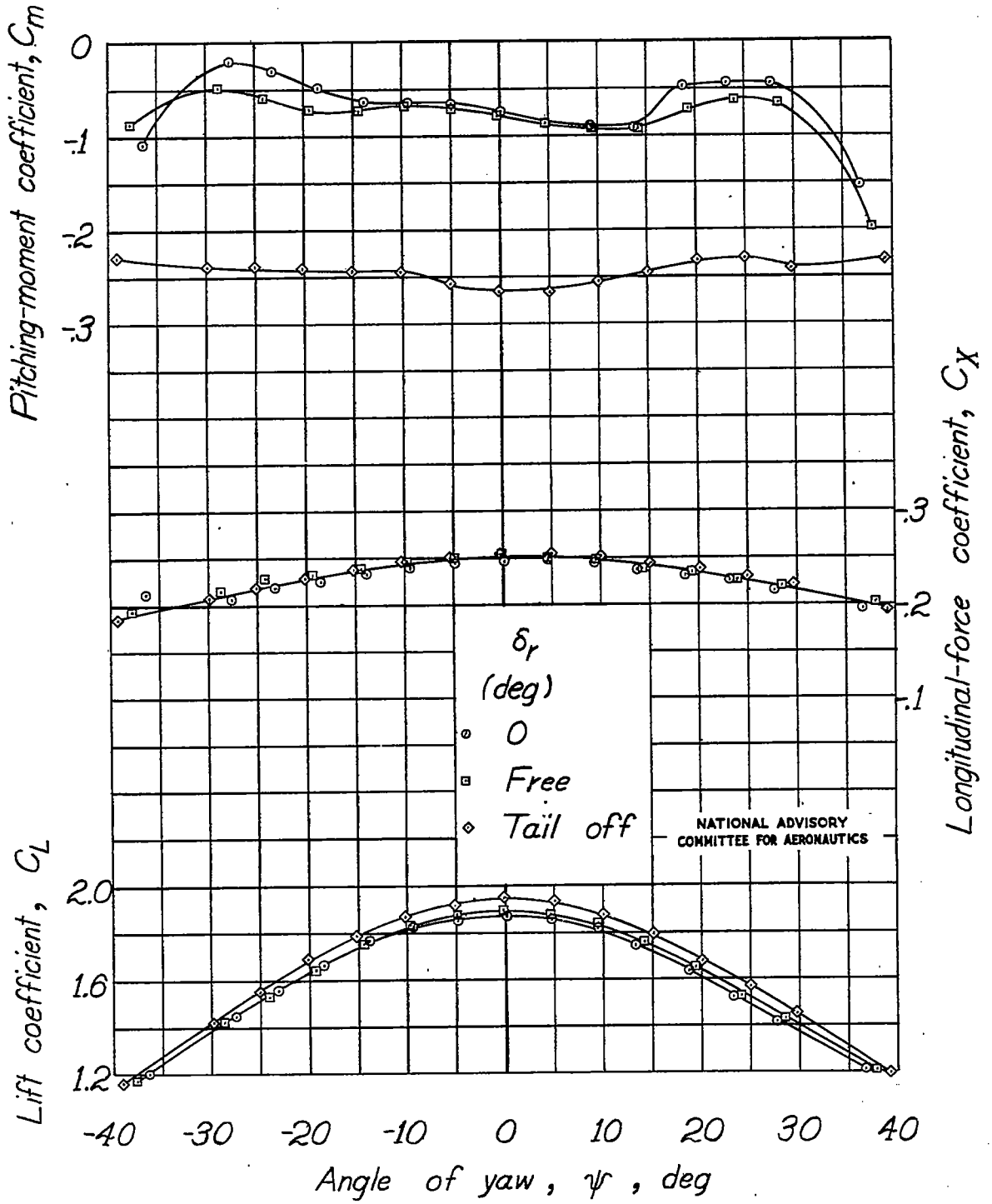

(a) Concluded.

Figure 15.- Continued.

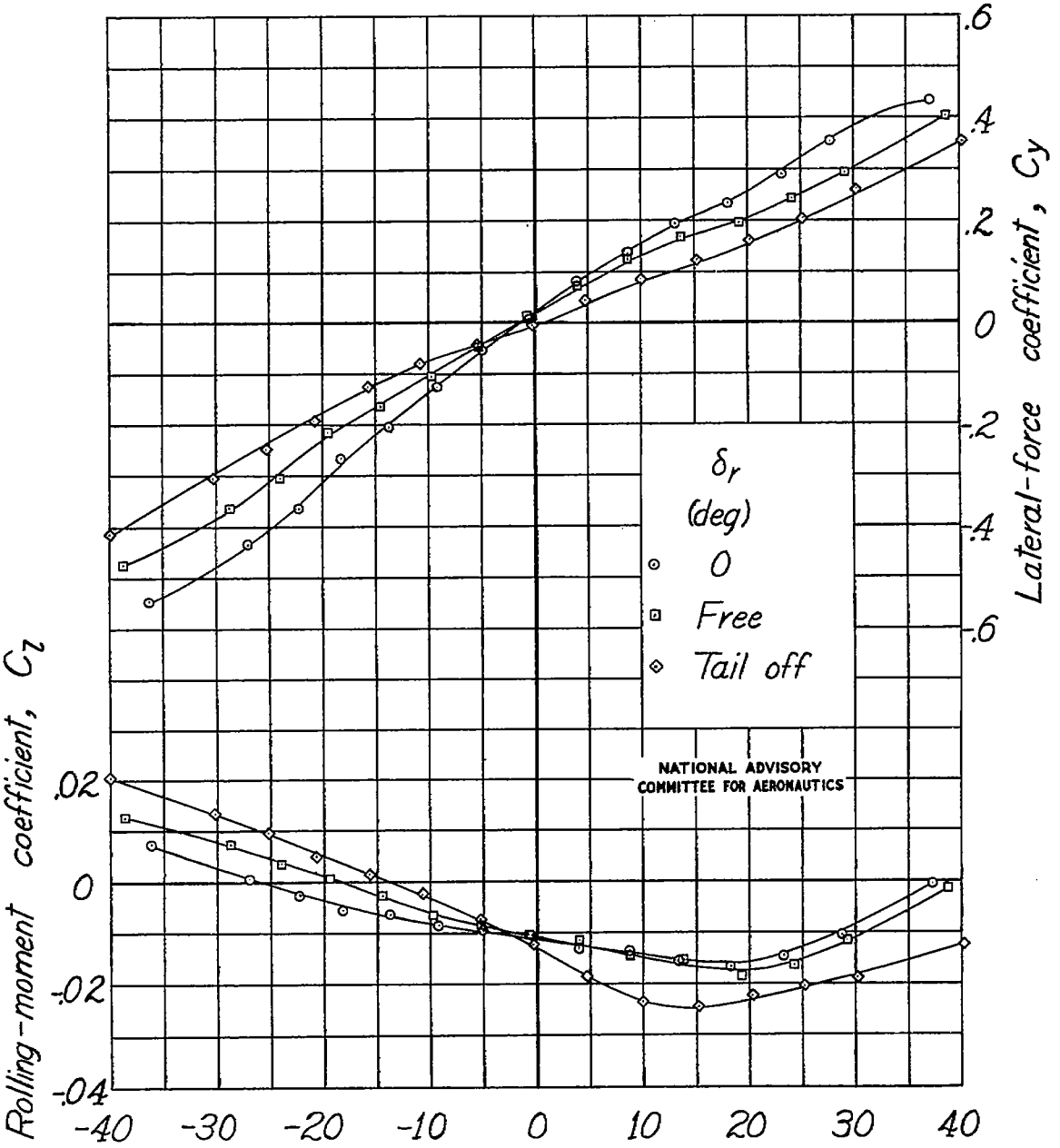

(b) Constant power.

Figure 15.- Continued.

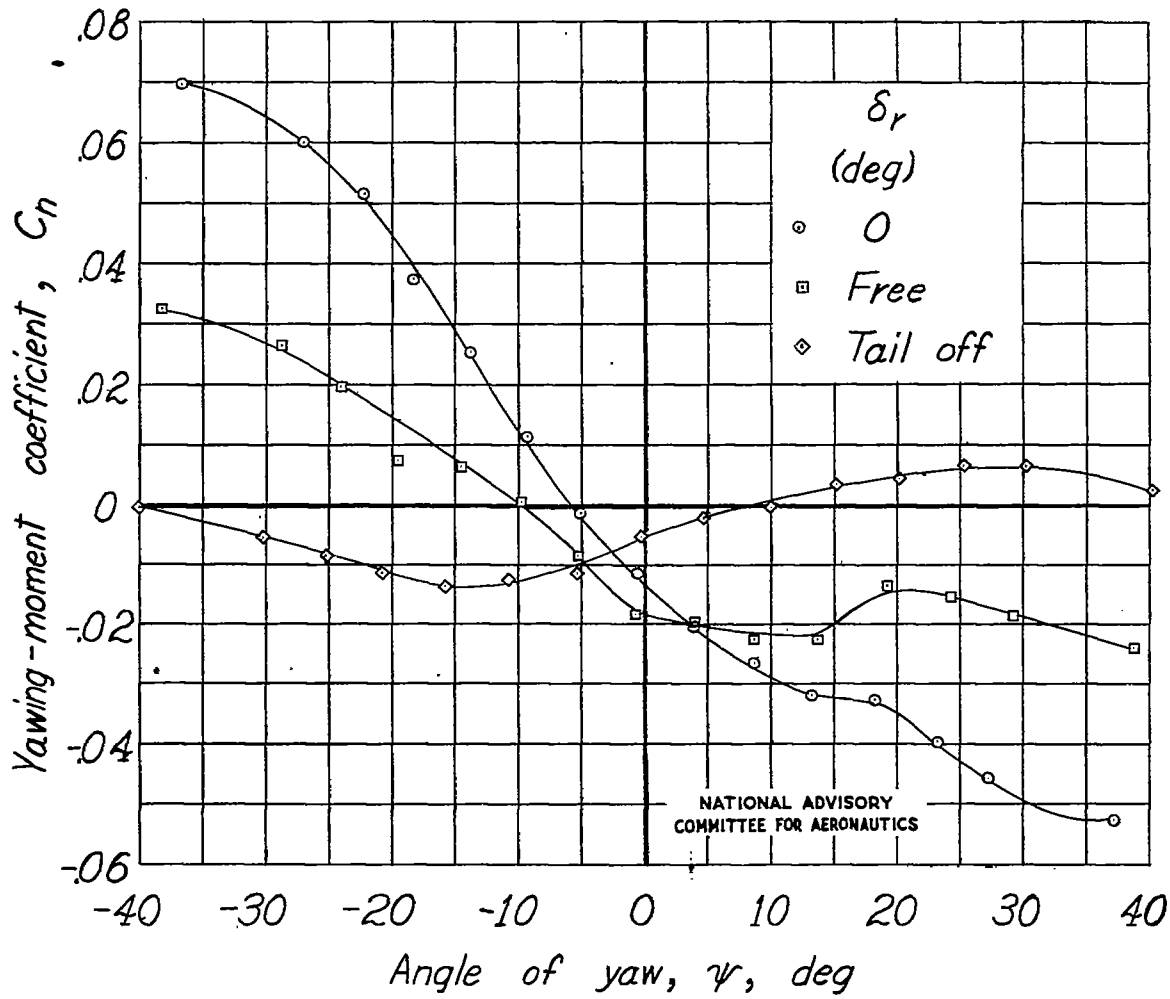

(b) Continued.

Figure 15.- Continued.

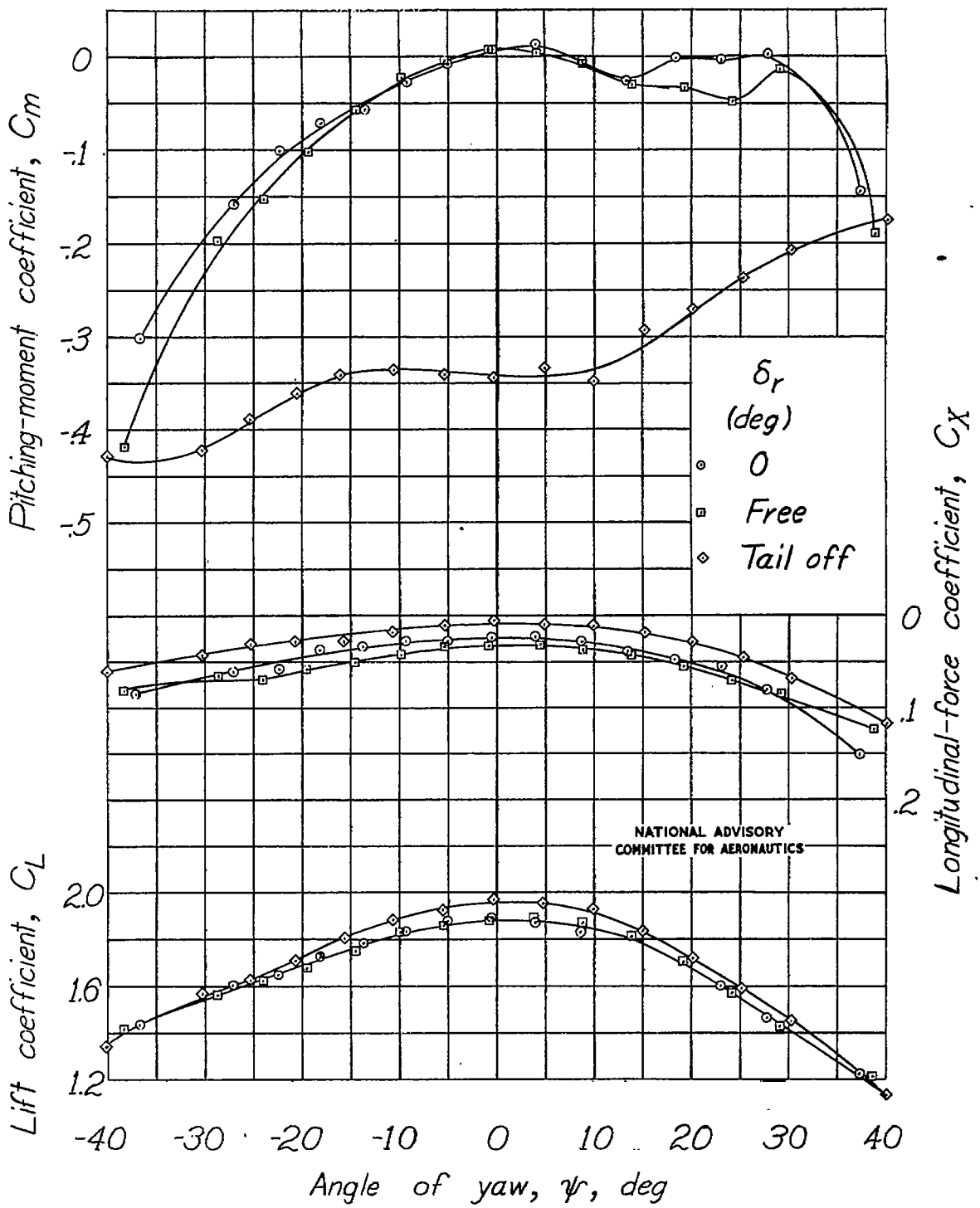

(b) Concluded.

Figure 15.-Concluded.

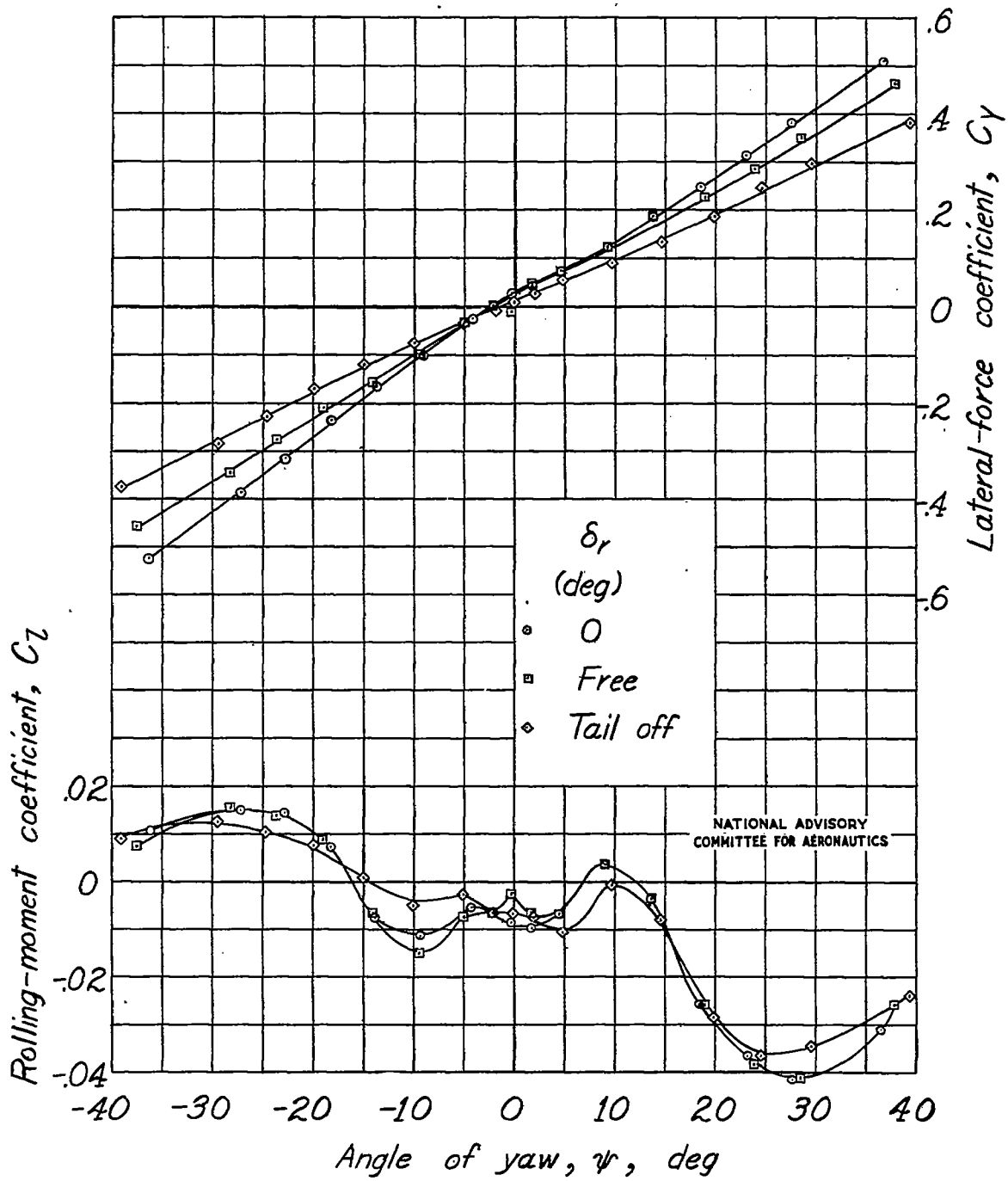

(a) Propeller windmilling.

Figure 16.- Aerodynamic characteristics in yaw of the model as a single-engine high-wing airplane with full-span double slotted flap. $\alpha \approx 9.4°$.

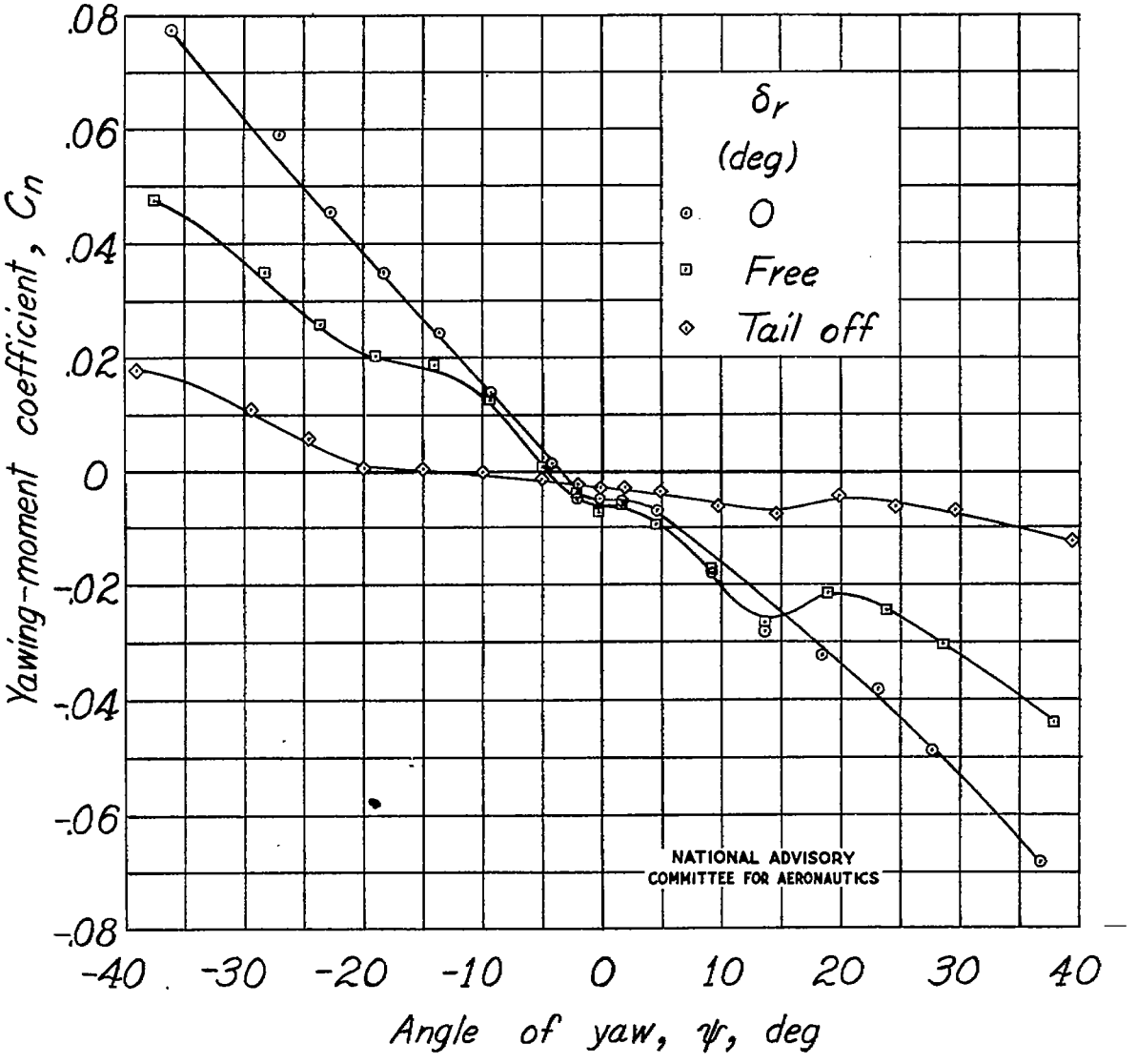

(a) Continued.

Figure 16 .—Continued.

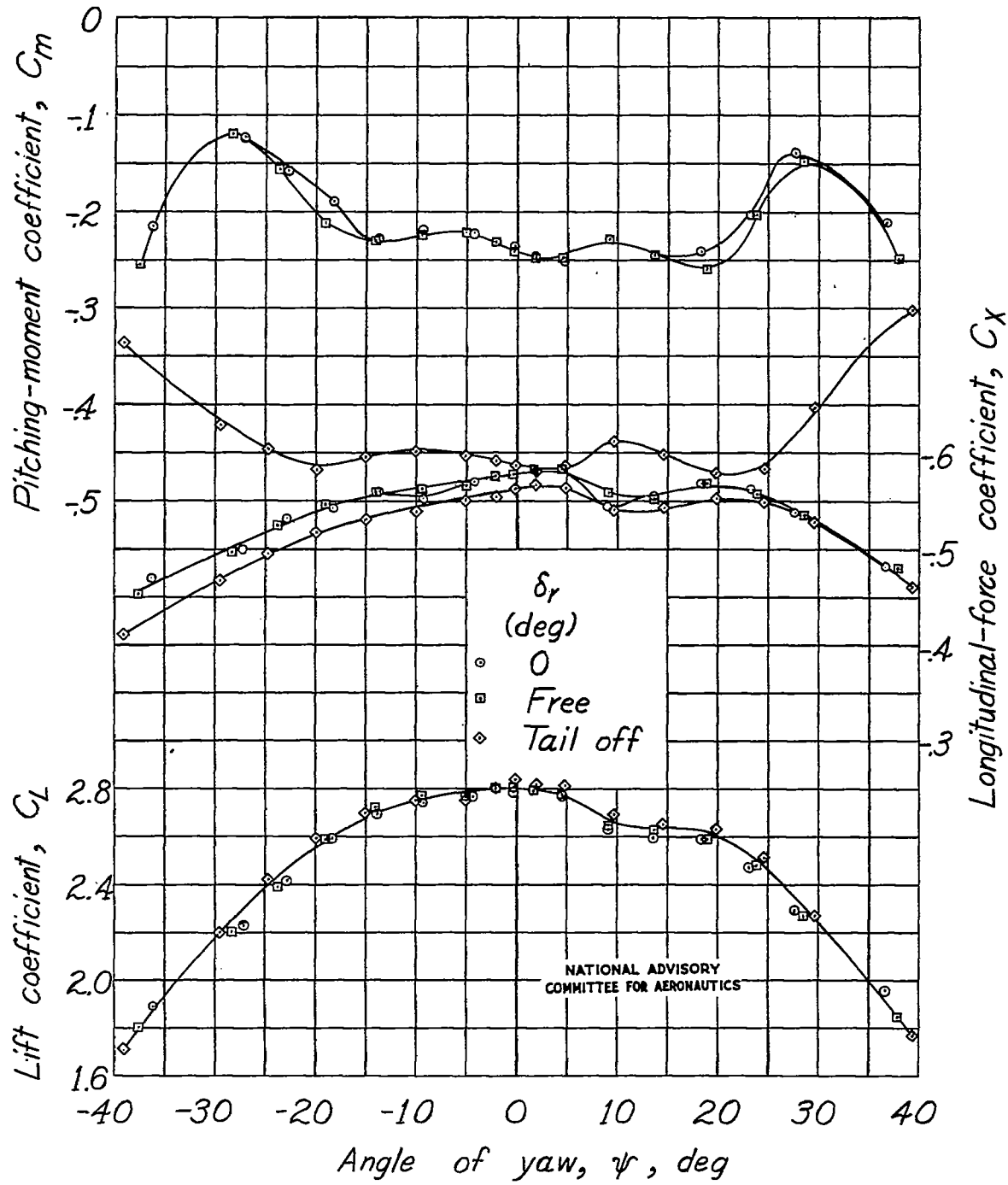

(a) Concluded.

Figure 16.- Continued.

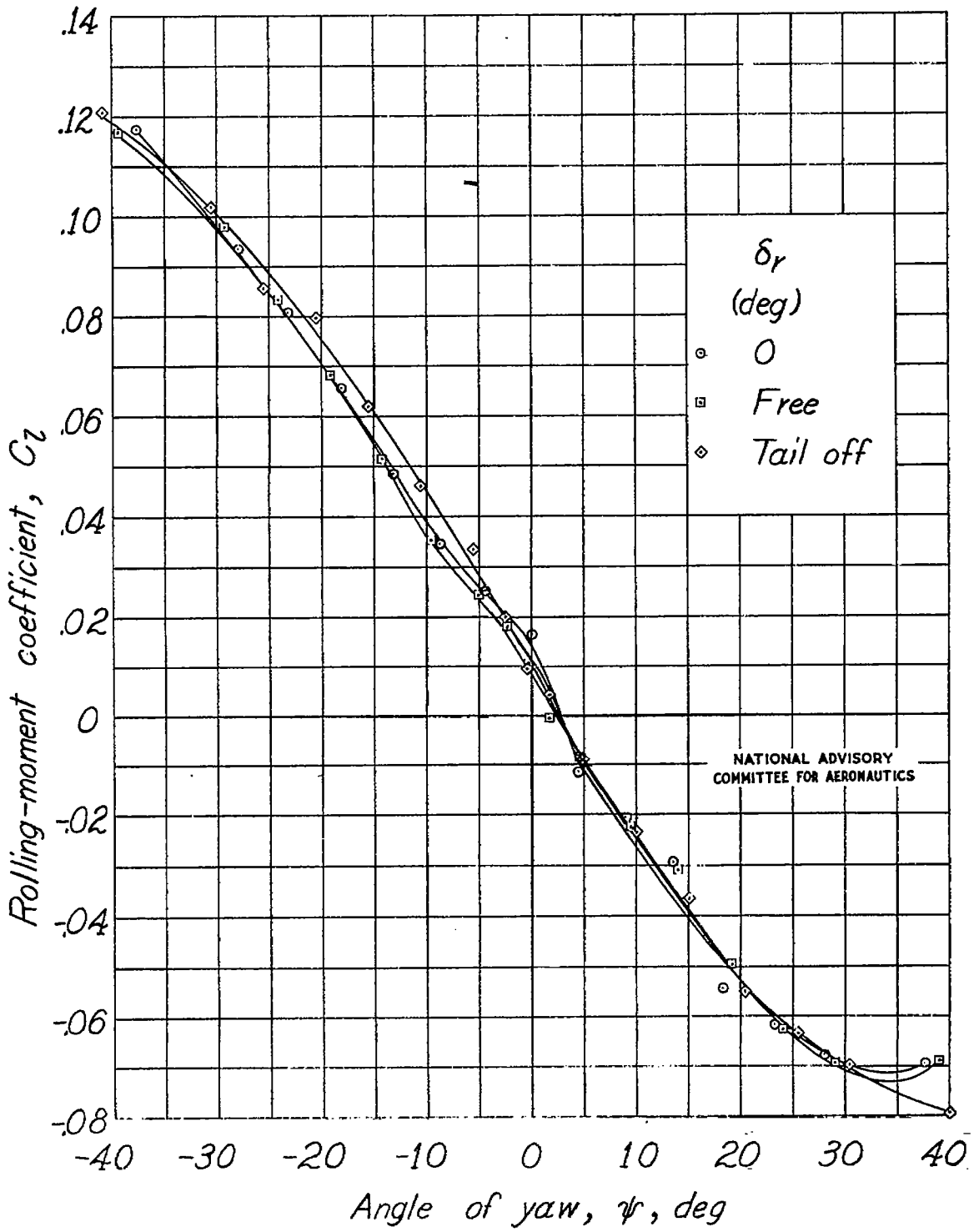

(b) Constant power.

Figure 16.-Continued.

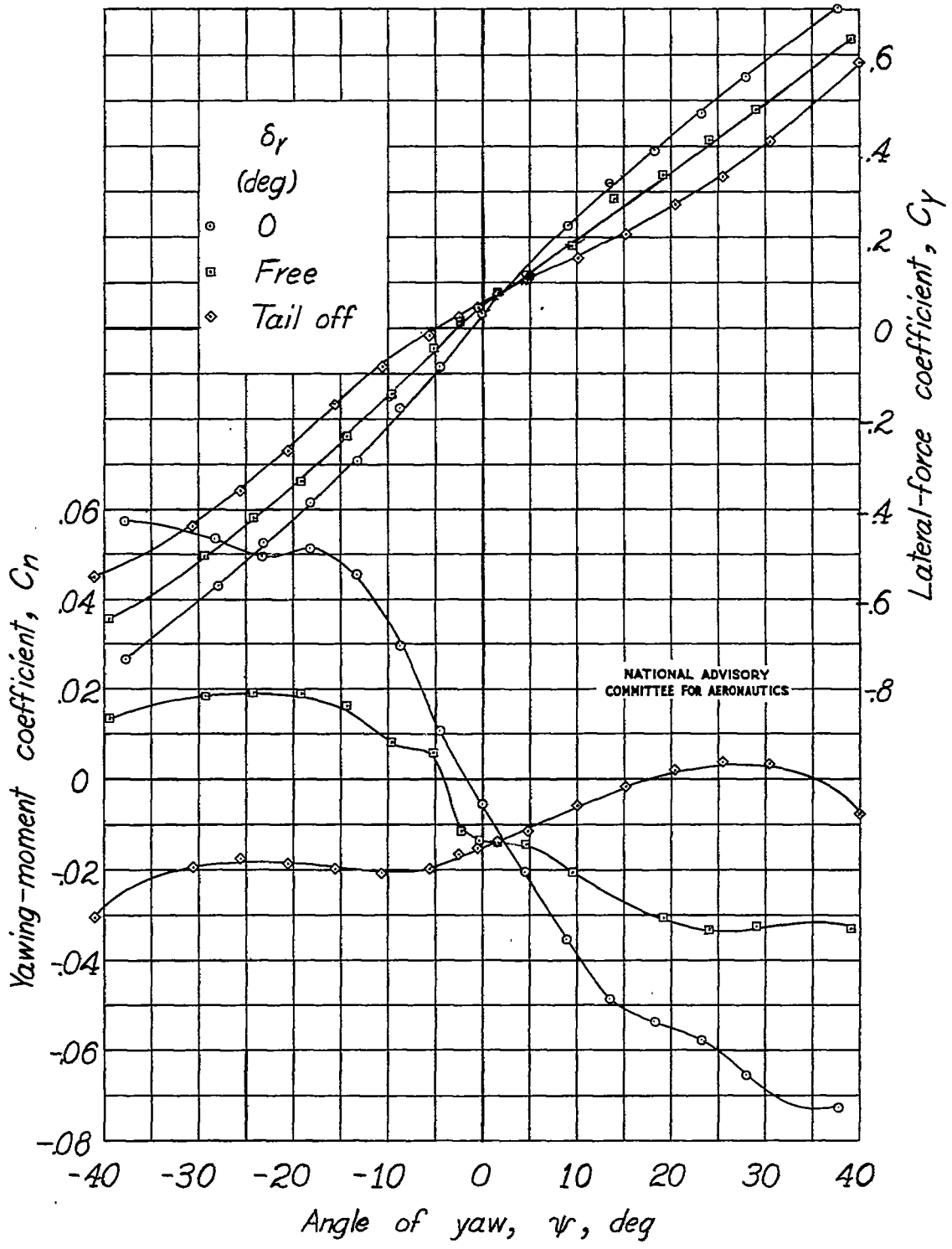

(b) Continued.

Figure 16.-Continued.

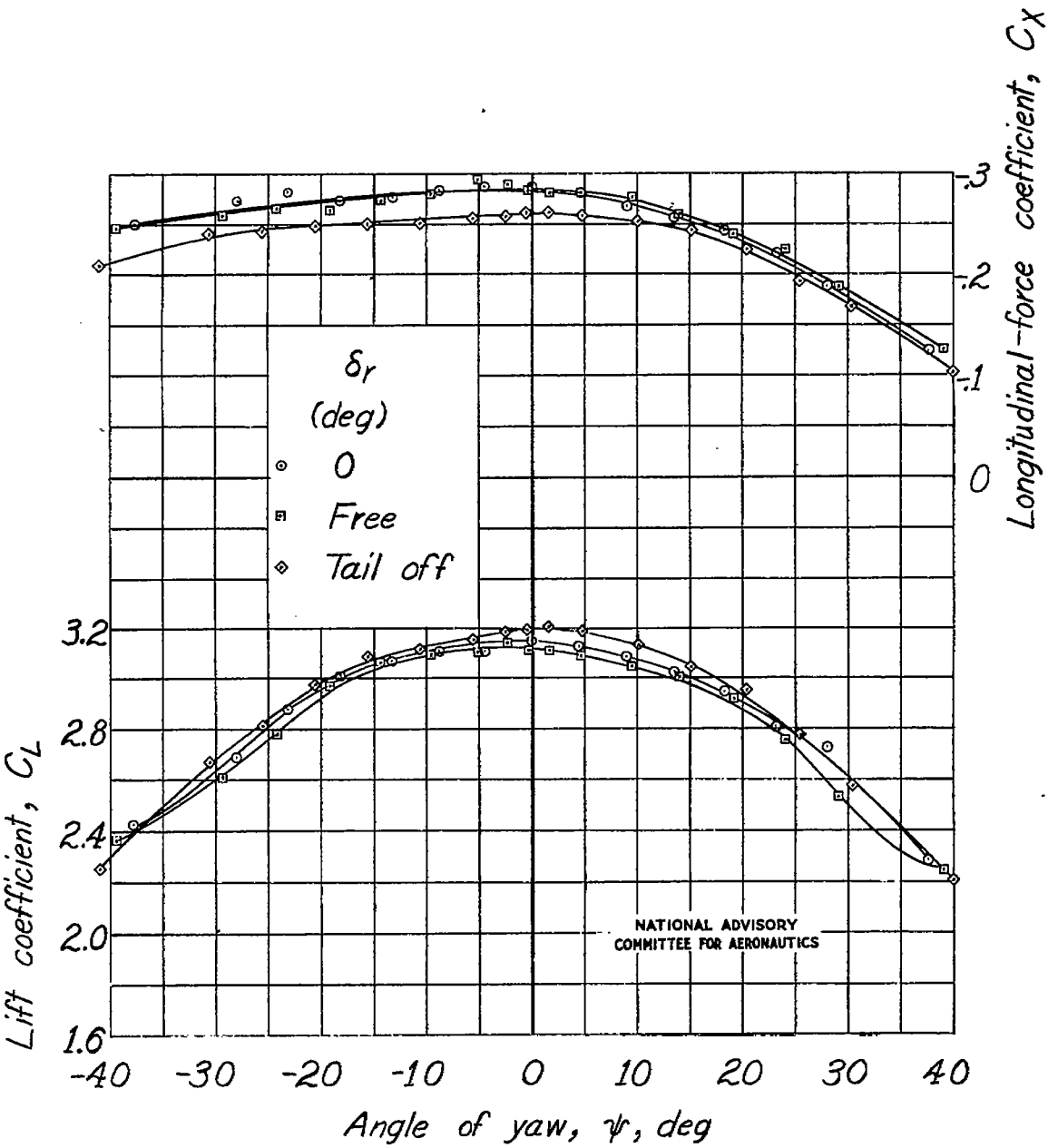

(b) Continued.

Figure 16.-Continued.

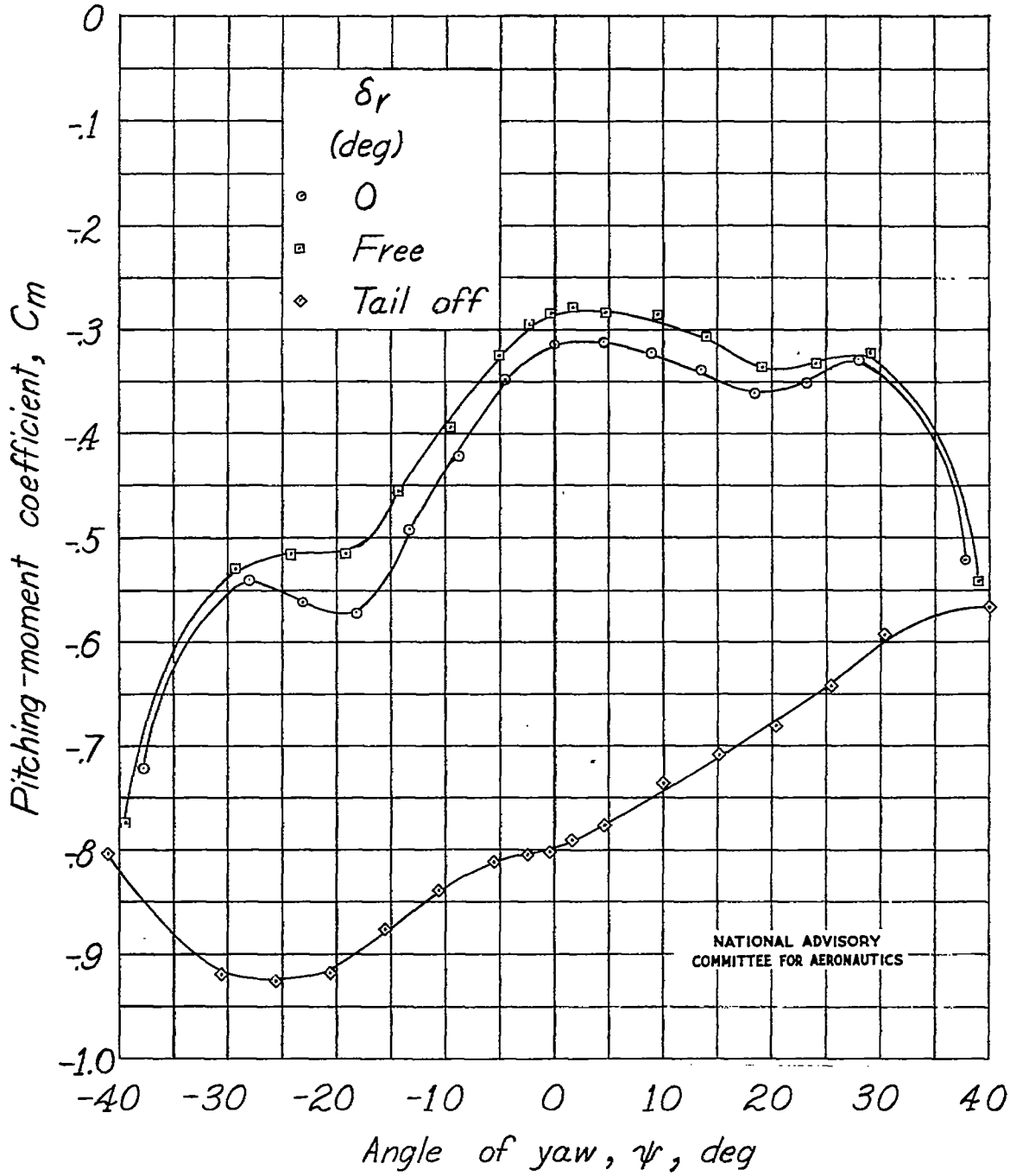

(b) Concluded.

Figure 16.—Concluded.

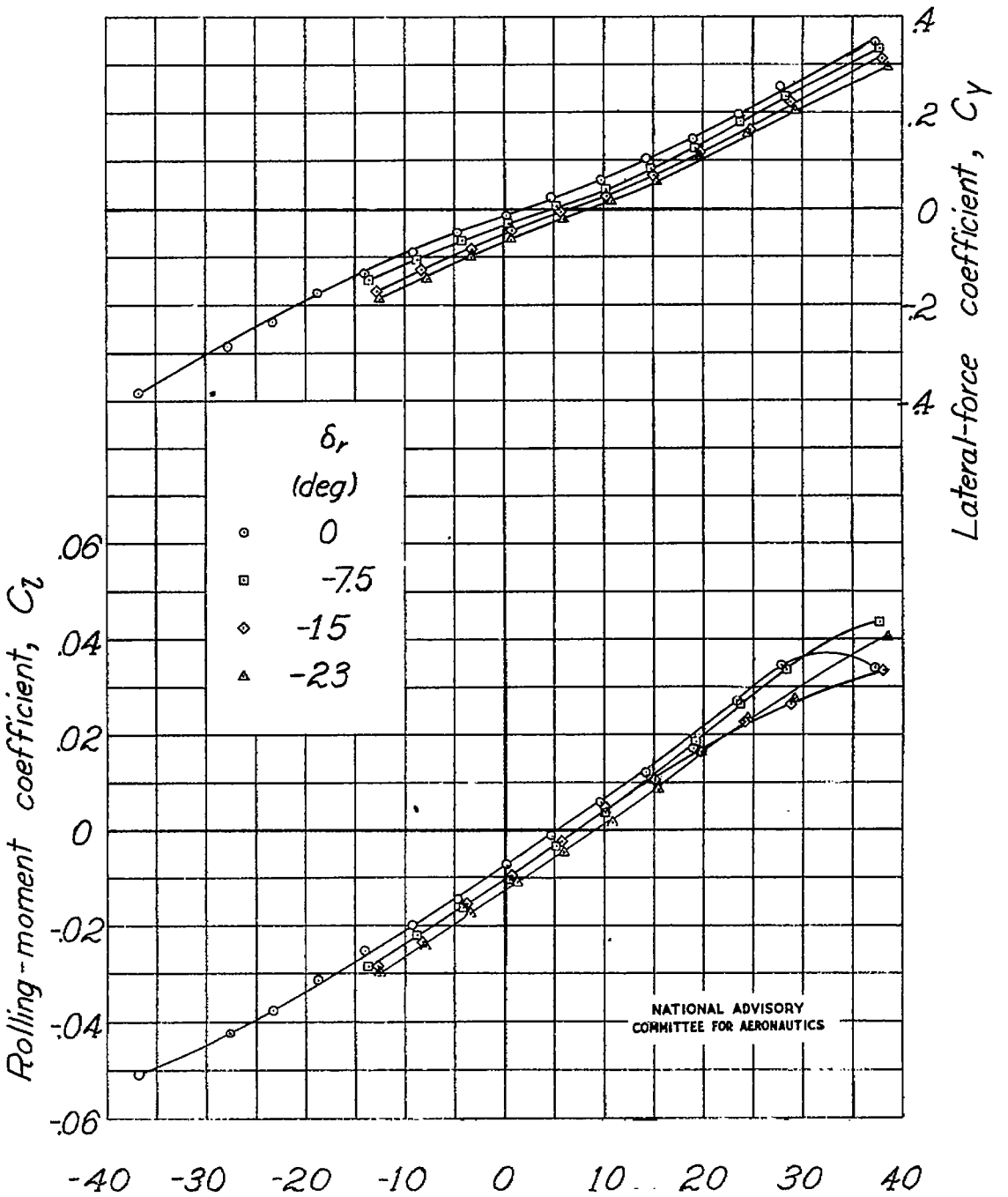

(a) Propeller windmilling.

Figure 17.- Effect of rudder deflection on the aerodynamic characteristics of the model as a single-engine high-wing airplane with flap neutral. $\alpha \approx 1.7°$.

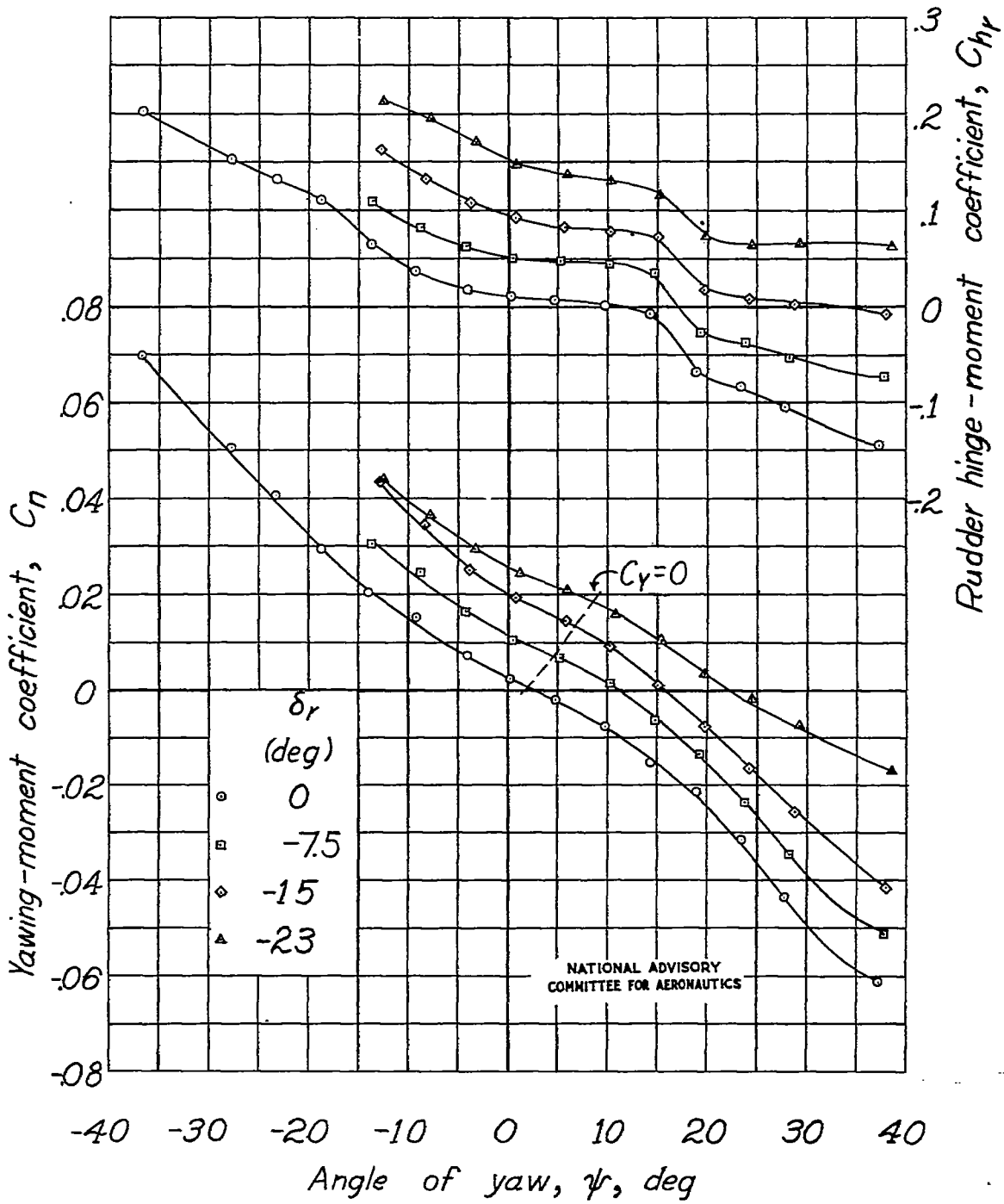

(a) Continued.

Figure 17.– Continued.

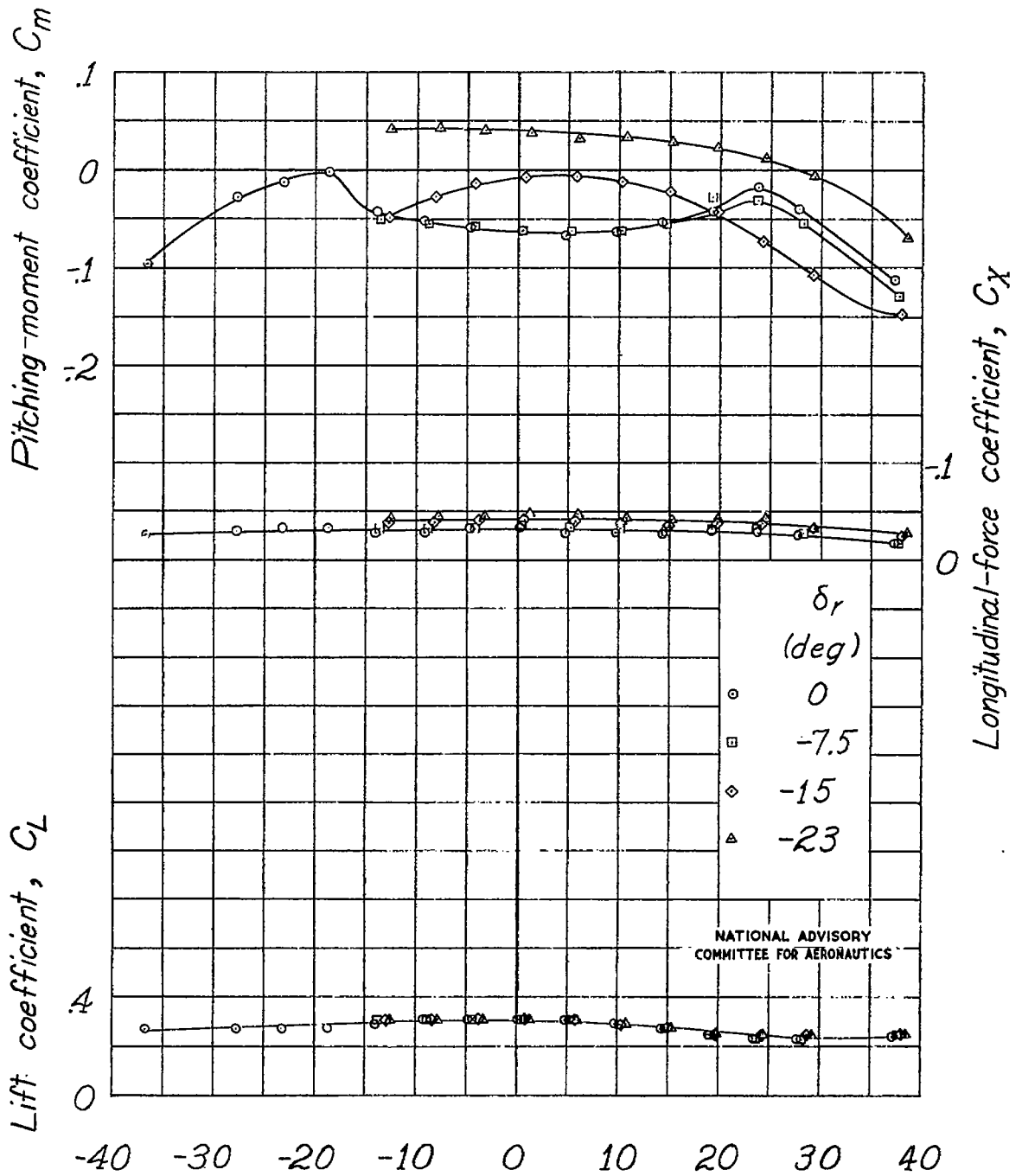

(a) Concluded.

Figure 17.- Continued.

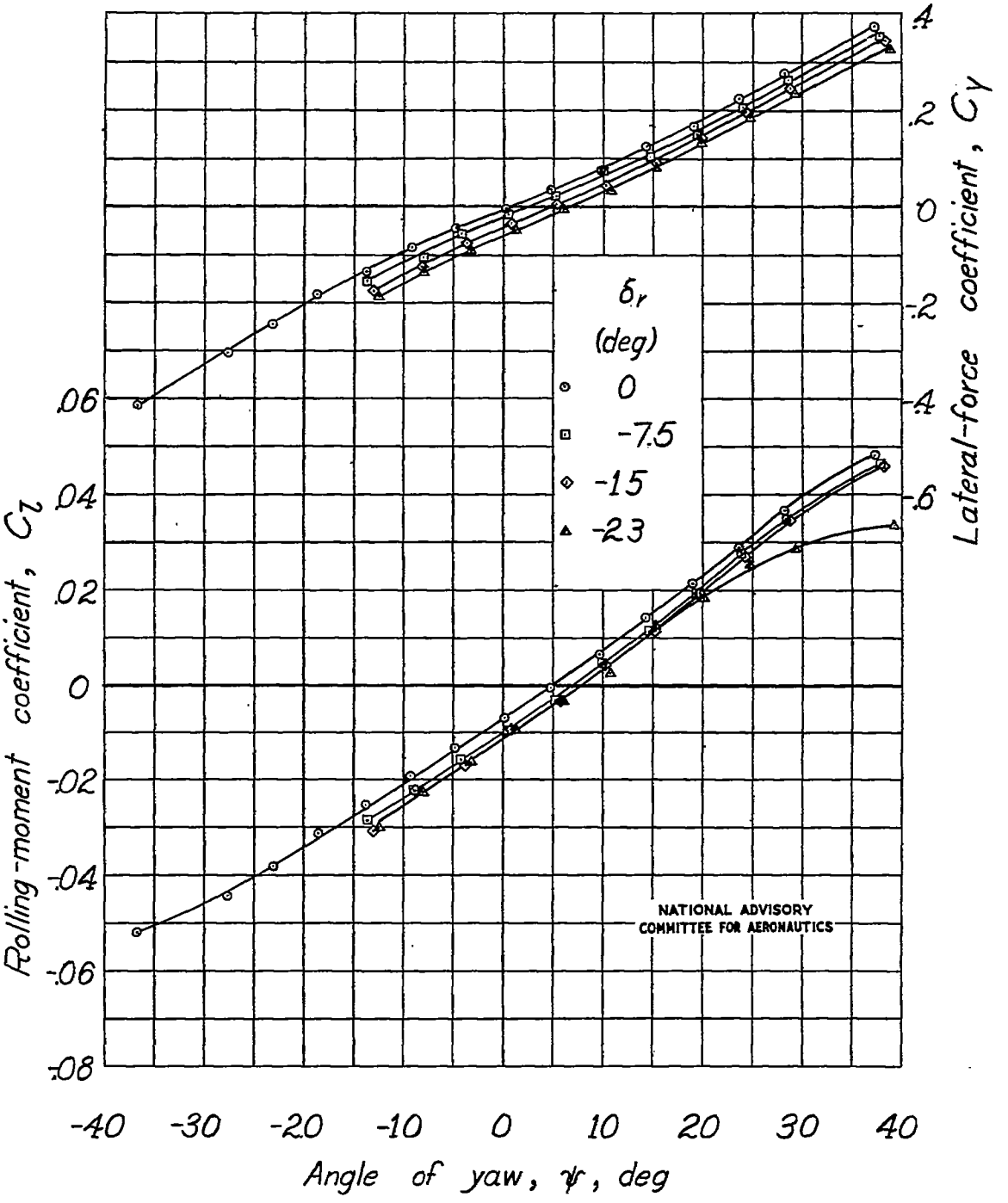

(b) Constant power.

Figure 17.-Continued.

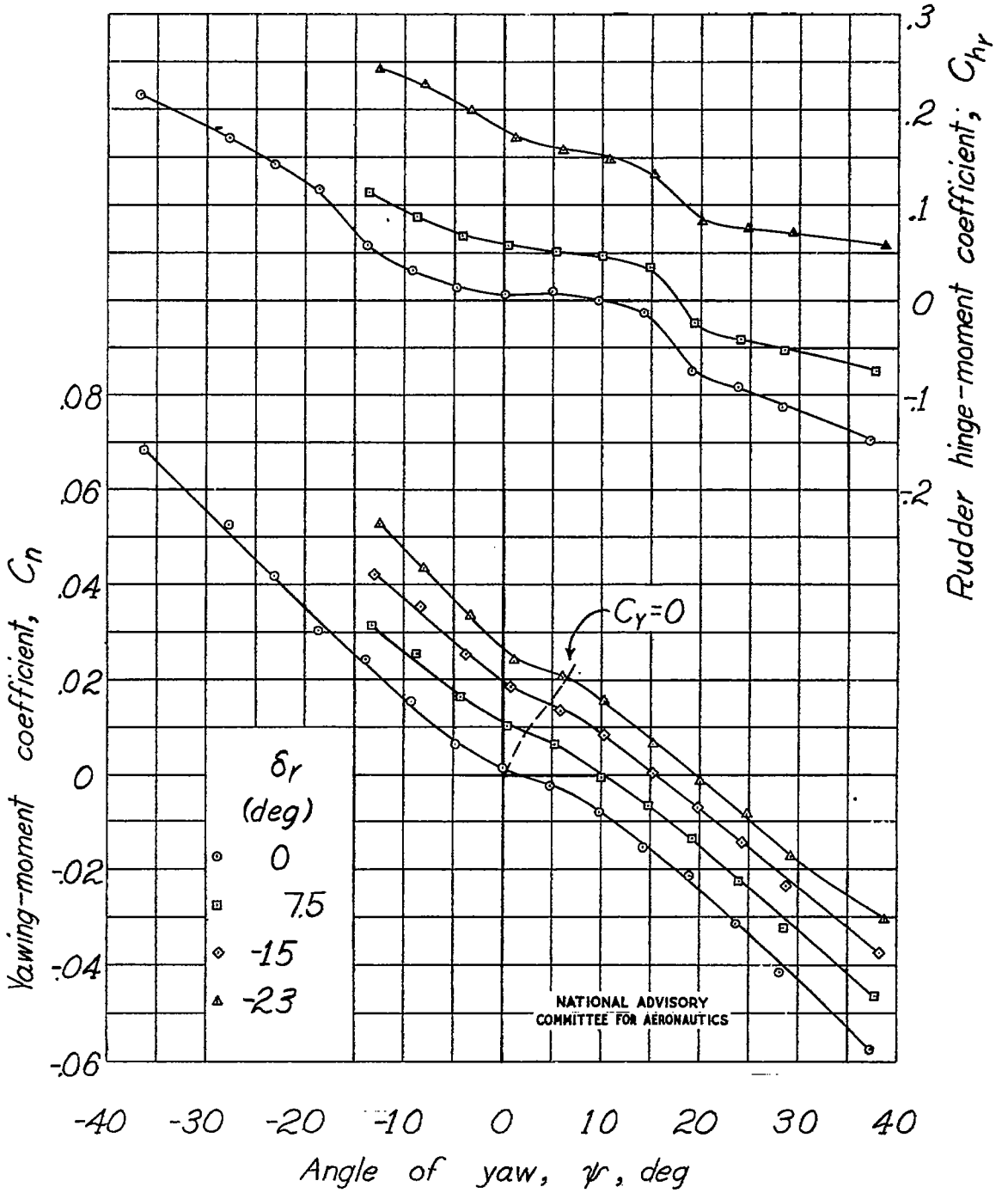

(b) Continued.

Figure 17.—Continued.

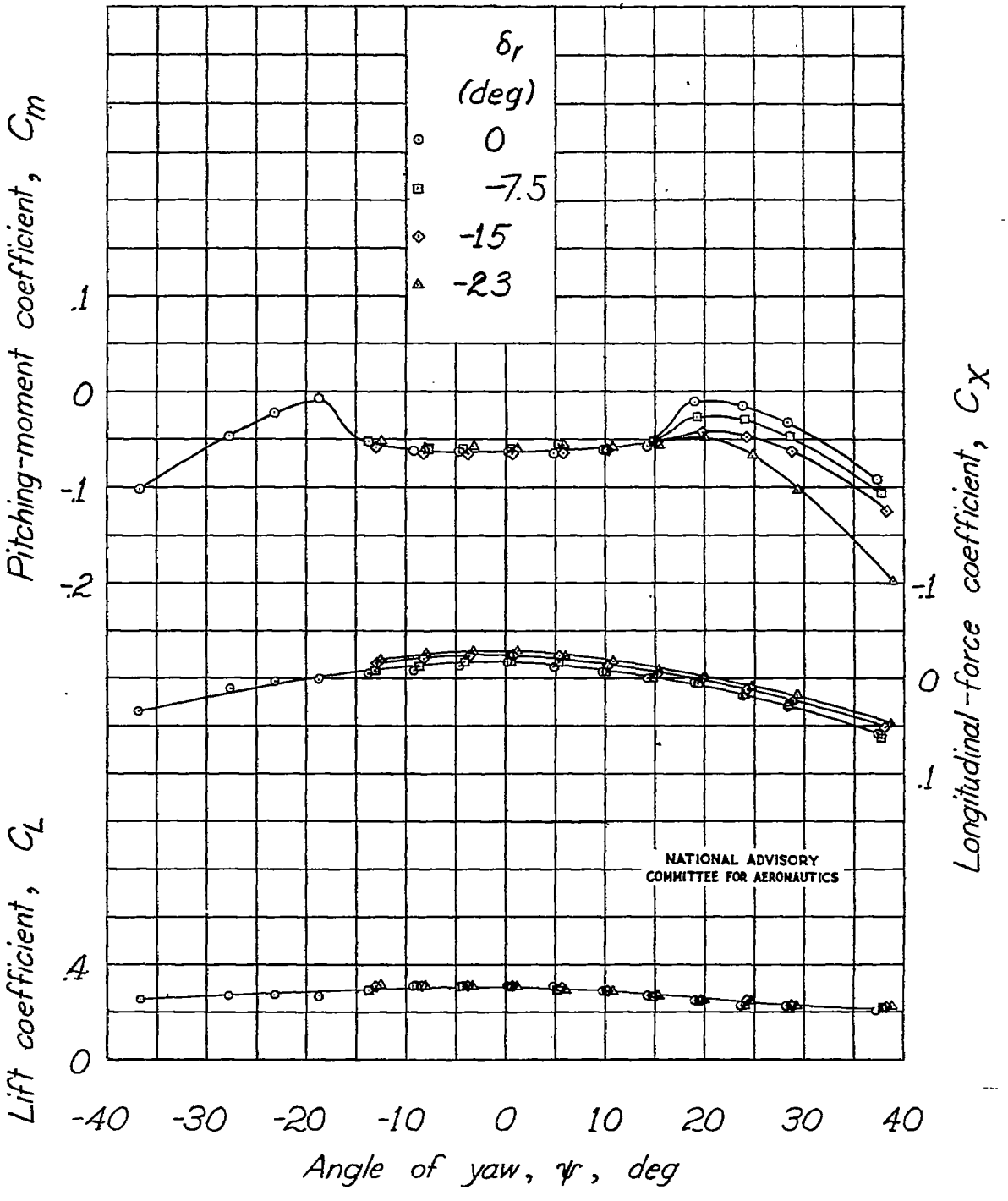

(b) Concluded.

Figure 17.–Concluded.

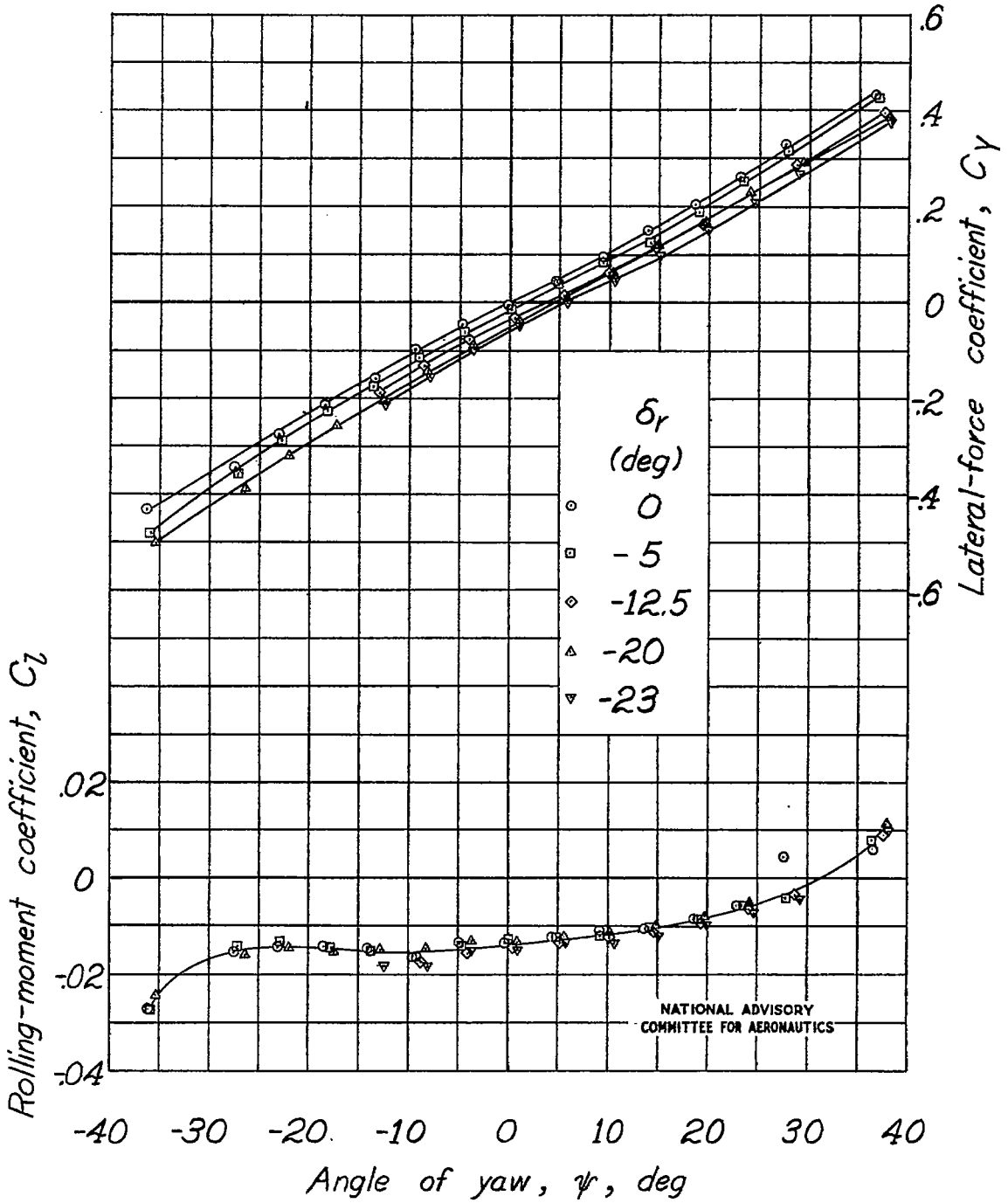

(a) Propeller windmilling.

Figure 18.—Effect of rudder deflection on the aerodynamic characteristics of the model as a single-engine high-wing airplane with full-span single slotted flap. $\alpha \approx 9.6°$.

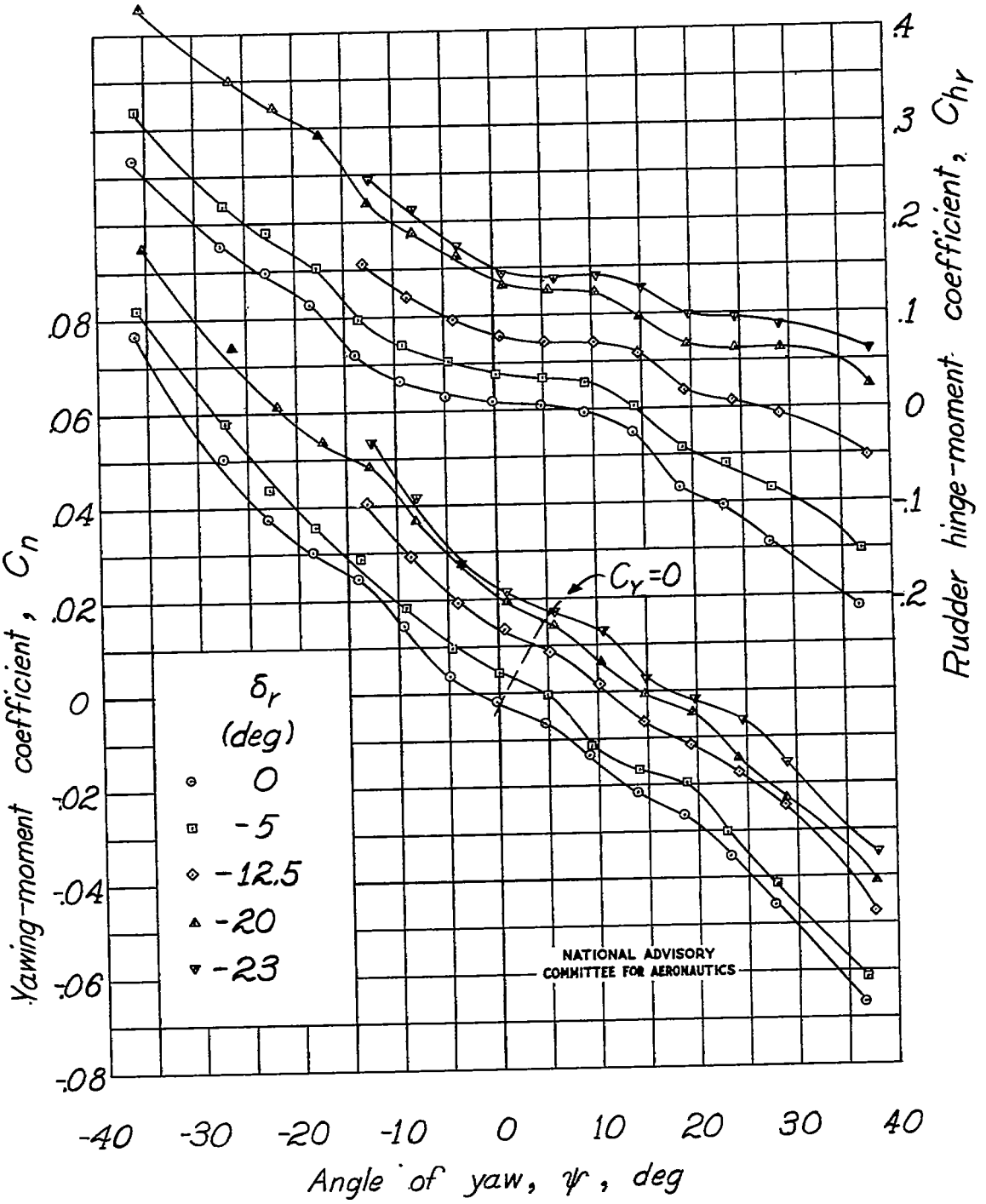

(a) Continued.

Figure 18.-Continued.

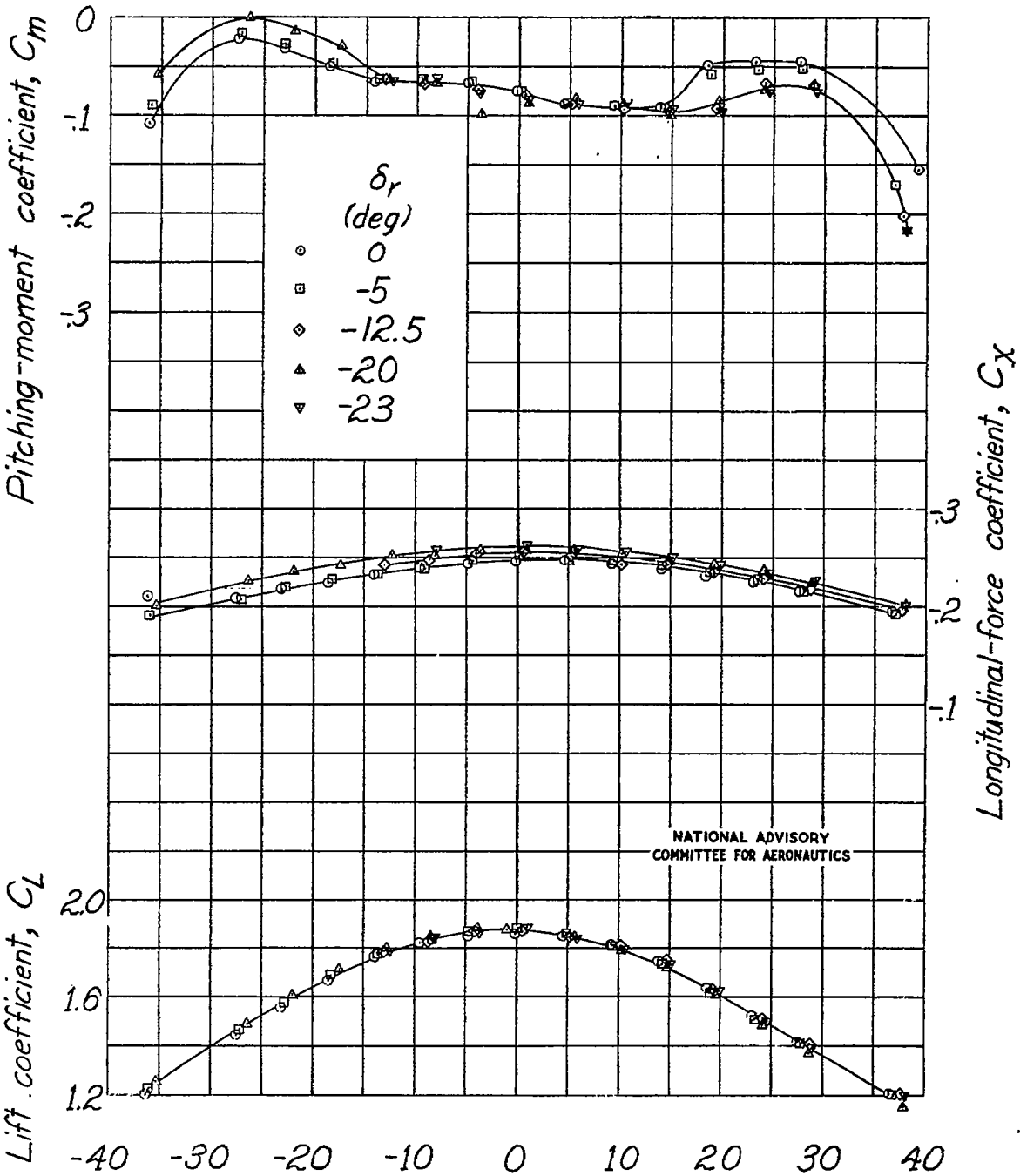

(a) Concluded.

Figure 18.- Continued.

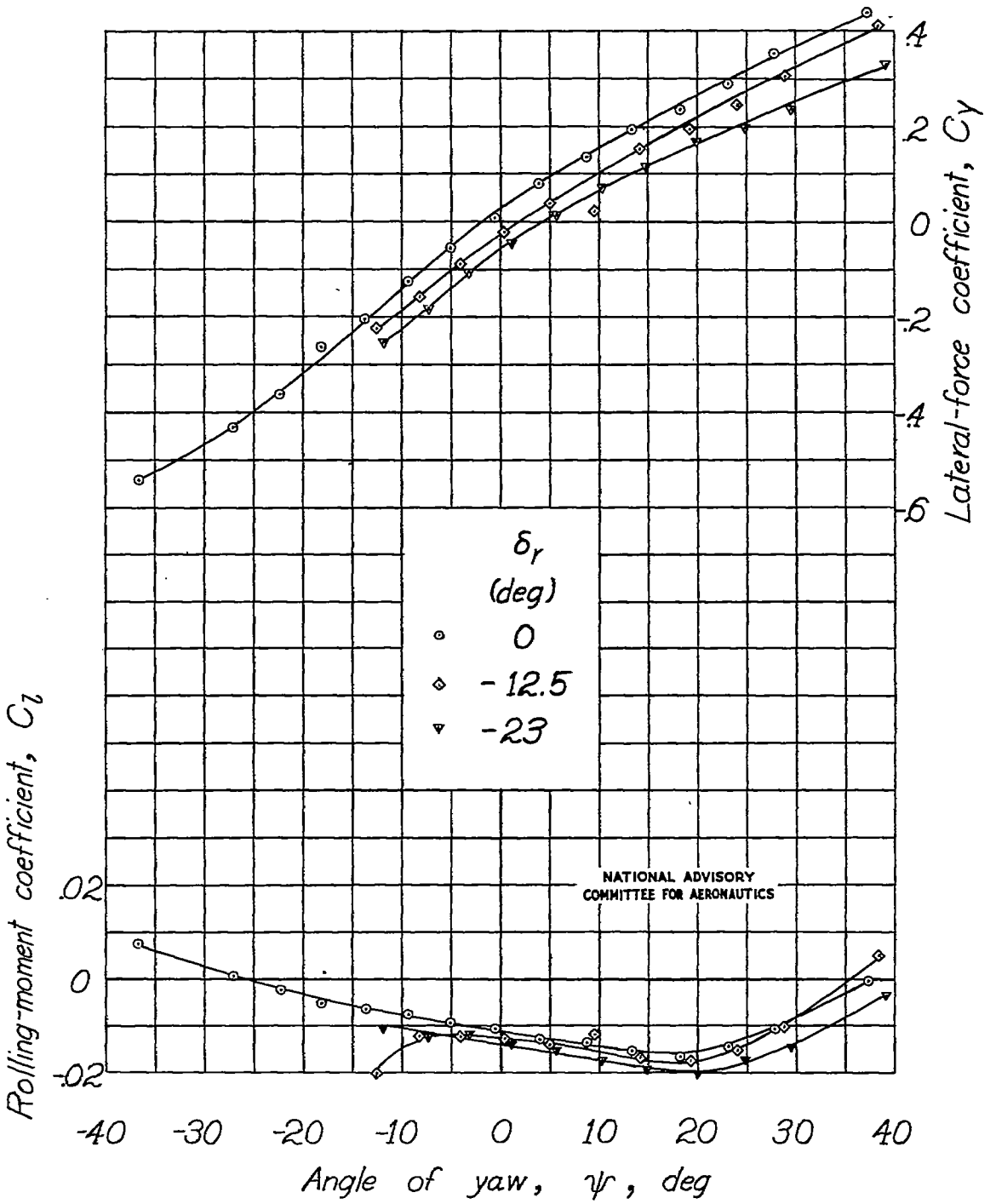

(b) Constant power.

Figure 18.–Continued.

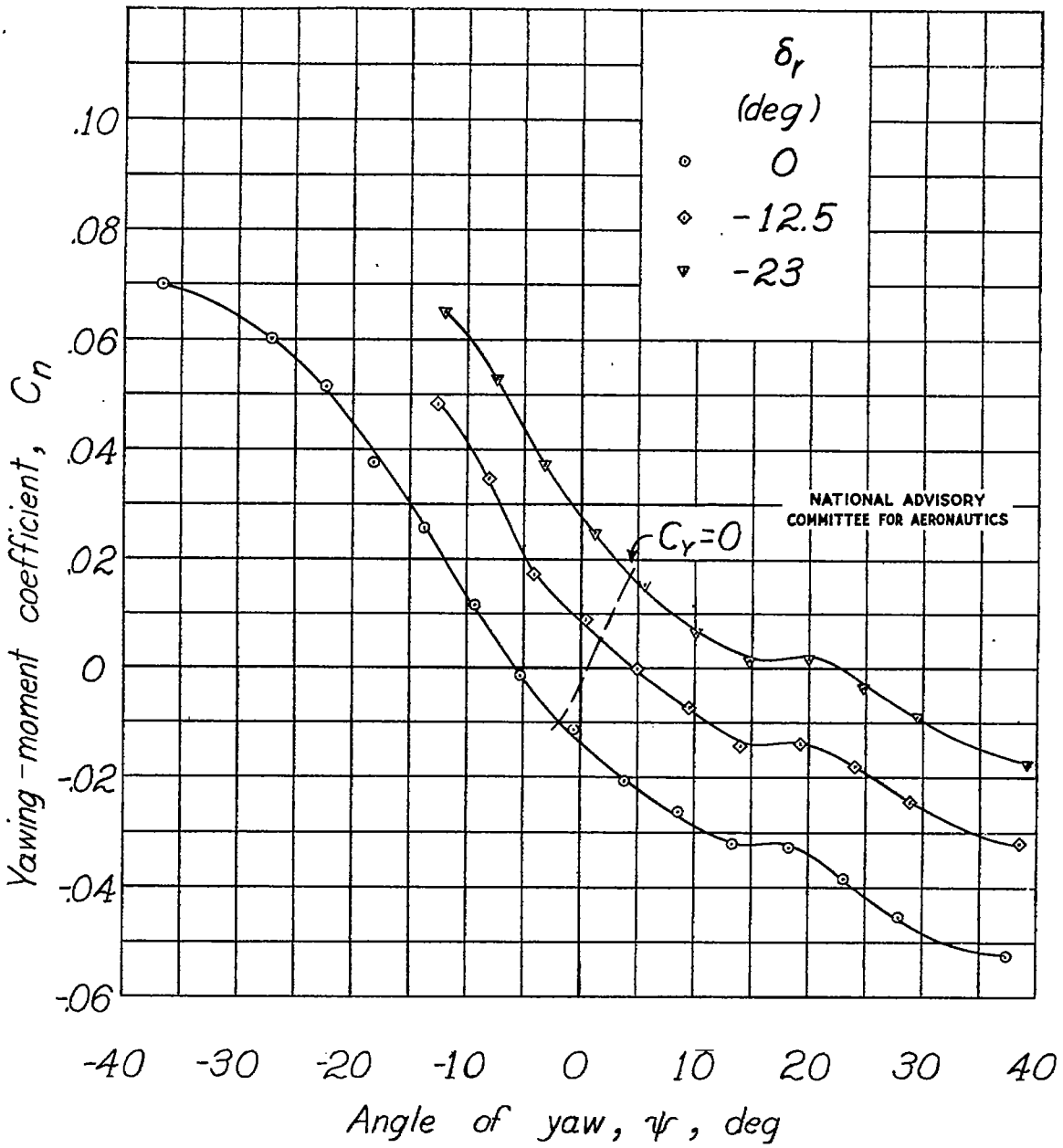

(b) Continued.

Figure 18.- Continued.

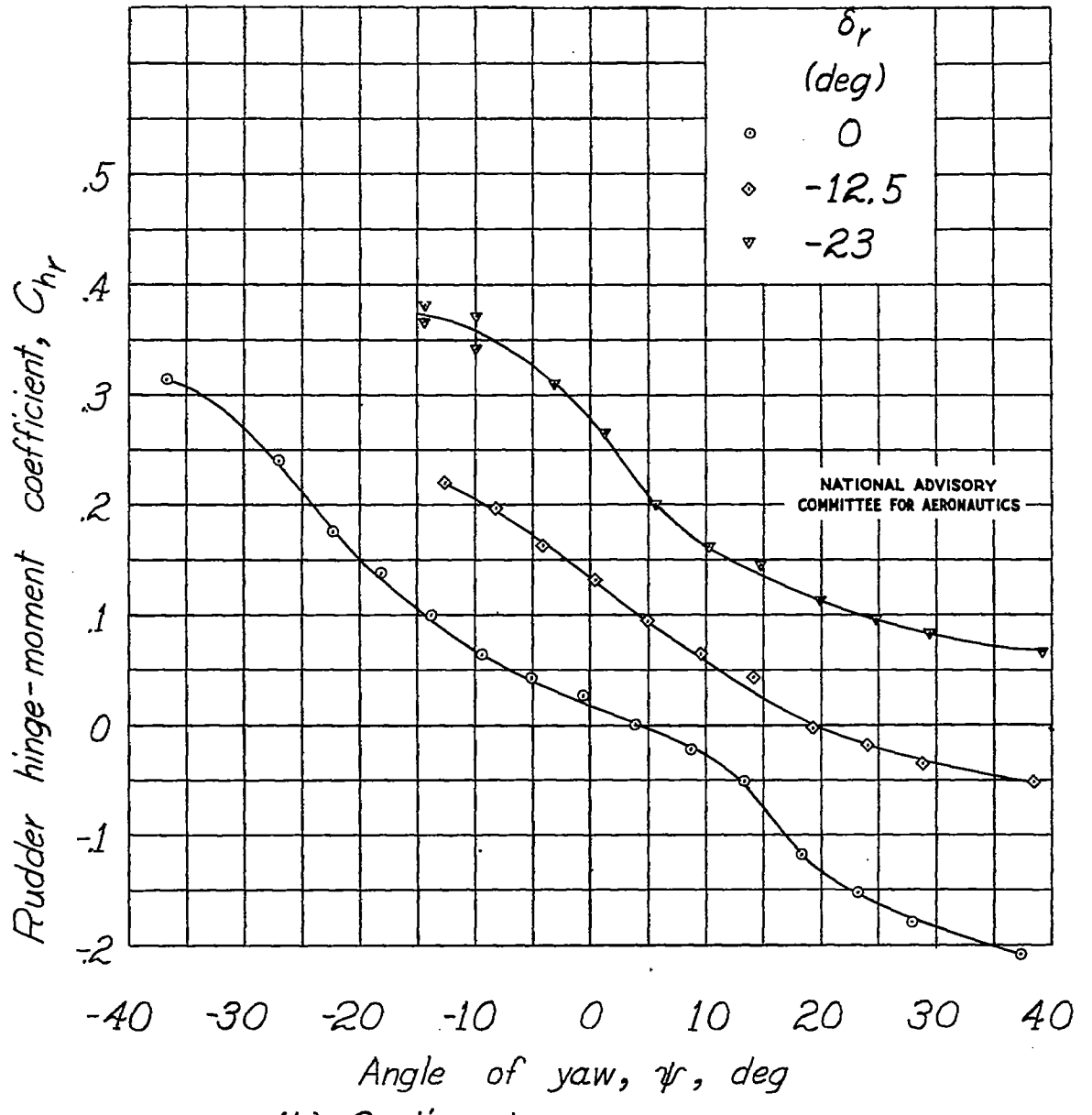

(b) Continued.

Figure 18.- Continued.

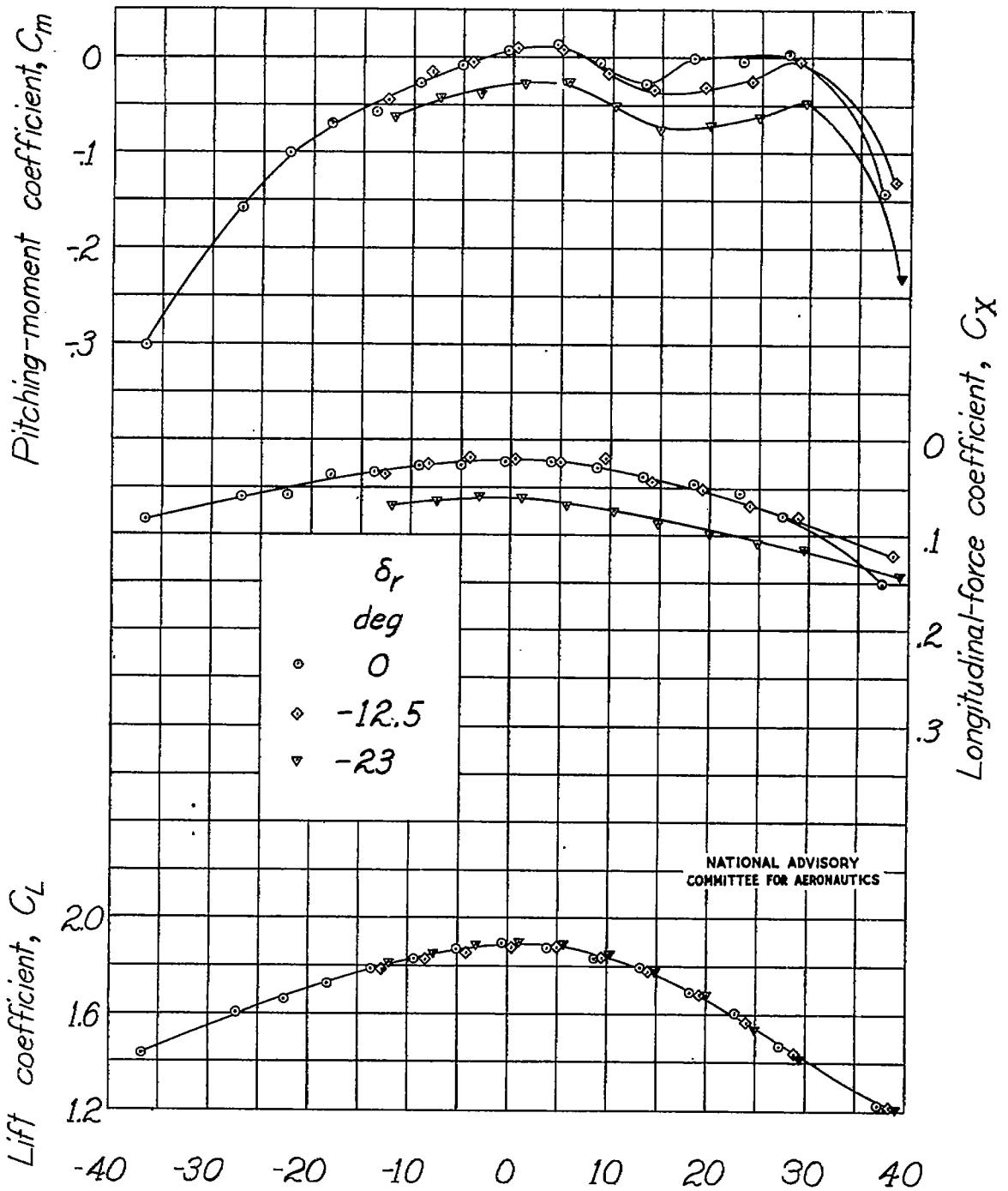

(b) Concluded.

Figure 18.- Concluded.

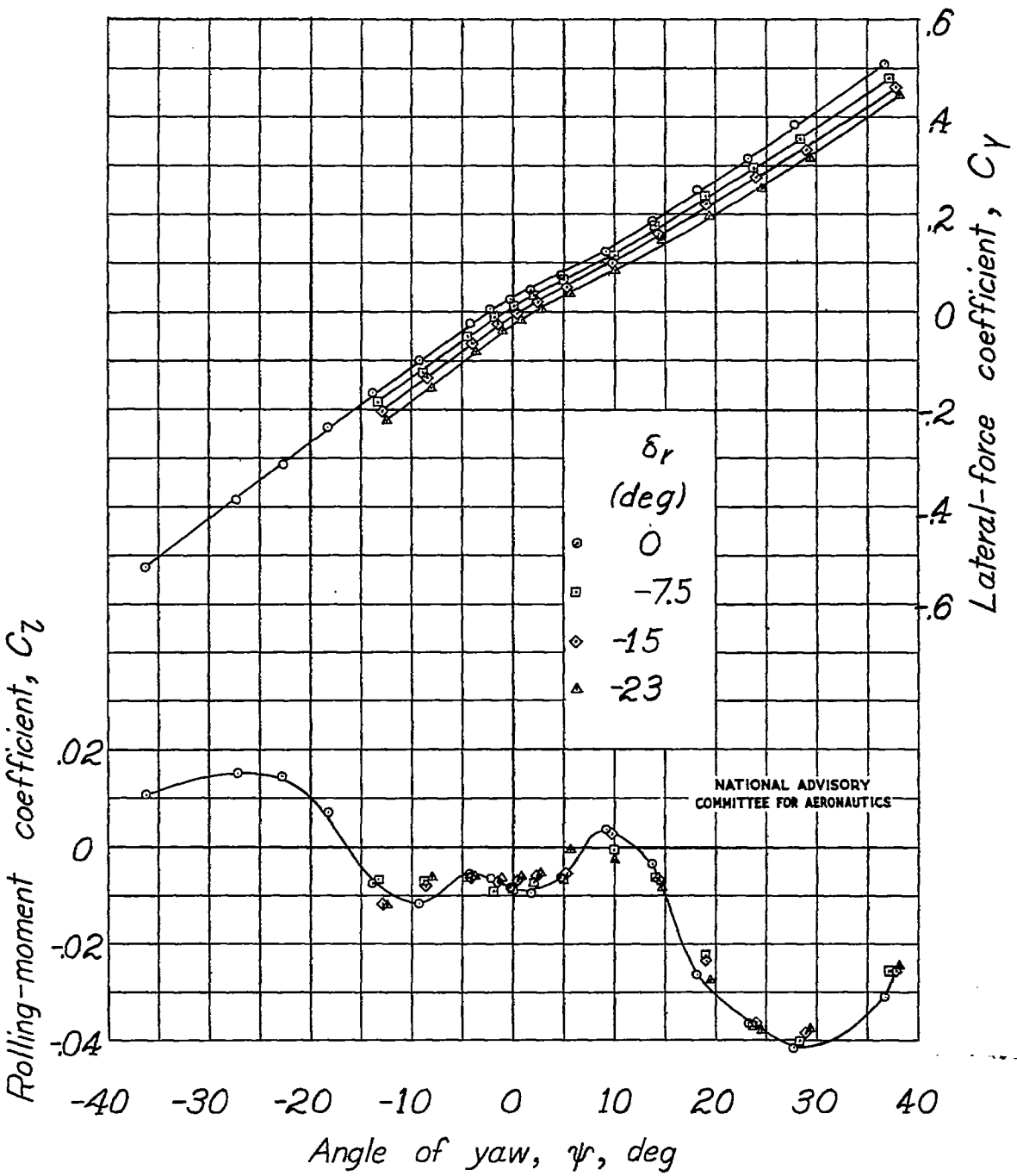

(a) Propeller windmilling.

Figure 19.- Effect of rudder deflection on the aerodynamic characteristics of the model as a single-engine high-wing airplane with full-span double slotted flap. $\alpha \approx 9.4°$.

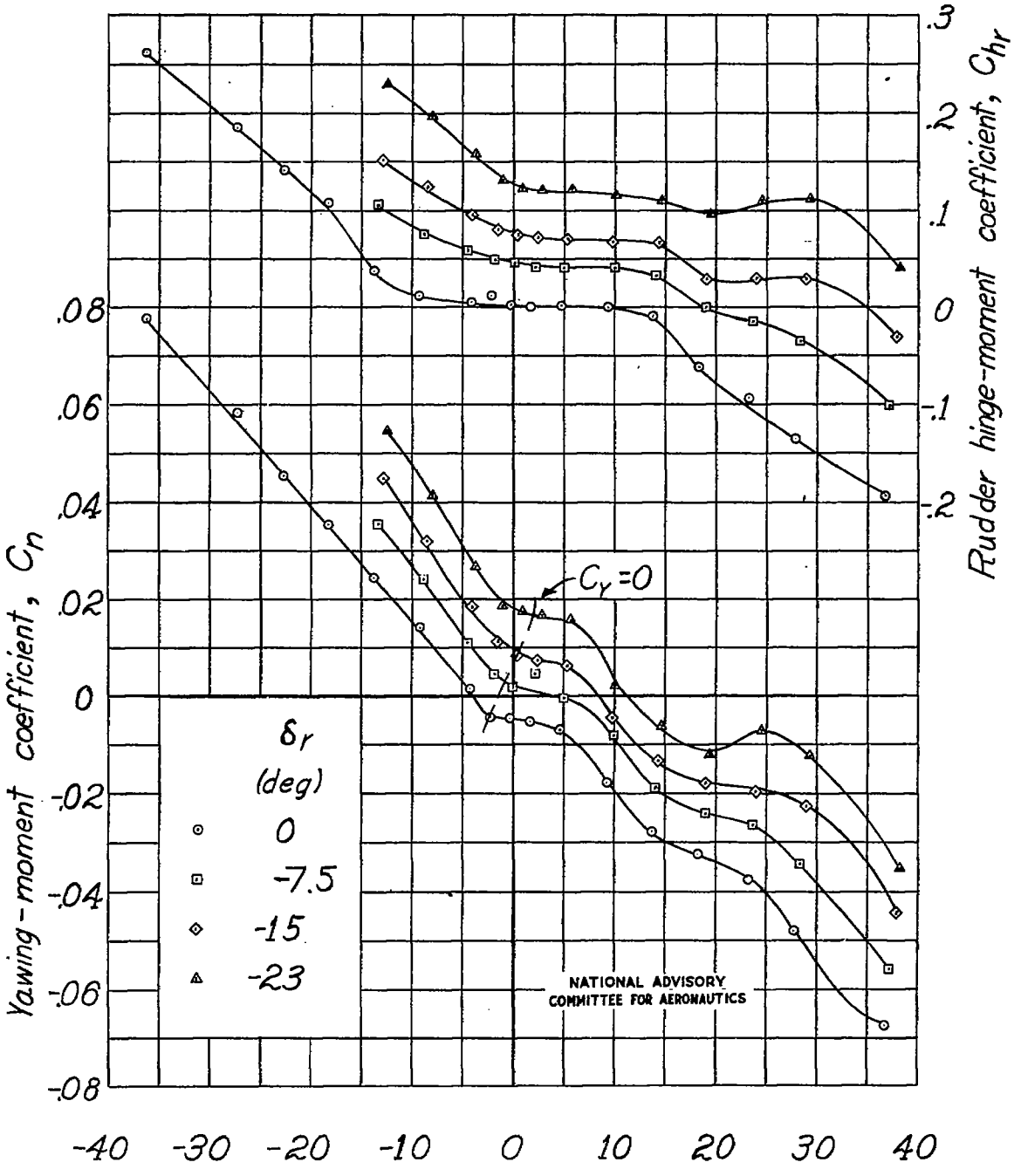

(a) Continued.

Figure 19.-Continued.

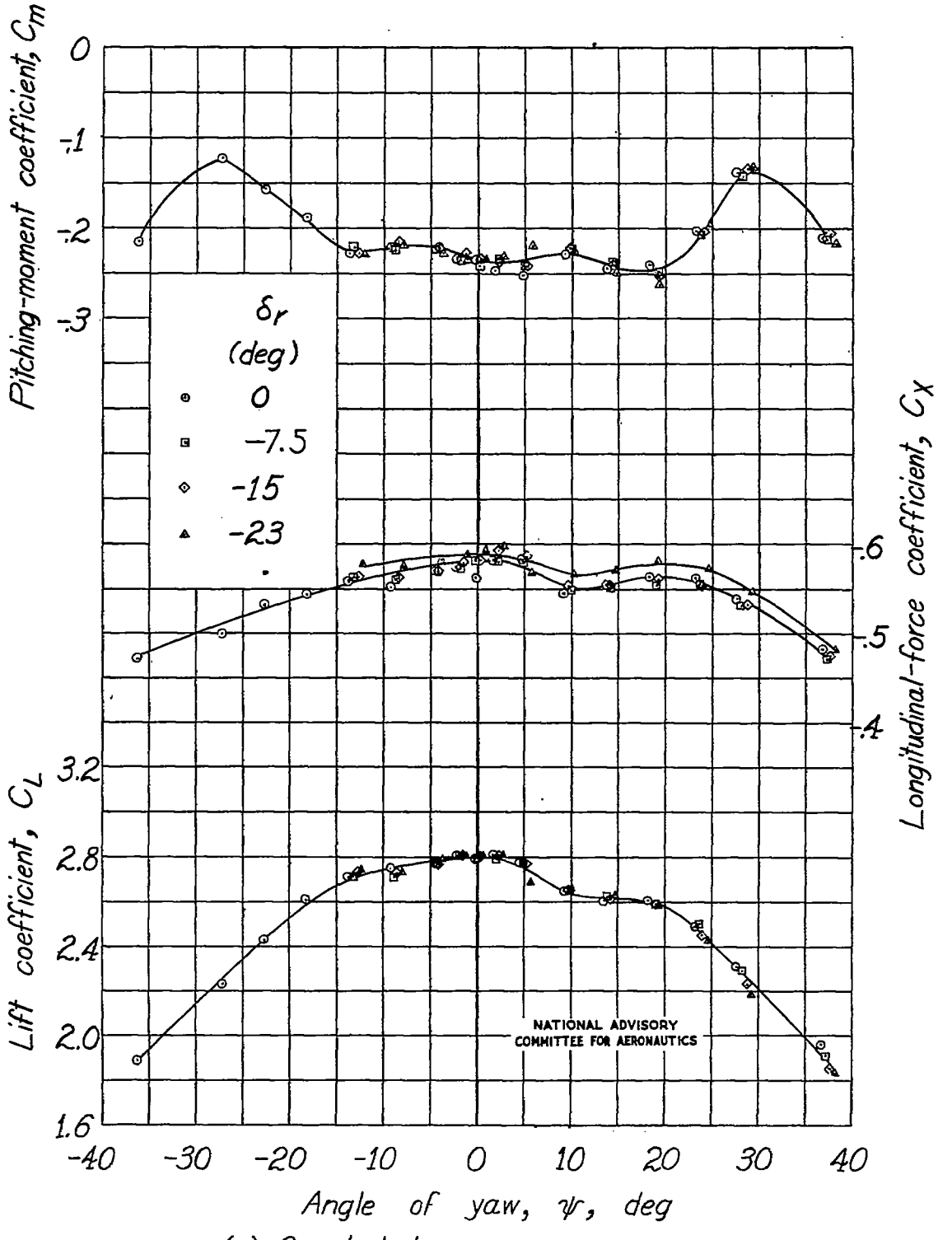

(a) Concluded.

Figure 19.—Continued.

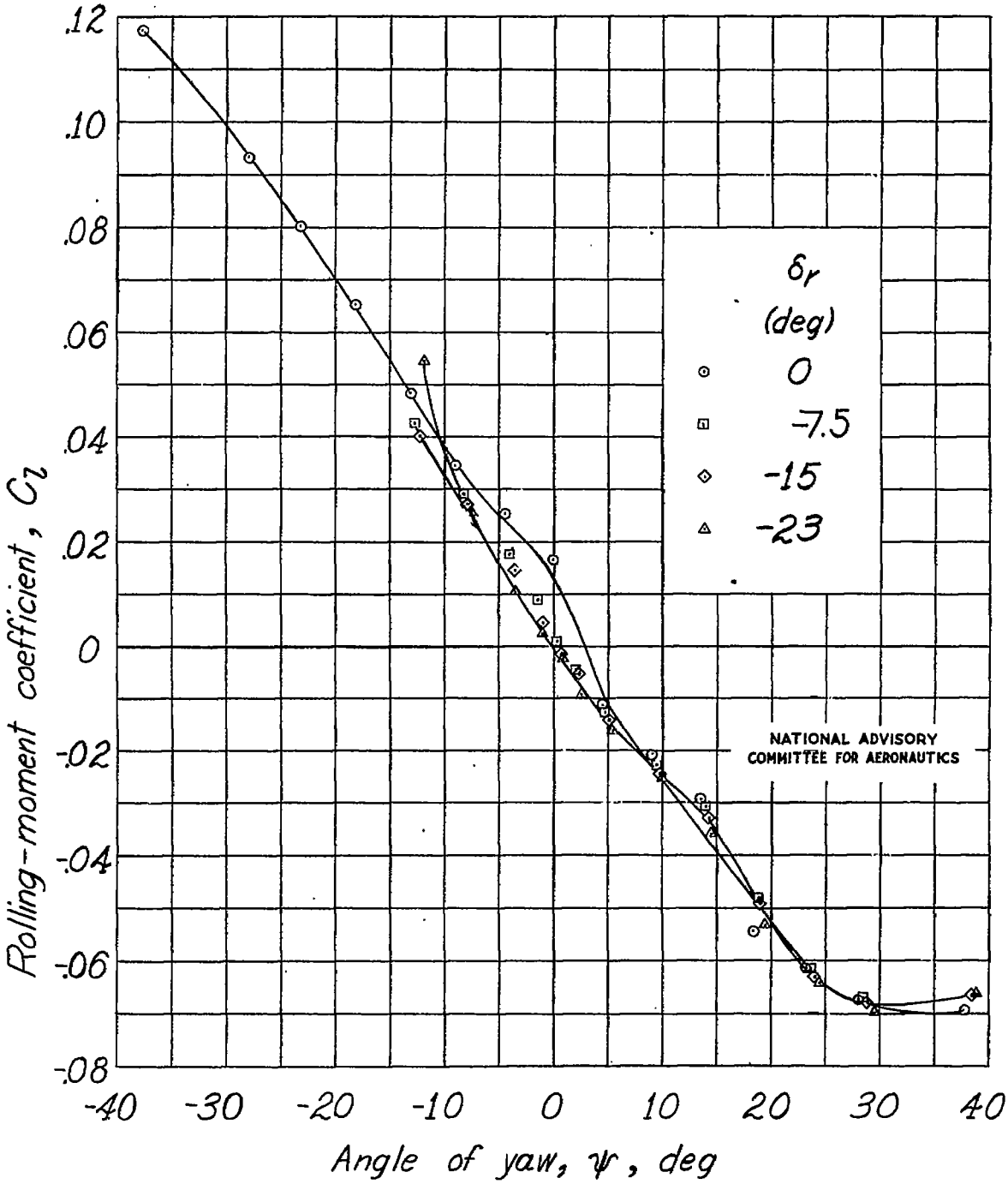

(b) Constant power.

Figure 19.- Continued.

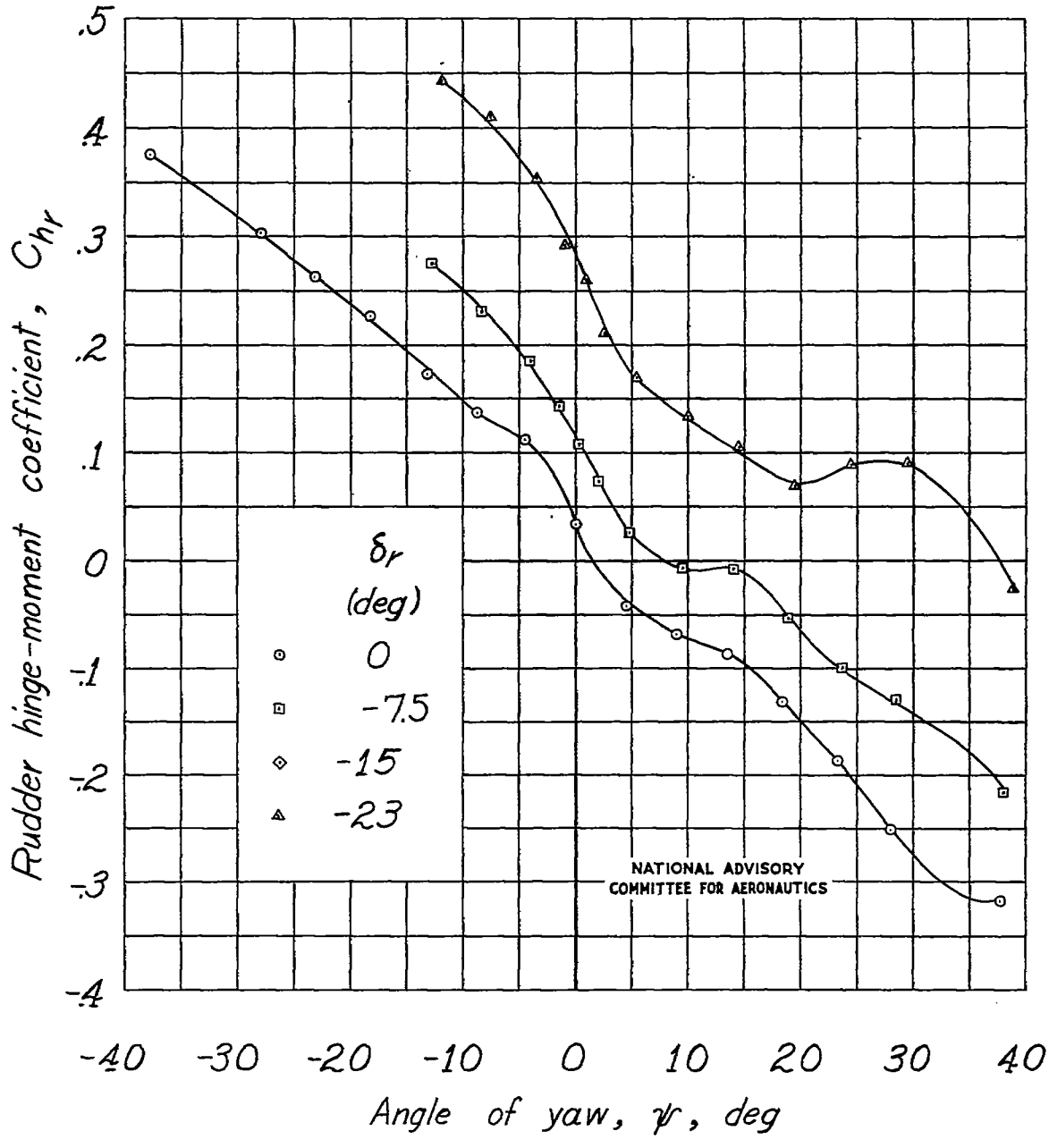

(b) Continued.

Figure 19.-Continued.

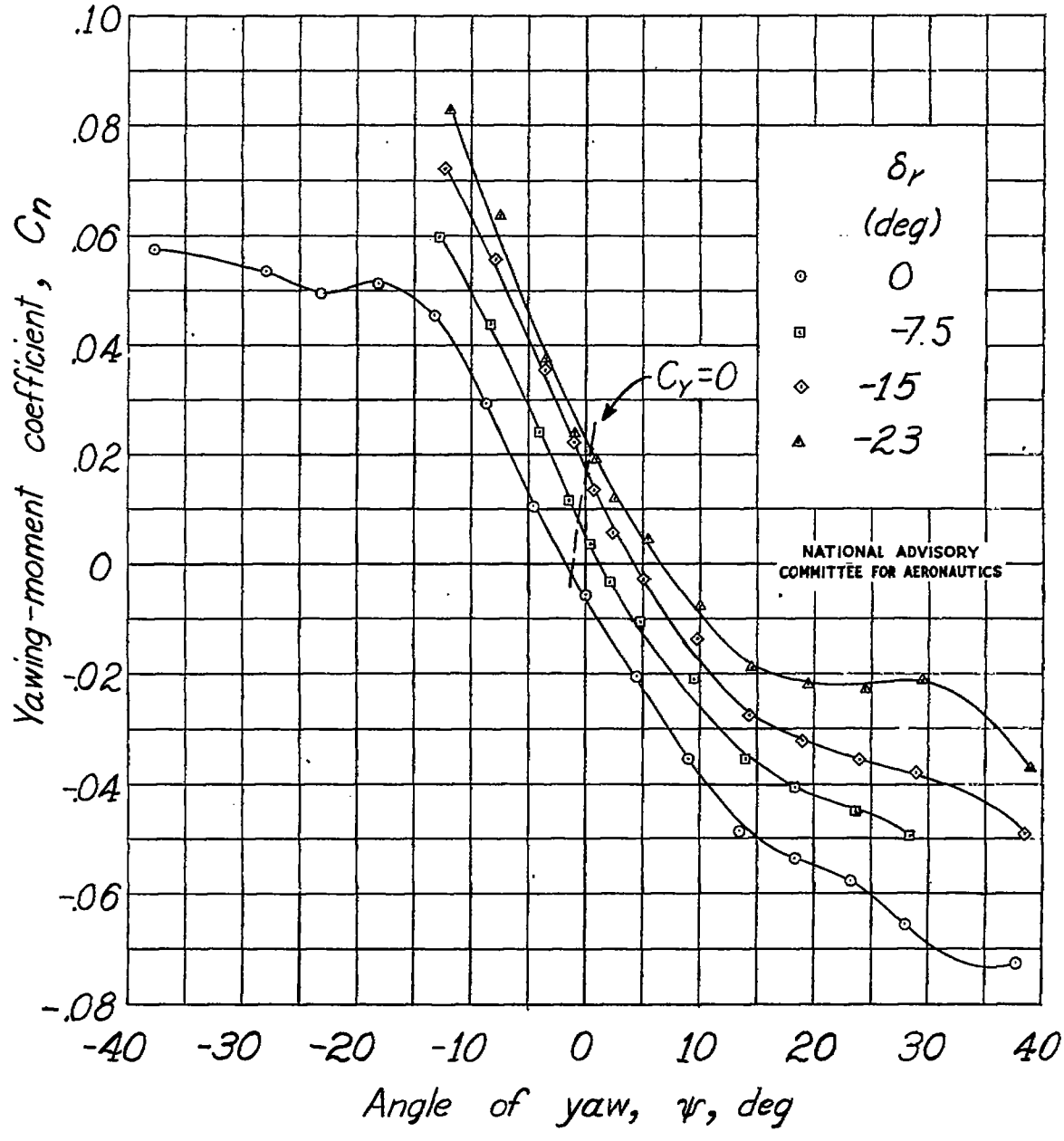

(b) Continued.

Figure 19.- Continued.

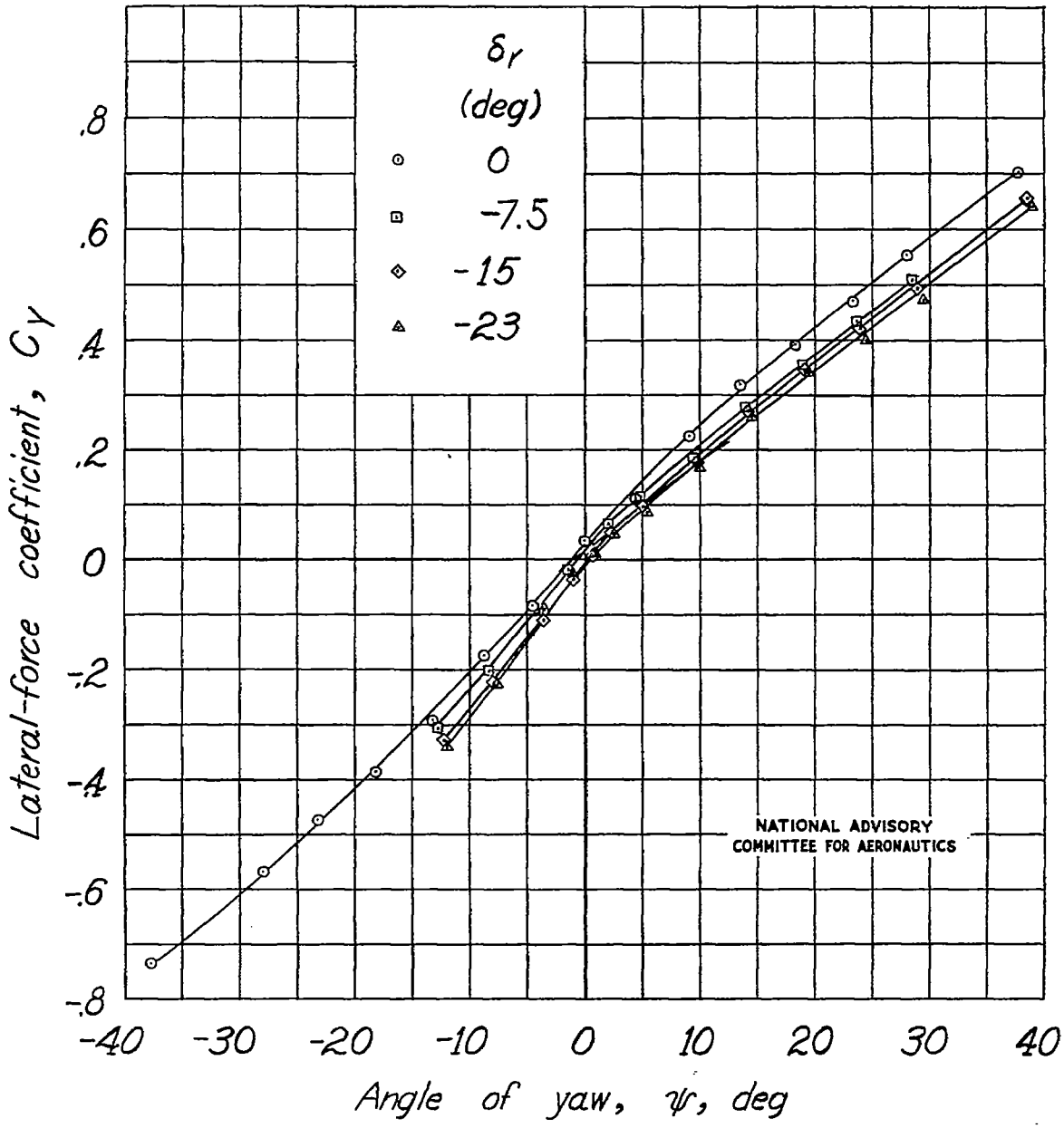

(b) Continued.

Figure 19.- Continued.

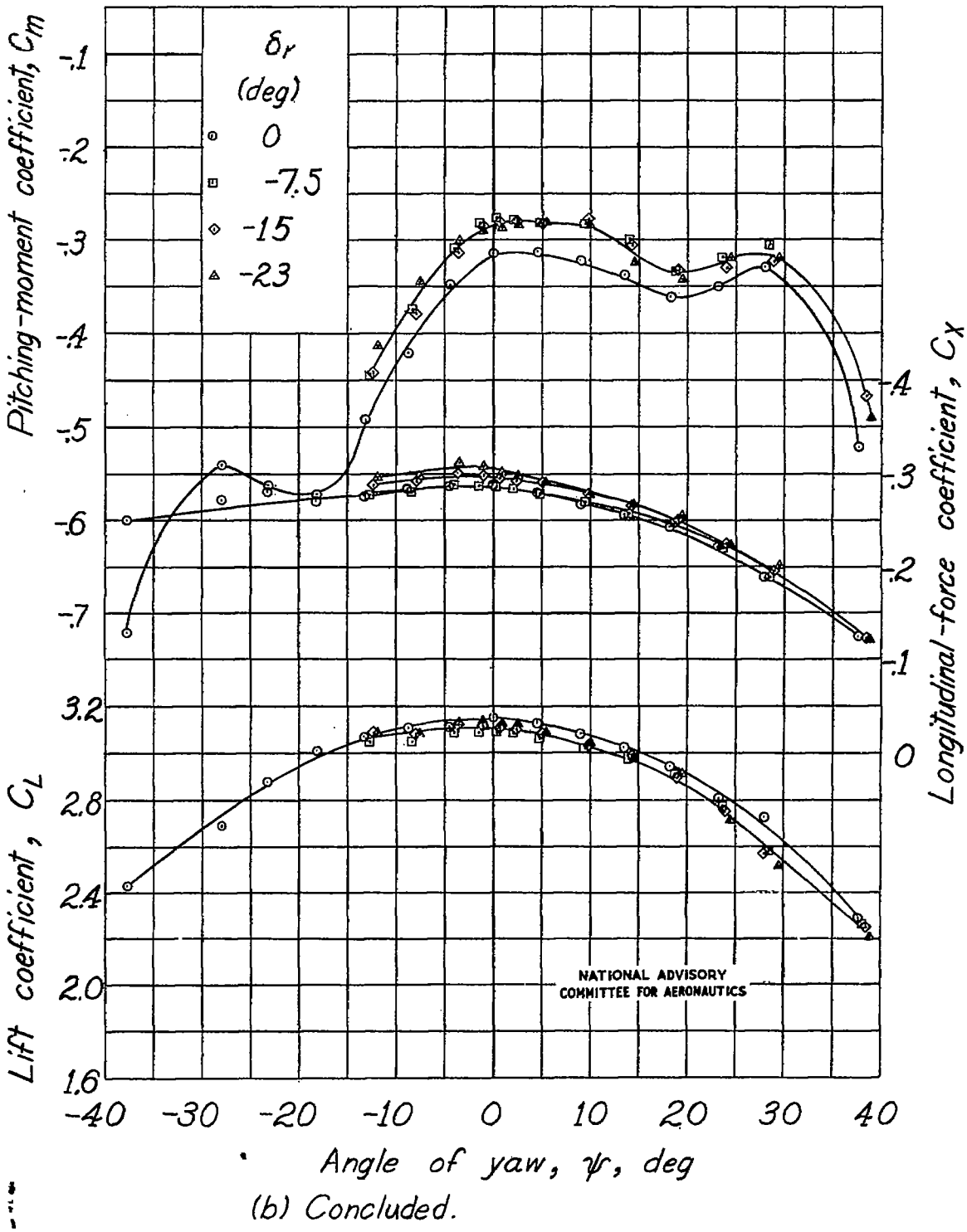

(b) Concluded.

Figure 19.- Concluded.